University of Nebraska - Lincoln

DigitalCommons@University of Nebraska - Lincoln

Biological Systems Engineering--Dissertations, Theses, and Student Research

Biological Systems Engineering

12-3-2021

Development and Characterization of a Decellularized Neuroinhibitory Scaffold Containing Matrix Bound Nanovesicles

Logan Piening
University of Nebraska-Lincoln, logan.piening@huskers.unl.edu

Follow this and additional works at: https://digitalcommons.unl.edu/biosysengdiss

Part of the Biological Engineering Commons, Biomaterials Commons, and the Bioresource and Agricultural Engineering Commons

DEVELOPMENT AND CHARACTERIZATION OF A DECELLULARIZED

NEUROINHIBITORY SCAFFOLD CONTAINING MATRIX BOUND

NANOVESICLES

By

Logan M. Piening

A THESIS

Presented to the Faculty of

The Graduate College at the University of Nebraska

In Partial Fulfillment of Requirements

For the Degree of Master of Science

Major: Agricultural & Biological Systems Engineering

Under the Supervision of Professor Rebecca Wachs

Lincoln, Nebraska

December, 2021

DEVELOPMENT AND CHARACTERIZATION OF A DECELLULARIZED

NEUROINHIBITORY SCAFFOLD CONTAINING MATRIX BOUND

NANOVESICLES

Logan Piening, M.S.

University of Nebraska, 2021

Advisor: Rebecca Wachs

Chronic low back pain (LBP) is a leading cause of disability but treatments for LBP are limited. Degeneration of the intervertebral disc leads to loss of neuroinhibitory sulfated glycosaminoglycans (sGAGs) which allows nerves from dorsal root ganglia (DRG) to grow into the core of the disc, leading to pain. Current treatments for LBP involve drugs that do not target the source of the pain and lack long term efficacy or use invasive surgeries with high complication rates. Treatment with a decellularized tissue scaffold that contains neuroinhibitory components may inhibit nerve growth and prevent disc-associated LBP. Here, a decellularized nucleus pulposus (NP) tissue scaffold was developed to be used as a treatment for low back pain. Results indicated that the decellularized tissue scaffold developed here removed over 99% of DNA and maintained 70% of the native sGAGs. After gelation, it was determined that the gel was not cytotoxic, and it exhibited neuroinhibitory properties. Following the research on a neuroinhibitory gel, the project shifted to the investigation of a recently discovered nanovesicle with active cargo that may be present in NP tissue. Matrix bound nanovesicles (MBVs) were successfully isolated from NP tissue. Analysis of the MBVs found within the decellularized tissue revealed that they polarized macrophages towards an inflammatory phenotype, which is different to

previous literature investigating MBVs. Culture of nucleus pulposus cells with MBVs demonstrated that the NP cells started growing on top of each other, although this was the only morphological change. This work also characterized the protein contents of the NP-derived suggesting that MBVs may be one reason that the NP cannot resolve inflammation during degeneration. The work presented here demonstrates that a decellularized NP tissue scaffold can be formulated into an injectable gel that exhibits neuroinhibitory properties for the treatment of low back pain. Along with this, the presence of MBVs were discovered within the decellularized NP and the NP derived MBVs had unique profile of contents and cellular responses.

Contents

List of Figures and Tables

List of Abbreviations

α-gal - α-galactosyl epitope

AF – annulus fibrosus

BDNF – brain-derived neurotrophic factor

DPBS – Dulbecco's phosphate buffered saline

DRG – dorsal root ganglia

EDX – X-ray spectroscopy

FBS – fetal bovine serum

HAADF – high-angle angular dark-field

HCl – hydrochloric acid

HMDS – hexamethyldisilazane

IACUC – Institutional Animal Care and Use Committee

LBP – Low back pain

LPS – lipopolysaccharide

MBV – matrix bound nanovesicle

miRNA – micro ribonucleic acid

NaOH – sodium hydroxide

NF-H – neurofilament-H

NGF – nerve growth factor

NP – nucleus pulposus

OCT – optimal cutting temperature

PBS – phosphate buffered saline

PBST – phosphate buffered saline with tween

PFA – paraformaldehyde

Pt/Pd – platinum/palladium

SB-16 - 3(N,N-Dimethylpalmitylammonio)-propane inner salt

SB3-10 - 3-(Decyldimethylammonio)-propanesulfonate inner salt

SD – sodium deoxycholate

SEM – scanning electron microscopy

sGAG – sulfated glycosaminoglycan

TEM – transmission electron microscopy

CHAPTER 1: INTRODUCTION

1.1 Significance of the Study

Low back pain impacts a large portion of the world population in their lifetimes. This study aimed to create a minimally invasive, thermally forming hydrogel that could be injected into a painful, degenerate disc in the clinic to stop painful nerves from growing into the disc and to stabilize the degenerate disc. Decellularized nucleus pulposus tissue was used for this purpose because it contains proteins, proteoglycans, and polysaccharides native to the healthy disc. In doing so, this treatment is meant as a minimally invasive treatment for low back pain. In addition to the formation of an injectable gel, this study also investigated and expanded the knowledge on matrix bound nanovesicles derived from nucleus pulposus tissue, which are a recently discovered vesicle that are believed to be found in all tissues and have demonstrated regenerative properties.

1.2 Purpose of the Study

The purpose of this study was to adapt a decellularization process [1] for whole porcine nucleus pulposus, then use this decellularized tissue to create a thermally forming, injectable hydrogel that could maintain cell viability while preventing nerve growth. Following the successful development of this neuroinhibitory hydrogel, the study shifted to investigate a recently identified particle in other tissues that modulate cell response, matrix bound nanovesicles. Because this work investigated two different projects, this thesis is separated into two different arms, the neuroinhibitory gel project and the nucleus pulposus derived matrix bound nanovesicle project.

1.3 Statement of the Hypothesis

This thesis tested a hypothesis specific to each project, which are described below.

1.3.1 Creation of a neuroinhibitory gel:

A previous decellularization process could be adapted for use here and the resulting decellularized tissue could be developed into a gel that exhibits neuroinhibitory properties.

1.3.2 Nucleus Pulposus Derived Matrix Bound Nanovesicles:

Matrix bound nanovesicles are present within the nucleus pulposus, and they modulate cell phenotypes present in this tissue.

CHAPTER 2: Creation of an Injectable Gel for Treatment of Low Back Pain

2.1 REVIEW OF LITERATURE
2.1.1 Low Back Pain

Low back pain (LBP) affects four out of five people in the world at least once in their lifetime, with 20% of those affected developing *chronic* LBP [2]. The high incidence of chronic LBP has made it the leading cause of years lived with disability for the past three decades [3]. Disc-associated LBP is a major contributor to chronic LBP, in which pain is attributed to the disc directly. Disc-associated LBP patients exhibit nerve growth deep within the previously aneural disc [4, 5]. These nerve fibers are stimulated and sensitized by the catabolic disc environment, leading to pain [6, 7]. The current gold standard of treatment for end-stage chronic LBP patients is a spinal fusion, which can be invasive, have high complication rates (14.3%-16% [8, 9] of patients), high costs [8-10],

long recovery times [11], and lead to reduced range of motion and increased potential for adjacent level degeneration [12, 13]. An alternative low-risk treatment that focuses on preventing a patient's pain progression holds great potential for the treatment of disc-associated LBP.

The intervertebral disc is composed of a gelatinous nucleus pulposus (NP) core surrounded by a lamellar annulus fibrosus (AF) as demonstrated in **Figure 1** [14]. The healthy disc is predominantly avascular and aneural and receives the majority of nutrients from diffusion through adjacent cartilaginous endplates [14, 15]. Aging and injury can trigger disc degeneration, resulting in thickening of the cartilaginous endplates, reducing diffusion of nutrients into the NP [16-18]. This reduction in nutrient diffusion can lead to NP cell senescence [19]. Senescent NP cells secrete inflammatory cytokines and degradative enzymes, creating a catabolic environment that breaks down matrix components such as aggrecan [20-22]. Intact aggrecan has neuroinhibitory properties due to sulfated glycosaminoglycan (sGAG) side chains and thus, naturally inhibits nerve growth into a healthy disc [23]. During degeneration, cleavage of these sGAG side chains reduces the neuroinhibitory properties of the disc [24-27]. Further, senescent NP cells secrete several molecules that increase nerve growth, such as nerve growth factor (NGF) and brain-derived neurotrophic factor (BDNF) [7, 28, 29]. The loss of potently neuroinhibitory sGAGs and increased expression of NGF and BDNF results in ideal conditions for the ingrowth of nerve fibers into degenerated discs. Once painful nerve fibers are present in the disc, they can be sensitized and stimulated by the harsh catabolic environment of the degenerating disc, leading to pain [30]. A treatment that contains neuroinhibitory sGAGs and other neuroinhibitory components has the potential to prevent

disease progression by preventing nerve growth. Decellularized tissue scaffolds fabricated from healthy NP tissue hold promise to reintroduce neuroinhibitory properties to the NP and prevent pain progression.
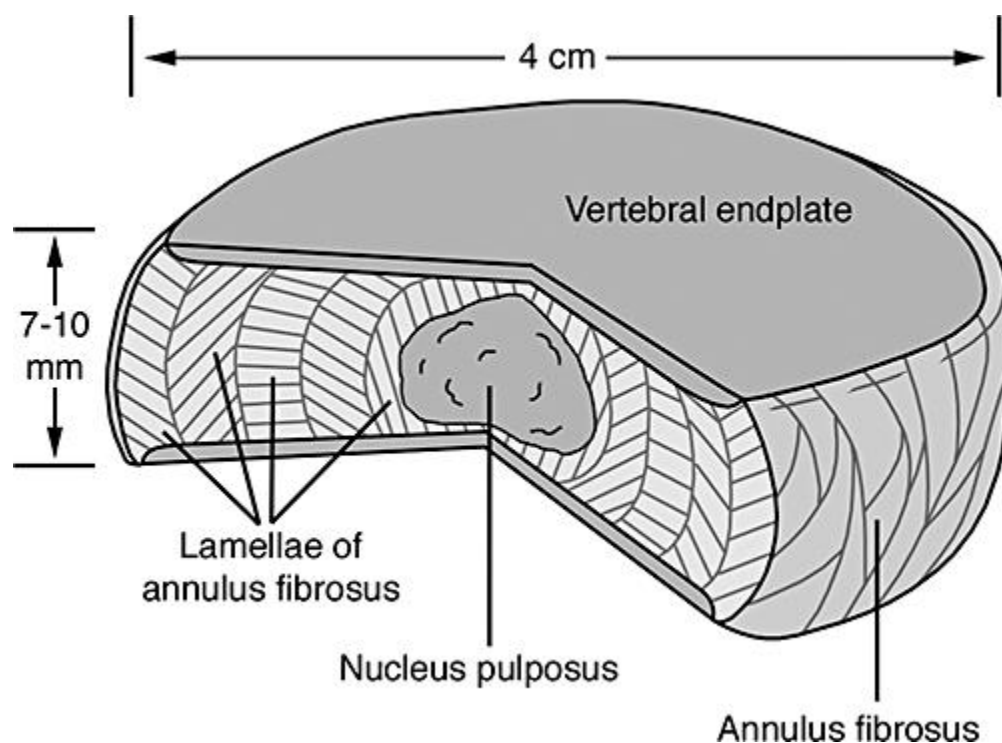
Figure 1. Anatomy of the intervertebral disc [14].

Decellularized tissue has been widely used over the past 50 years to engineer tissues such as: urinary bladder matrix [31], dermis [32, 33], and small intestinal submucosa [34-36]. Decellularized tissues have been successful in treatments because decellularized scaffolds have similar properties, compositions, and architecture to native tissue, thereby improving their function and cellular recognition in vivo compared to other treatments [37]. For decellularization of the NP, maintenance of the extracellular matrix proteins and proteoglycans is crucial for its eventual function in the disc. Several groups have developed decellularization methods for the NP by using various detergents of differing concentrations and incubation times [38-44]. These decellularization methods focus on

improving the removal of cellular materials while maintaining native molecules, such as sGAGs [1, 38-44].

2.1.2 Decellularized Nucleus Pulposus Scaffolds

In all cases of clinical implantation of animal tissue, it is not feasible to implant animal tissue directly into the human body, as doing so will cause a multitude of immune responses and be rejected quickly. However, decellularization fixes this problem, as antigens from cells are removed in the decellularization process, leaving behind structural and other native molecules [37]. This is significant because, in clinical settings, one would be able to use much more readily available animal tissue compared to much rarer and hard to come by human tissue. This has led several researchers to investigate methods to decellularize nucleus pulposus tissue from other species, to be used in the future as clinical treatments. The two main species used for NP decellularization are porcine and bovine, due to their similarities in size and composition to human NP, as well as availability due to raising livestock [45].

Decellularization is a balance between the removal of cellular material and the maintenance of native proteins. Decellularized NP tissues have demonstrated the ability to cause stem cells to increase expression of anabolic proteins aggrecan and collagen type II, indicative of an NP-like phenotype [38-44]. This suggests that decellularized NP has the potential to promote a healthy nucleus pulposus environment, without pain. Several groups have developed decellularization protocols for either bovine or porcine NP. All literature of NP decellularization investigated the presence of DNA, as a marker of cellular contaminants, and native proteins through the measurement of sGAGs and/or collagen. The DNA removal of these decellularization methods ranged from 71% to ~98%, while the

sGAG maintenance ranged from ~54% to 97% [38-44]. The normalized collagen content ranged from 135% to 190% [38-44]. Lastly, cell viability was determined either qualitatively or quantitatively once the material had been applied to cells and all decellularization processes appeared to have minimal cytotoxicity [38-44]. The results of the analysis of NP decellularization methods are displayed in **Table 1**. Other characterization methods that were employed with less frequency involved staining tissue sections, generally with H&E and observing macroscopic changes between the control and decellularized tissue, determining the mechanical properties of the tissue following decellularization, determining the difference in swelling with water, and determining the effects of the decellularized tissues on stem cells [38-44]. In general, the decellularized tissues remained similar to fresh tissues in terms of micro- and macro-architecture, although staining did reveal less sGAG content in the decellularized tissues compared to control [38-44]. Mechanical properties of decellularized NPs were generally not significantly different from control tissues, the swelling capabilities of the decellularized NPs were lower than controls most likely due to loss of sGAGs [38-44]. The results demonstrated here helped to guide the choice of analysis, as well as set benchmarks for how effectiveness of the decellularization process. However, to date, no group has investigated the neuroinhibitory properties of decellularized NP.

Table 1. Analysis of Various NP Decellularization.

Species	DNA Removal	sGAG Maintenance	Collagen Content	Cell Viability	References
Porcine	93%	89%	135%	Qualitative	[38]
Bovine	~85%	~54%	Qual.	N/A	[40]
Bovine	71%	97%	Qual.	92.30%	[41]
Porcine	~98%	~81%	177%	N/A	[42]
Porcine	~97%	~85%	190%	~83%	[43]
Bovine	93%	89%	135%	Qualitative	[44]

2.1.3 Injectable Formulations

Even after the successful decellularization of NP, there is still a problem of how to reintroduce this scaffold back into the body. Leaving the decellularized scaffold intact would mean that surgery would be required to implant the scaffold into the patient's disc, causing unnecessary damage to the outer AF. Intact scaffolds could also be the incorrect size and leave voids within the tissue. One alternative method is to make the decellularized scaffold injectable, generally through enzymatic digestion and thermal re-gelation [46-50]. The enzymatic digestion and regelation method holds promise for the NP, as it can allow the reforming of a gelatinous structure, similar to the native NP, in situ.

Injectable hydrogels made from digested and re-gelled decellularized tissue have been developed as possible treatments for many diseases, from myocardial infarctions [51] to nerve degeneration [52] and osteoarthritis [53]. This process generally involves the use of an enzyme that can digest tissue, such as pepsin, followed by some form of supplementation, either with molecules that can naturally crosslink, drugs, cells, solutions to control the buffering capacity and ionic strength, or chemical crosslinkers. The digested tissue is then injected to the appropriate location and allowed to form a gel. Injectable hydrogels are generally used because they are non-invasive, easily targetable, and the gels form to the space that they are injected into [54, 55]. Injectable hydrogels are also an attractive form of treatment because they can be chemically modified, optimized to include specific drugs or cells, and the mechanical properties can be tuned to what is specifically needed for certain situations.

While there have been several groups to develop decellularization processes for the NP, only a few have investigated the injectability of their solutions [38-44]. Briefly, Zhou

et. al. developed a decellularization method for porcine NP, then used this decellularized tissue scaffold to create a hydrogel by combining their crushed, lyophilized tissue with 20 mg/mL chondroitin sulfate, PBS, and cells in DMEM [42]. The authors then used genepin as a crosslinker to fully form the gel. It was found that the gel was injectable and that there was an improvement in disc height, water content, and extracellular matrix synthesis in the model of intervertebral disc degeneration, indicative of a healthier NP over time [42]. Yu et. al. also developed a decellularization process for bovine NP and used this decellularized tissue scaffold to create a hydrogel by digesting their decellularized tissue with pepsin and adjusting the ionic strength with PBS [44]. Digestion of decellularized tissue with pepsin is a common method of solubilizing extracellular matrix tissue, without destroying the native molecules [44, 49, 56, 57]. The authors found that the gel was able to form on its own without the need for additional crosslinkers. It was demonstrated that the gel was injectable and that it did not cause any substantial immune response [44]. As demonstrated here, injectable hydrogels for the NP may be able to form on their own or need to supplement specific molecules that can form a hydrogel. While chemical crosslinkers are useful in being able to fine tune the mechanical properties of the injectable hydrogel, they can introduce unintended cytotoxicity [58]. To account for the need for supplementation in some tissues, molecules that naturally form a hydrogel, such as type I collagen can be supplemented to allow a gel to form after injection. Once the gel has formed, it will be able to modulate cell response.

2.1.4 Immunomodulatory Tissue Scaffolds

The immune response induced by a tissue scaffold is one of the critical factors for the success of the scaffold. If a scaffold or biomaterial can guide the immune response to become pro-regenerative, it will have increased therapeutic efficacy, and increase the time

that the biomaterial can function due to decreased degradation rate. In terms of immunomodulation for tissue engineering scaffolds, the key immune cell to target is the macrophage. Macrophages are innate immune cells and play many roles in immunity as well as tissue homeostasis. During times of tissue damage or infection, macrophages are polarized towards an inflammatory phenotype, where they secrete inflammatory cytokines and chemokines in order to fight off infection and alert other cells of what is happening [59]. This phenotype is termed the M1-like phenotype. During times of tissue remodeling and maintenance, macrophages can enter into an alternatively activated, pro-remodeling phenotype where they secrete anti-inflammatory cytokines and aid in the remodeling process through phagocytosis of damaged molecules [60]. This phenotype is termed the M2-like phenotype. These phenotypes exist along a spectrum of activation, however, there are known molecules that can drive macrophages to specific phenotypes. A few of these molecules include lipopolysaccharide for the M1-like phenotype and IL-4 and IL-13 for the M2-like phenotype [59]. The ideal macrophage response to a decellularized scaffold would be to polarize towards an M2-like phenotype, so that the macrophage can begin to remodel the scaffold accordingly. However, this response may be dependent upon the specific tissue, as the ideal response for NP tissue may be to push the tissue towards a more fibrillar state that lacks pain, instead of leading to more inflammation, which currently occurs during degeneration. It is important to understand the roles macrophages play in immunity and tissue homeostasis to modulate them to create a successful implantable scaffold.

Several decellularized tissue scaffolds have been investigated for their roles in modulating the response of macrophages, namely small intestinal submucosa [61, 62],

skeletal muscle [63], and urinary bladder matrix [64]. There has not been clinical or histological evidence of delayed rejection of efficiently decellularized extracellular matrix biomaterials, suggesting that if the tissue is decellularized well enough, macrophages are polarized towards an M2-like phenotype [65]. The effect of inadequate decellularization was tested on porcine small intestinal submucosa, by varying the decellularization process to have non-decellularized, moderately decellularized, and completely decellularized tissue [66]. The authors demonstrated that the macrophage response was mostly M1-like in both the non-decellularized and moderately decellularized groups, however, the response shifted towards a predominantly M2-like response in the completely decellularized group, as demonstrated in **Figure 2** [66]. The response to inadequately decellularized scaffolds is also important in the clinic as decellularized porcine heart valves are often used as a treatment for heart related diseases, however, inadequately decellularized porcine heart valves have been linked to deaths of patients [67]. All of the papers cited here support the claim that properly decellularized tissue scaffolds polarize macrophages towards an M2-like phenotype, whereas treatments without decellularized tissue scaffolds or inadequately decellularized tissue scaffolds showed predominantly M1-like responses [61-64]. Carbodiimide crosslinking of decellularized small intestinal submucosa caused a more M1-like response in macrophages, compared to the uncrosslinked tissue scaffold, which caused an M2-like response as described [61]. This suggests that there are certain factors within the decellularized tissue scaffold that polarize macrophages towards an M2-like phenotype but are not able to be reached by the macrophages when the tissue scaffold is more crosslinked. One possible explanation for this is the presence of matrix bound nanovesicles within the decellularized tissues that modulate macrophage phenotype and have previously

been seen to polarize macrophages towards an M2-like phenotype, similar to the whole tissue effects described here [68, 69]. These vesicles will be discussed later in this thesis.
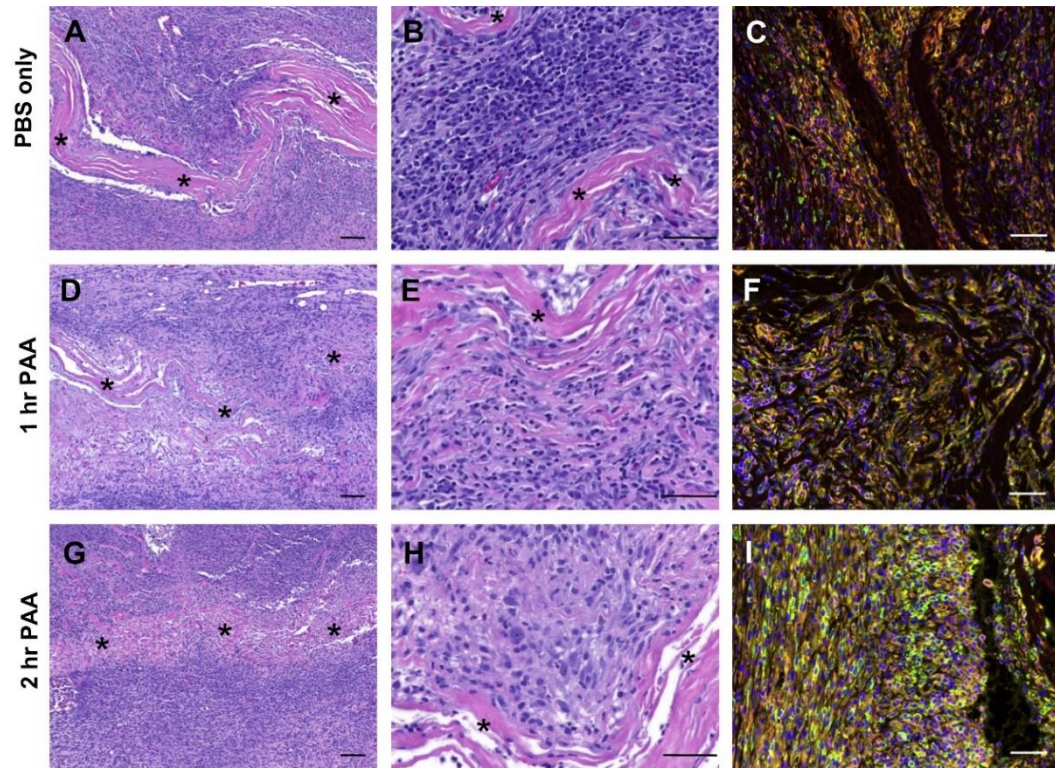
Figure 2. Decellularized small intestinal submucosa polarizes macrophages toward M2 when fully decellularized. Small intestinal submucosa not decellularized (PBS only), moderately decellularized (1 hr PAA), and completely decellularized (2 hr PAA). Macrophages were cultured on the tissues for 14 days and were stained for CD68 (pan macrophage marker, purple), CCR7 (M1 marker, orange), and CD206 (M2 marker, green) and counterstained with DAPI. Fully decellularized tissue caused a mostly M2 response, whereas tissues that were not fully decellularized caused a mostly M1 response [66].

2.1.5 Summary for Neuroinhibitory Gel

Tissue specific decellularized scaffolds are useful as treatments for diseases because they contain the native proteins, proteoglycans, and polysaccharides of the healthy tissue, without the antigenic materials that may cause an immune response. The decellularized tissue scaffolds can modulate the immune response, generally towards an M2-like phenotype. To use this decellularized tissue scaffold as a minimally invasive clinical treatment, the tissue can be digested and supplemented to create a hydrogel. This

process has previously been performed with decellularized NP tissue, however, the neuroinhibitory properties of these NP gels have not been investigated before.

2.2 METHODS

2.2.1 Decellularization Process and Analysis

2.2.1.1 Whole Disc Decellularization

Cervical spines from commercial line Landrace/Yorkshire/Duroc young female pigs (~200 days of age) were aseptically collected and frozen (-80 °C) following humane slaughter at the United States Meat Animal Research Center Abattoir (Clay Center, NE, USA; USDA Material Transfer Agreement). Intact spines were thawed for two days at 4 °C. The spines were then cleaned aseptically and the NPs of the C2-C7 intervertebral discs were surgically removed. Control NPs from each spine were either: 1) fixed in 4% paraformaldehyde (PFA) for 30 minutes, followed by 3 x 15 min washes in 1X phosphate buffered saline (PBS) for imaging, 2) eluted in media for cytotoxicity studies, or 3) frozen at -80 ℃ and lyophilized for 2 days (FreeZone 4.5 L Freeze Dryer (7750020, Labconco)) for additional analyses described below. Remaining NPs were decellularized following the process as outlined in **Table 2**. This procedure was adapted from Wachs et. al. 2017 [1] by processing each whole intact NP at room temperature in a 50 mL tube (89039, VWR) filled up to the 45 mL mark, spinning on an orbital shaker (EW-07650, Stuart) at 18 rpm. Changes made to the previous protocol include replacing Triton X-200 (discontinued) with sodium deoxylcholate (SD), excluding RNase digestion, altering times for detergent washes, and including 1X PBS and water washes at the end of the process. Triton X-200 was replaced with SD because triton X-200 was discontinued and SD had previously been used in decellularization methods for NP tissue, with positive results [38]. RNase was excluded from the decellularization process because it was determined that it caused

cytotoxicity with limited effect on the final RNA content. RNase is a fairly stable enzyme and so would remain in the tissue for long periods of time, while the RNA it was meant to cleave was relatively unstable and the vast majority of it would have degraded by the end of the process, naturally. On the other hand, DNase was included as it is relatively unstable and thus would have degraded by the end of the decellularization process, while the DNA it was meant to cleave was very stable and could still be present at high quantities following the decellularization process. The times for detergent washes were altered to reduce the cytotoxicity of the decellularized tissue scaffold, because preliminary work had demonstrated that reducing several of the detergent times had little effect on the decellularization efficacy but led to decreased cytotoxicity. Lastly, PBS and water washes were added at the end of the decellularized process to ensure as much residual detergent was removed as possible, again to decrease the cytotoxicity of the tissue scaffold. At the end of decellularization, NPs were either processed with fixation, elution, or lyophilization. A minimum of three spines were used for each analysis to account for biological variability (n=3 experiments). To account for increased variability in decellularized NP samples compared to control NP samples, at least one unprocessed control NP and at least three decellularized NP were analyzed for each spine.

Table 2: The time spent in each wash step of the decellularization process

	Wash liquid	Time
1	ddH$_2$0	7 hours
2	100 mM Sodium/50 mM Phosphate buffer	Overnight (10-12 hours)
3	125 mM SB3-10 in 50 mM Sodium/10 mM Phosphate buffer	4 hours

4	100 mM Sodium/50 mM Phosphate buffer	15 minutes
5	3% (w/v) SD/0.6 mM SB-16 in 50 mM Sodium/10 mM Phosphate buffer	1 hour
6	100 mM Sodium/50 mM Phosphate buffer	3 x 15 minutes
7	125 mM SB3-10 in 50 mM Sodium/10 mM Phosphate buffer	1.75 hours
8	100 mM Sodium/50 mM Phosphate buffer	15 minutes
9	3% (w/v) SD/0.6 mM SB-16 in 50 mM Sodium/10 mM Phosphate buffer	45 minutes
10	100 mM Sodium/50 mM Phosphate buffer	3 x 15 minutes
11	DNase (75 U/mL) in 50 mM Sodium/10 mM Phosphate buffer	34 hours
12	50 mM Sodium/10 mM Phosphate buffer	3 x 90 minutes
13	1X PBS	3 x 3 hours
14	ddH$_2$O	3 x 15 minutes
Chemical Information For Decellularization Process		
3-(Decyldimethylammonio)-propanesulfonate inner salt (SB3-10) (D4266, Sigma-Aldrich)		
3(N,N-Dimethylpalmitylammonio)-propane inner salt (SB-16) (H6883, Sigma-Aldrich)		
Sodium deoxylcholate (SD) (D6750, Sigma-Aldrich)		
DNase (D4527, Sigma-Aldrich)		

2.2.1.2 DNA Content

DNA content of control and decellularized NP samples was analyzed using the Quant-iT PicoGreen dsDNA Assay Kit (P7589, Thermo Fisher) according to the manufacturer's instructions to verify removal of antigenic DNA remnants after decellularization. Briefly, lyophilized control and decellularized NP samples were digested in 1 mL of 16 U/mL papain (P3125, Sigma-Aldrich) in 0.2 M sodium phosphate buffer containing 0.0975 M sodium acetate (W302406, Sigma-Aldrich), 0.0137 M ethylenediaminetetraacetic acid (E6758, Sigma-Aldrich), and 0.005 M cysteine HCl (C1276, Sigma-Aldrich) overnight in a 65 °C water bath. The remainder of the assay was conducted per the manufacturer's instructions, DNA was quantified using the provided standards and normalized to the dry weight of the tissue scaffold. A total of n = 3 control NPs and n = 9 decellularized NPs were used for the outlined experiments.

2.2.1.3 Sulfated Glycosaminoglycan Content

sGAG content of control and decellularized NP samples was quantified to determine maintenance of sGAG after decellularization as a potential source of neuroinhibitory properties. A Blyscan Glycosaminoglycan assay kit (B1000, Biocolor) was utilized according to the manufacturer's instructions. Briefly, lyophilized control and decellularized NP samples were digested in papain as described above (see DNA Content). The remainder of the assay was conducted per the manufacturer's instructions by adding 1 mL of the provided dye reagent to 100 µL of each sample and shaking at room temperature for 30 minutes. The tubes were then centrifuged at 12,000 rpm for 10 minutes to pellet out the now insoluble sGAG. The remaining liquid was carefully poured off and the bound dye was liberated through the addition of 500 µL of the provided dissociation reagent and vortexing. sGAG absorbance was quantified on a plate reader at 656 nm according to the

provided standards and normalized to the dry weight of the tissue scaffold. A total of n =

3 control NPs and n = 12 decellularized NPs were used for the outlined experiments.

2.2.1.4 Collagen Content

Maintenance of collagen was determined after decellularization by analyzing

collagen content in control and decellularized NP samples. Depending on the type of

collagen, hydroxyproline can make up between 12.8-14.7% of the mass [70]. Thus, a

middle value of 13.5% was used as the percentage of hydroxyproline in collagen as a

conversion from hydroxyproline to collagen. A hydroxyproline assay (ab222941, Abcam)

was conducted according to manufacturer's instructions with slight modifications to

determine collagen content. Briefly, lyophilized control and decellularized NP samples

were digested in 1 mL of 16 U/mL papain (see above) at 65 °C overnight. This digested

NP was lyophilized overnight to concentrate the tissue. The resulting lyophilizate was

hydrolyzed with 200 µL of 5 M sodium hydroxide (NaOH) at 120 °C for 1 hour, then

neutralized on ice with 200 µL of 5 M hydrochloric acid (HCl). The remainder of the assay

was conducted per the manufacturer's instructions by moving 10 µL of each sample and

standard into a 96 well plate and allowing the liquid to evaporate at 65 °C on a hot plate.

Once the liquid had evaporated and crystals formed, 100 µL of oxidation reagent was added

to every well and incubated at room temperature for 20 minutes. 50 µL of provided

developer solution was then added to each well and incubated at 37 °C for 5 minutes.

Lastly, 50 µL of provided DMAB concentrate was added to each well and incubated at 65

°C while covered. The absorbance of the plate at 560 nm was read using a plate reader.

From the absorbance data a standard curve of soluble hydroxyproline was determined.

Once the soluble hydroxyproline content of each well was known, that value was

multiplied by three to get the total hydroxyproline (according to manufacturer) then divided

by 0.135, the value of hydroxyproline to collagen, to get the total collagen. The resulting data were normalized to the dry weight of the tissue scaffold. A total of n = 4 control NPs and n = 4 decellularized NPs were used for the outlined experiments.

2.2.1.5 Cytotoxicity of Residual Chemicals

Cytotoxicity of any residual chemicals in the decellularized NP tissue scaffold was evaluated by measuring the change in metabolic activity of human NP cells treated with media eluted from the decellularized NP using the AlamarBlue Assay (Thermo Fisher, 88951) in accordance with ISO Standards 10993:5 [71] and 10993:12 [72]. This cytotoxicity processing is necessary because low levels of the decellularization chemicals may remain in the tissue scaffold and diffuse out after being implanted into a patient. Briefly, 100 mg of wet decellularized NP tissue scaffold was eluted in 1 mL complete NP media (ScienCell, 4801) for 72 hours at 37 °C. Human NP cells from a single, fetal donor (ScienCell, 4800), were grown to passage 4, then split and seeded in a 48 well plate coated with Poly-L-Lysine at a density of 7500 cells/well. The cells were allowed to adhere for 24 hours before they were treated with eluted media. After cells were incubated for 48 hours with the eluted media, alamarBlue reagent was added to each well at a 1:10 ratio and incubated at 37 °C for 2 hours. The absorbance of the media was analyzed using a microplate reader (Synergy H1, Biotek, VT, USA) at 570 and 600 nm. The reduction of alamarBlue was calculated according to manufacturer's instructions. All samples including untreated controls were measured in triplicate. A total of n=3 decellularized spines, with 4 NP samples taken from each n, for a total of 12 decellularized NP were used in the outlined experiments.

2.2.1.6 α-galactose Epitope Immunostaining

The α-galactosyl epitope (α-gal) content of decellularized NP scaffolds was tested because α-gal is known to elicit an immune response in humans, as humans and old-world monkeys do not express this epitope [73]. Immunostaining was used to test whether the α-gal epitope was present in the NP tissue after decellularization. Fixed control and decellularized NP samples were utilized for α-gal immunostaining. Porcine muscle tissue was used as an additional positive control for α-gal due to its high cellularity and high α-gal presence. After fixation and storage at 4 °C in PBS, the PBS was removed, and the tissues were soaked in a 30% sucrose solution at 4 °C overnight. The samples were then frozen in optimal cutting temperature (OCT) compound (4586, Scigen) and cryo-sectioned at 30 µm (CM1950, Leica). Sections were post-fixed to slides in 4% PFA for 30 minutes, followed by 2 x 15-minute washes in 1X PBS and another wash for 15 minutes in PBS with tween (PBST) (0.1% Tween 20 (BP337, Fisher Scientific) in 1X PBS). The sections were then blocked using blocking buffer (3% goat serum (G9023, Sigma-Aldrich), 0.3% Triton X-100 (93443, Sigma-Aldrich) in 1X PBS for 1.5 hours, followed by primary mouse α-gal antibody incubation (ALX-801-090-1, ENZO) (1:1000 in blocking buffer) overnight at 4 °C with mild agitation. The sections were washed 6 x 15 minutes in 1X PBST, then incubated with secondary antibody anti-mouse 488 (ab150117, Abcam) for 4 hours at room temperature with mild agitation. The sections were again washed 6 x 15 minutes with 1X PBST. Finally, sections were counterstained with DAPI (D1306, Thermo Fisher) (1:1000 in 1X PBS) for 10 minutes, washed 3 x 5 minutes in 1X PBS, mounted using Prolong Gold (P36934, Fisher Scientific) and a glass coverslip. All steps were conducted at room temperature unless otherwise specified. Images were taken using a Zeiss Axio Observer at 10X magnification and quantified by counting the number of positive α-gal epitopes in

three 10X images of control NP, decellularized NP, and muscle tissue from three different animals using ImageJ. A total of n=3 samples were used for each group with a minimum of 3 images analyzed per n.

2.2.2 Creation of Injectable Neuroinhibitory Gel
2.2.2.1 Comparison of DMEM + HEPES Gelation of Collagen and Tissue scaffold

The intact AF provides a barrier to delivery to the NP; thus, an injectable formulation is essential. To create an injectable gel made from decellularized NP tissue, previous enzymatic digestion protocols were adapted [46, 74]. Twenty mg of lyophilized, decellularized NP was digested by 1 mg/mL of pepsin (P6887, Sigma-Aldrich) in 0.05 N HCl for 44 hours with spinning at 300 rpm using a magnetic stir bar. Prior work with altering the ionic strength by adjusting the concentration of PBS in solution found that lower ionic strengths allowed the tissue scaffold to gel much more robustly than high ionic strengths. This is because ionic strength has been demonstrated to have a strong effect on the gelation time, number of fibrils, and size of fibrils of collagen [75, 76]. Because of the low concentration of PBS, the buffering capacity of the solution would be impacted, as PBS was the only buffering capacity in the solution. To combat this, PBS was proposed to be replaced by DMEM (D2429, Sigma-Aldrich), to control ionic strength, and HEPES (H0887, Sigma-Aldrich), to control buffering capacity, so that these variables could be controlled independently of each other. Several experiments were performed to determine if this change was feasible and what concentrations would be optimal. Briefly, microcentrifuge tubes with 300 µL of solution were prepared on ice with concentrations of DMEM of 0.5X, 0.33X, 0.25X, and 0X and the collagen concentration was set at 2 mg/mL. The HEPES concentration was kept constant at 7.5 mM, as this is similar to the buffering capacity of 1X PBS, and prior work had demonstrated that buffering capacity had little

impact on gelation, so this value was used to keep buffering capacity consistent with previous work. The pH of each tube was adjusted to ~7.4 using 1 M NaOH. The different groups were: tissue + collagen, collagen alone, or tissue alone. Within each of these groups, different preparations were made using the above DMEM concentrations. The digested tissue was neutralized using 5M NaOH and was added to the appropriate tubes to a final concentration of 14.56 mg/mL or was replaced with water in the collagen only group. In the tissue only group, collagen was replaced with 0.02N acetic acid, to keep the pH the same as the other groups, as this is what the collagen was dissolved in. 100 µL of each tube was pipetted in duplicate into a 96 well plate and the absorbance was measured at 405 nm every minute for 45 minutes in a plate reader pre-heated to 37 °C. The absorbance at 405 nm was used to determine the opacity of the solution, which is an indicator of collagen fibril formation [1]. A total of n=3 preparations of different digests were performed following the methods described above.

2.2.2.2 Digestion and preparation of decellularized NP gel

Following the previous study, the concentration of DMEM was chosen to be 0.5X, as this concentration balanced gelation of both the collagen and tissue, and collagen was increased slightly to 2.5 mg/mL to improve mechanical properties, as it was noted that the previous gels were fragile and difficult to handle. The digested NP tissue alone did not form a robust gel at 37 °C, so rat tail type I collagen (354249, Corning) was supplemented to create a more robust gel. Type I collagen was selected because there is an increase in type I collagen with aging and degeneration and it forms a gel more consistently than type II collagen. Since the goal of this material is not to regenerate a healthy disc, but rather to act as a neuroinhibitory supplement, collagen type will not impact this property. The neutralized tissue digest, as described here after it had been neutralized, was added to pre-

mixed tubes containing DMEM and HEPES so that the final concentration of DMEM would be 0.5X and HEPES would be 7.5 mM. Collagen was added last up to a concentration of 2.5 mg/mL, to prevent premature crosslinking. The final pH of the resulting solution was adjusted to ~7.4 using 0.25M NaOH. The final formulation with supplemented collagen was termed regelled NP.

2.2.3 Characterizing the Physical Properties of the Regelled NP

2.2.3.1 Gelation kinetics

Following the formulation of the regelled NP, 100 µL of regelled NP was prepared and pipetted in triplicate into a 96 well plate. The plate was then placed into a microplate reader, pre-heated to 37 °C and the absorbance was read once every minute for 45 minutes at 405 nm, following the same protocol as discussed in "3.1.2.1 Comparison of DMEM + HEPES Gelation of Collagen and Tissue scaffold". The change in absorbance from the initial value and the normalized absorbance, (Equation 1), were calculated to show the percent of the maximum absorbance over time. A total of n = 3 different preparations were used with 3 samples analyzed for each n.

$$1) \quad NA = \frac{A_2 - A_1}{Max - A_1}$$

NA = normalized absorbance

A_2 = absorbance at a specific time

A_1 = initial absorbance

Max = maximum absorbance value over the time course

2.2.3.2 Mechanical characterization

Mechanical characterization consisted of rheology of the gel and was compared to previously published data on healthy human NP tissue, however, the gel created here was

meant as a supplement to the degenerate disc to prevent pain progression, not as an NP replacement. Rheology testing was performed on gels using an Anton Paar MCR 302 with sand blasted plates and a humidity bath. Briefly, regelled NP and collagen control gels were formed by injecting the gel solutions into 8-mm diameter silicone molds (666305, Grace Bio-Labs), using 21 G needles (305129, BD), between two glass slides and thermally cross-linked at 37 °C for 45 minutes. The gels were then allowed to soak in 1X PBS for 30 minutes to become fully hydrated. An initial amplitude sweep was conducted to determine the limiting strain value of the linear viscoelastic region by measuring a shear strain range from 0.001-1% with 20 data points, angular frequency of 6.21 Hz, and the reading from 0.1 to 100 rad/s. Following the amplitude sweep, a frequency sweep from 0.1-100 rad/s at 0.01% strain, 20 data points were conducted on each gel at 37 °C in a humidity bath. Collagen gels with a concentration of 2.5 mg/mL were used as controls. A dynamic shear modulus of G* = 17 kPa and tan δ = 0.3 at 1 rad/s were used as mildly degenerate human NP rheological values and G* = 7.4 kPa and tan δ = 0.4 at 1 rad/s was used as healthy human NP rheological values [77, 78]. G* was calculated as $G* = \sqrt{G'^2 + G''^2}$ and tanδ = G"/G' where G' = storage modulus and G" = loss modulus. N = 8 collagen control experimental replicates and 3 regelled NP groups, each with 6 replicates, for a total of 18 regelled NP samples.

2.2.3.3 Scanning electron microscopy

SEM was performed to assess formation of collagen fibers after NP digestion and re-gelation. Fixed control NPs, decellularized NPs, collagen only gels and regelled NPs were processed for SEM using a graded dehydration method. Samples were dehydrated in increasing concentrations of ethanol (30%, 50%, 70%, 85%, 90%, 95%, and 100% in ultrapure water) for 15 minutes each at room temperature. Following this, the samples were

incubated in increasing percentages of hexamethyldisilazane (HMDS) (16700, Electron Microscopy Services) (25%, 50%, 75%, and 100% in ethanol) for 30 minutes each at room temperature in a fume hood. Finally, the samples were submerged in 100% HMDS overnight in a fume hood until the HMDS had completely evaporated. The dehydrated samples were secured to a pin stub mount using conductive tape and sputter coated in platinum/palladium (Pt/Pd) for 20 seconds (106 Autosputter Coater, Cressington). The coated samples were then imaged using a FEI Helios FIB/SEM 660 at a voltage of 5-10 kV, current of 0.2 nA, 3 µs dwell time using secondary electron mode and Everhart-Thornley detector unless a through lens detector was needed for finer resolution at higher magnifications. ImageJ was used to quantify the fiber diameter by drawing a line across each distinguishable fiber and measuring the distance of the line. A total of n = 3 different samples were characterized and at least 3 images per sample were analyzed for each group at 100,000X magnification to quantify fiber diameter.

2.2.4 Culture and Analysis of NP Cells with Regelled NP
2.2.4.1 NP cell culture

Human NP cells (4800, ScienCell) were cultured in a T75 flask (CLS430641U, Sigma Aldrich) coated with 15 µg of Poly-L-Lysine (0413, ScienCell). NP cells were cultured in Complete Nucleus Pulposus Cell Media (4801, ScienCell), which was changed every two to three days. The NP cells were grown to confluency in hypoxia (3.5% oxygen, 10% CO_2, 86.5% N_2) in a modular incubator chamber (MIC-101, Billups-Rothenberg) at 37 °C before being used. NP cells from passages 2 and 3 were used in the following experiments to negate the effects of dedifferentiation. These cells were acquired from a single, fetal donor and the identity of the cells was verified by the company through immunofluorescence with antibodies for fibronectin and vimentin (ScienCell).

2.2.4.2 3D cell culture within regelled NP or collagen control gels

NP cells were added to non-crosslinked regelled NP or collagen control solutions to attain a cell concentration of 2 million cells/mL. 30 µL of the gel and cell suspension was transferred to a sheet of parafilm to prevent sticking, then placed in the incubator at 37 °C for 40 minutes to crosslink before being transferred individually to 48-well plates. 400 µL of complete NP cell media was added to each well. Media was replaced every 2-3 days over the course of 7 days.

An alamarBlue metabolic assay (88951, Thermo Fisher Scientific) was conducted on days 0, 1, 3, and 7 after initiation of culture to determine cell health. The alamarBlue assay measures the metabolic activity of cells by reducing resazurin in the electron transport chain to resoruflin. This reduction causes a change in color from blue to purple/pink that can be measured. Cells that are more metabolically active will reduce resazurin at a faster rate than less metabolically active cells, leading to a greater color change. At the desired time point, alamarBlue reagent was added to each well at a 1:10 ratio and the plates were incubated at 37 °C in hypoxia for 3 hours. 200 µL of media from each well was moved in duplicate to a 96 well plate. The wells were then rinsed with 1X PBS before adding 400 µL of complete NP media and placing the plates back in the incubator under hypoxia. The absorbance of the removed media was analyzed using a microplate reader at 570 and 600 nm. The reduction of alamarBlue was calculated according to manufacturer's instructions following equation 2. The reduction was then normalized to the DNA content of the respective wells, following the conclusion of the experiment. Gels were then frozen in water at -80 °C at respective time points for sGAG, collagen, and DNA assays. A total of n = 6 experimental replicates from each preparation,

with the collagen having 1 preparation and the regelled NP having three different preparations for a total of 6 collagen and 18 regelled NP.

$$2) \quad \% \; Reduction = \frac{(E_{oxi}600 \; x \; A_{570}) - (E_{oxi}570 \; x \; A_{600}) \; x \; 100}{(E_{red}570 \; x \; C_{600}) - (E_{red}600 \; x \; C_{570})}$$

$E_{oxi}570$ = molar extinction coefficient (E) of oxidized alamarBlue reagent at 570 nm = 80586

$E_{oxi}600$ = E of oxidized alamarBlue reagent at 600 nm = 117216

A_{570} = absorbance of test wells at 570 nm

A_{600} = absorbance of test wells at 600 nm

$E_{red}570$ = E of reduced alamarBlue reagent at 570 nm = 155677

$E_{red}600$ = E of reduced alamarBlue reagent at 600 nm = 14652

C_{570} = absorbance of negative control well (media, alamarBlue reagent, no cells) at 570 nm

C_{600} = absorbance of negative control well (media, alamarBlue reagent, no cells) at 600 nm

At study end, all gels were lyophilized overnight. Due to the small masses remaining following lyophilization, the mass could not accurately be determined for normalization. Instead, the data were normalized to each gel, which was a known volume of solution. Three gels from each time point and group were digested in 1 mL of 16 U/mL papain (see above) overnight at 65 °C. sGAG, DNA, and hydroxyproline assays were conducted as described previously in the "Validation of Whole Disc Decellularization Methods" section. A total of n = 3 experimental replicates from each preparation, with the collagen having 1 preparation and the regelled NP having three different preparations for a total of 3 collagen and 9 regelled NP samples.

2.2.5 Evaluation of Neuroinhibitory Properties of Regelled NP
2.2.5.1 Dorsal root ganglia explant isolation process

Studies using primary rat dorsal root ganglia explant culture tested the neuroinhibitory properties of the regelled NP. DRGs are located close to the disc and can

sprout pain-sensing neurons into degenerate disc, leading to pain, thus they are an ideal model cell type to validate neuroinhibition in vitro [4]. All animal experiments were conducted in accordance with the Guide for the Care and Use of Laboratory Animals and approved through the University of Nebraska-Lincoln's Institutional Animal Care and Use Committee (IACUC). Adult male Sprague Dawley rats (CD Rat 001, Charles River) aged 11-15 weeks were euthanized and L1-L6 DRGs were surgically removed and placed in cold trimming media: Neurobasal-A media (10888022, Thermo Fisher Scientific) with 10% Fetal Bovine Serum (FBS) (26140079, Thermo Fisher Scientific), 1% GlutaMax (35050061, Thermo Fisher Scientific), 1% Penicillin/Streptomycin (15140122, Thermo Fisher Scientific) and 2% B-27^{TM} Plus Supplement (A3582801, Thermo Fisher Scientific). DRGs were transferred into a 60 mm petri dish with cold trimming media and excess tissue around the DRG was trimmed using surgical spring scissors under a stereo microscope (Stemi 508, ZEISS). Trimmed lumbar DRGs were divided into two or three equally sized pieces before culture.

2.2.5.2 Gel-within-gel fabrication and DRG explant culture

To accurately model the growth of DRG neurons into a degenerative disc in vitro, we utilized our previously established gel-within-gel 3D culture method to model the in vivo environment of the DRG and NP [79]. Cut DRGs were embedded and cultured in type I collagen outer hydrogel which surrounded an inner 'NP-like' gel. Inner gels consisted of either regelled NP or type I collagen. Collagen inner gels were used as a positive control due to its neuro-permissive properties [79, 80]. To prepare the model, regelled NP and collagen gels were prepared as previously described herein with a final collagen concentration of 3.6 mg/mL, to match the final regelled NP collagen concentration, which

equate to the summation of the added type I collagen (2.5 mg/mL), and the collagen from the digested tissue (1.1 mg/mL).

To form the inner gels, 100 µL of non-crosslinked collagen control or regelled NP were transferred into a 96 well plate with custom laser-cut plastic gel lifters and incubated for 60-90 minutes at 37 $^{\circ}$C, 5% CO_2. The inner gels were carefully lifted out and placed into a 48 well plate using the gel lifters. On ice, 150 µL of the prepared collagen outer gel was then pipetted to the outside of the inner gel, and a DRG explant was carefully embedded in the outer gel, close to the boundary between the two gels. The gel-within-gel was then incubated at 37 °C, 5% CO_2 for 1 hour to induce collagen gel crosslinking, prior to media addition. The DRGs were cultured in complete media: Neurobasal-A media with 10% FBS, 1% GlutaMax, 1% Penicillin/Streptomycin, 2% B-27^{TM} Plus Supplement and 0.05% Nerve Growth Factor (556NG100, Thermo Fisher Scientific) at 37 °C and 5% CO_2 for 15 days with half media changes every three days. Brightfield images were taken every 3 days starting on day 6 using a Cytation 1 Biotek, to acquire z-stack images of either 2x2 or 3x3 montages (depending on neurite length) encompassing the total neurite growth of all DRGs. This experiment was repeated three times with at least three inner gels per group. DRGs without any substantial neurite outgrowth in any direction after 15 days in vitro were excluded from this study.

2.2.5.3 Neuroinhibition analysis

A total of three experiments with 11 total collagen controls and 20 regelled NP gels were imaged and analyzed. On day 15, gels were fixed in 300 µL of 4% PFA for 1 hour at room temperature. DRGs were then washed 3 x 15 minutes with 1X PBS and stored in 1X PBS at 4 °C protected from light until immunostaining. Fixed DRGs in gels were stained

for neurofilament-H (NF-H). Briefly, the gels were permeabilized in 200 µL of blocking buffer (0.5% Triton X-100, 4% goat serum in 1X PBS) for 1 hour at room temperature. The blocking buffer was removed and 200 µL of primary antibodies against NF-H (mouse α-NF-H, Ab528399, DSHB) (1:500 in blocking buffer) were added to each well for 36 hours at 4 °C. The primary antibody was removed, and the gels were washed 3 x 4 hours in PBST (0.05% Tween 20 in 1x PBS) with mild agitation on a rocker plate at room temperature. Secondary antibody (α-mouse 488, ab150117, Abcam) (1:500 in blocking buffer) was added and incubated overnight at 4 °C, protected from light. The secondary antibody was removed, and the gels were washed 3 x 4 hours in PBST at room temperature, with mild agitation on a rocker plate, protected from light. The gels were stored in 1X PBS at 4 °C, protected from light until imaged. Following staining, the gels were imaged using a widefield fluorescence plate imager (Cytation 1, Biotek) at 488 nm to visualize the neurons. Representative images were taken on a ZEISS Confocal microscope LSM 800. Brightfield photos of the whole gel-within-gels were taken using a digital camera (EOS Rebel T6i, Canon) attached to a stereomicroscope (Stemi 508, Zeiss) to be used for drawing the boundaries between gels.

Using Adobe Photoshop CC 2019, the brightfield images were overlaid over the fluorescent images taken from the Cytation plate imager and gel boundaries were drawn. Gels without distinct boundaries were excluded from analysis. ImageJ software, Simple Neurite Tracer tool, and a modified Sholl analysis were used to quantify the: 1) maximum radial distance, 2) total distance travelled in the inner gel, 3) number of neurites extending within the inner gel at specific distances from the gel boundary, and 4) the number of neurites extending away from the inner gel at specific distances from the DRG body [79].

The maximum radial distance was determined by drawing a straight line the tip of the longest neurite to where it initially crosses the gel boundary. The maximum neurite length was determined by tracing the longest nerves using the simple neurite tracer tool up until the gel boundary. Only the largest values were used from each image for both the radial distance and neurite length. Sholl analysis has previously been used to determine the amount of neurite branching based on distance from the cell body [81, 82]. This method was modified here to represent distance from the boundary of the inner and outer gels, as well as the number of neurites growing away from the DRG body. Sholl analysis was able to determine the number of neurites at a given distance from the gel boundary. A total of n=3 experiments were conducted with at least 3 replicates per condition in each experiment.

2.2.6 Statistical Analyses

Statistical analysis was conducted using the GraphPad Prism 7.03 software. Statistical significance was determined in the DNA experiment on the decellularized tissue scaffold between the control and the treatments using an unpaired T-test with Welch's correction. Statistical significance was determined in the sGAG, collagen, α-gal, and SEM fiber diameter experiments using a one-way ANOVA with multiple comparisons with Tukey's post-hoc test. A two-way ANOVA with multiple comparisons between days (Sidak's post-hoc test) and within each treatment group (Tukey's post-hoc test) was used to determine significance for the DNA, sGAG, collagen and alamarBlue assays in the NP cell culture in gels. A two-way ANOVA with multiple comparisons between groups at the same time was used to determine significance for the gelation kinetics of the ionic strength experiment. In the neuroinhibition experiments, t-tests with Welch's correction were used for the maximum neurite length, maximum radial distance analyses, and distance of the

DRG from the boundary, while a two-way ANOVA with multiple comparisons and Sidak's post-hoc test was used for the Sholl analysis to determine significance. Significance was set as $p \leq 0.05$ for all analyses. Error bars for all graphs represent the standard deviation.

2.3 RESULTS

2.3.1 Development of an Injectable Decellularized Tissue Scaffold

2.3.1.1 Decellularization Process and Analysis

To analyze the efficacy of the NP decellularization process, the concentrations of DNA, sGAG, and collagen were determined. The PicoGreen assay demonstrated 99.0% reduction in DNA in the decellularized NP samples compared to the control NP tissue, with the decellularized NP samples having a normalized DNA content of 1.19 ± 0.94 ng DNA/mg tissue compared to 111.78 ± 5.18 ng/mg in the control NP, suggesting that native cells and antigens were successfully removed (**Fig. 3A**). The Blyscan assay demonstrated retention of 74.0% of sGAGs in the decellularized NP compared to the control NP samples, with control NP samples having sGAG content of 50.27 ± 5.40 µg/mg and the decellularized NP samples having 37.19 ± 5.27 µg/mg (**Fig. 3B**). The hydroxyproline assay results suggested that collagen took up a greater proportion of the total mass of the decellularized NP compared to control NP (227.3 ± 49.1 µg/mg decellularized NP vs 146.9 ± 54.7 control NP), however the decellularized and control NP were not significantly different from each other (**Fig. 3C**). Enrichment of collagen in decellularized NP compared to control NP was due to the removal of cells and other antigens thereby reducing the overall mass, while maintaining the amount of collagen in the tissue. The ratio of sGAG:hydroxyproline was calculated to be 10.16:1 in control tissue and 4.85:1 in decellularized NP.

Cytotoxicity of remaining chemicals after decellularization was tested using an alamarBlue assay to measure the metabolic activity of NP cells treated with eluted media from decellularized NP samples compared to control NP cells with normal growth media. Control NP cells exhibited a reduction of alamarBlue of $92.8 \pm 3.36\%$, whereas NP cells treated with eluted media had a reduction of alamarBlue of $80.28 \pm 9.30\%$, which are significantly different. When normalized to control, NP cells treated with eluted media had a metabolic activity of $86.5 \pm 10.0\%$ (**Fig 3D**). The eluted NP cells have a 14% reduction in metabolic activity, which is below the recommended value by ISO 10993:5 for cytotoxicity [83]. Cytotoxicity of the final regelled NP on DRG cultures was assessed below during neuroinhibition studies.
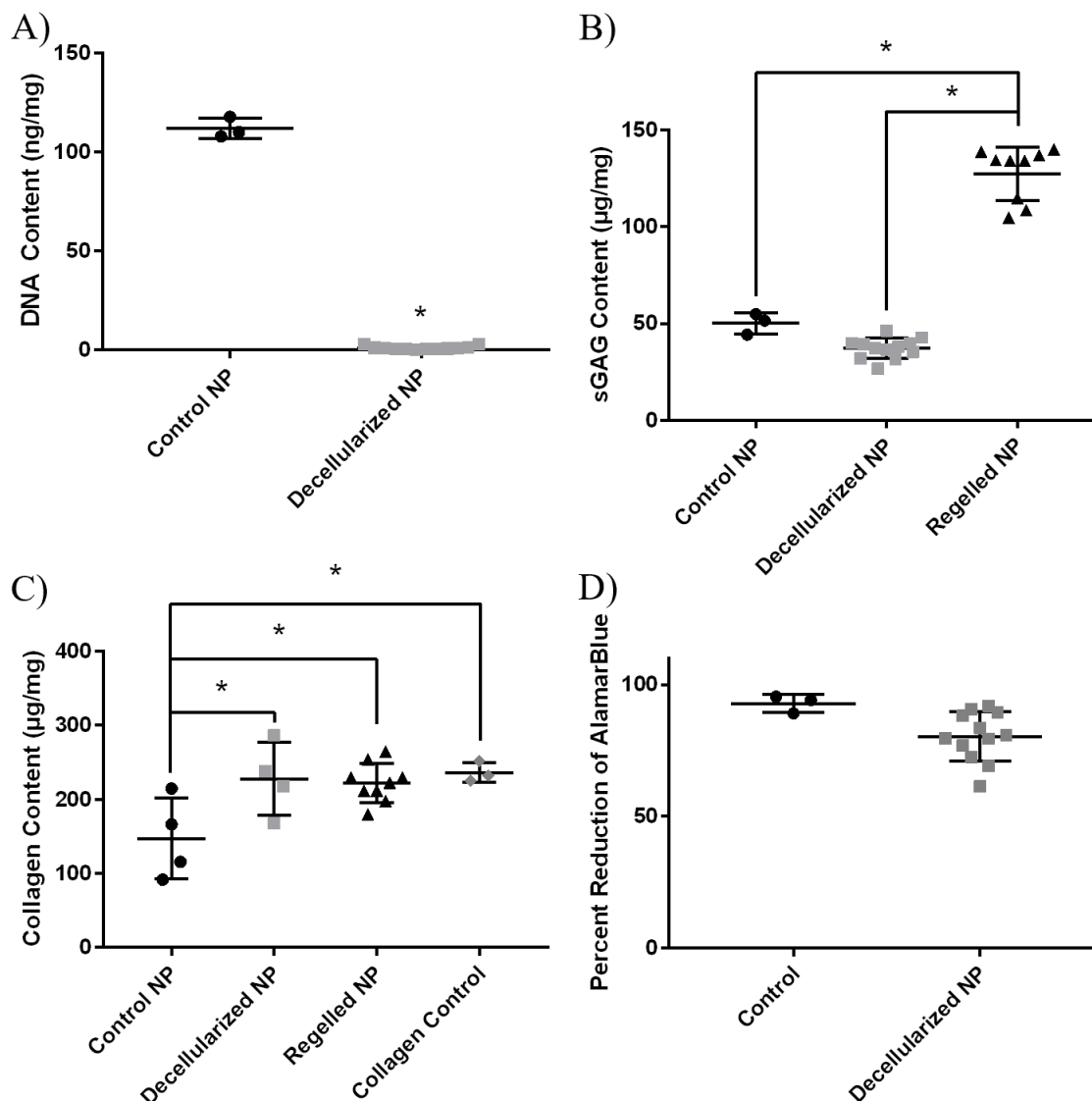
Figure 3. The decellularization process removes cells while maintaining extracellular matrix proteins. DNA (A), sGAG (B), and collagen (C) concentrations were compared before and after the decellularization process and after making into a gel. DNA was significantly reduced in the decellularized NP compared to control, while sGAG and collagen were maintained. D) Metabolic activity of NP cells treated with conditioned medium from decellularized NP tissue scaffold, normalized to untreated control shows a slight reduction to 86% of the control, which indicates minimal cytotoxic effects. *Indicates significant difference $p < 0.05$.

Following the characterization of the decellularization process, the concentration of an antigenic epitope was also investigated to ensure removal of antigenic materials. α-gal epitopes are an antigen that is present in porcine tissue, but not humans, so lack of removal can cause an immune response. Quantification of α-gal epitopes revealed very few

α- were present in either the control or decellularized NP samples. **Figure 4A-I** shows representative images of α-gal in muscle, control NP, and decellularized NP. Analysis of α-gal epitopes (**Fig. 4J**) revealed there was a significant reduction in the number of α-gal epitopes in the control NP samples and decellularized NP samples compared to the muscle tissue, but no difference between control and decellularized NP.

Figure 4. Control NP and decellularized NP contain negligible amounts of α-gal antigen. Representative individual channel images for α-gal epitope (green), cell nuclei (blue, DAPI), and phase channels in muscle (A-C), control NP (D-F), and decellularized NP (G-I). Red arrows indicate positive staining for the α-gal epitope. Comparison of number of epitopes normalized to

μm^2 in muscle, control NP, and decellularized NP (J). Both the control and decellularized NP had significantly fewer positive alpha gal epitopes compared to muscle. Scale bar = 200 μm. *Indicates significant difference $p < 0.05$.

2.3.1.2 Creation of Injectable Neuroinhibitory Gel

Ionic strength of a collagen solution plays a crucial role in how fibrils form. The effects of ionic strength were investigated on digested tissue, collagen only, and on digested tissue with collagen. **Figure 5A-D** demonstrates the average change in absorbance of digested tissue, collagen only, or digested tissue with collagen at 0.5X, 0.33X, 0.25X, or 0X DMEM concentrations, respectively. Digested tissue with collagen always tended to have a much greater change in absorbance than that of tissue alone or collagen alone, which suggests some form of interaction between the two that accounts for more than additive absorbances. Because 0.5X DMEM balanced the crosslinking of the collagen alone, as well as the tissue alone, which is necessary for integration of the two solutions together to form a cohesive gel, 0.5X DMEM was selected to be used for the final solution.
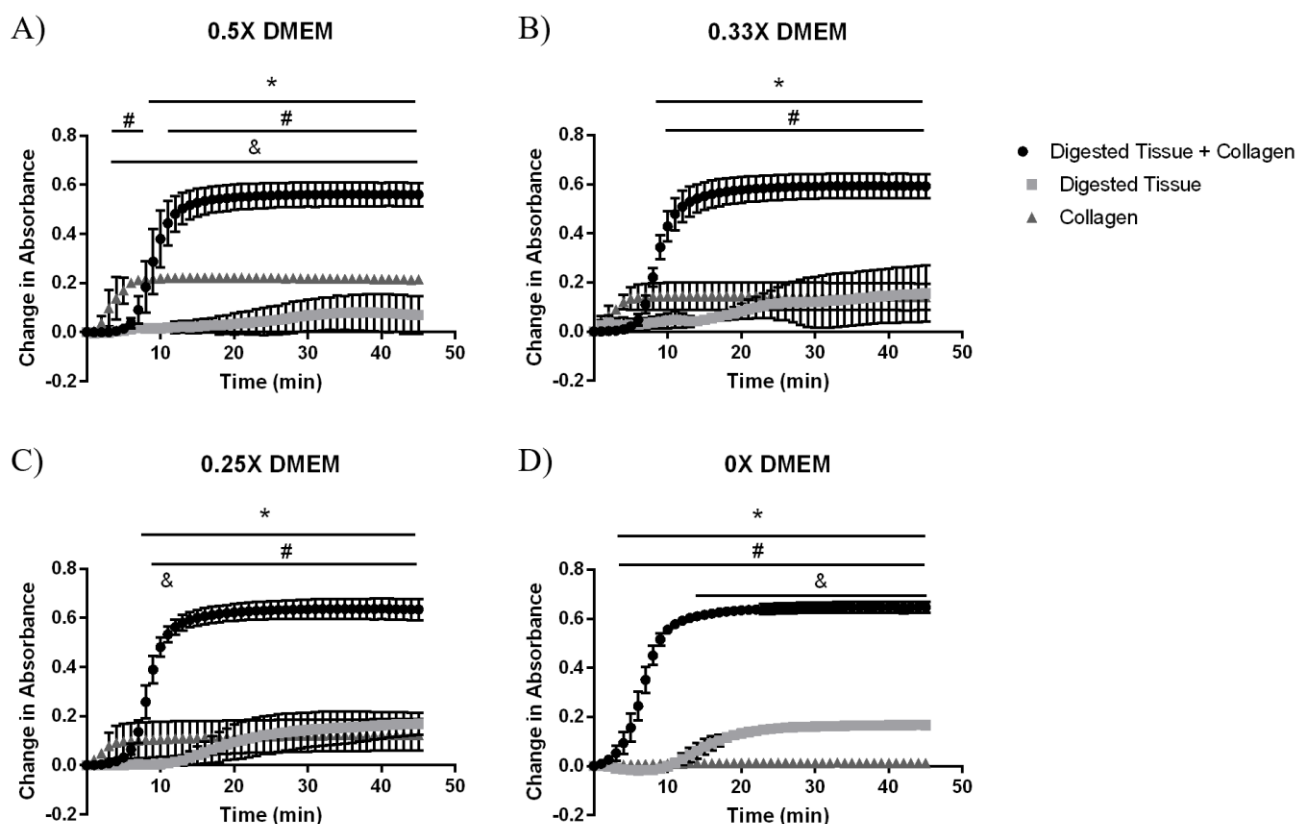
Figure 5. Ionic strength has opposite effects on collagen and digested tissue. Gelation kinetics graphs of digested tissue + collagen, digested tissue alone, and collagen alone at DMEM concentrations of A) 0.5X, B) 0.33X, C) 0.25X, D) 0X. * = significant difference between Digested Tissue + Collagen vs Digested Tissue, # = significant difference between Digested Tissue + Collagen vs Collagen, & = significant differences between Digested Tissue vs Collagen.

2.3.1.3 Characterization of the Physical Properties of the Regelled NP

Following optimization of the gelation solution, the next steps were to investigate

the strength of the gel and compare to native tissue. The gelation kinetics and mechanical

properties analysis focused on regelled NP with 0.5X DMEM and 2.5 mg/mL of added

collagen, to increase the robustness of the gel. The normalized gel absorbance was used to

determine the start and end of the gelation process. Collagen gels started and finished

forming before the regelled NP, starting at 3 minutes, and reaching 95% of its maximum

value after 12 minutes. The regelled NP started forming later at 8 minutes and reached 95%

of its maximum value after 17 minutes (**Fig. 6A** and **6B**). Results from rheological analysis

of the regelled NP and control collagen displayed a stable dynamic shear modulus (400-

530 Pa and 300-400 Pa respectively) and tan δ (0.4-0.7 for both regelled NP and collagen)

from 0.1 to 20 rad/s followed by an increase up to 100 rad/s where all samples had a

dynamic shear modulus of ~11,000-12,000 Pa and a tan δ of 0.72-1.4 for the regelled NP

and 17,500 Pa and a tan δ of 0.63 for the collagen (**Fig. 6D**). In comparison, human NP

ranges in dynamic shear modulus from 7.4-19.8 kPa and tan δ of 0.424-0.577 [77, 78, 84].
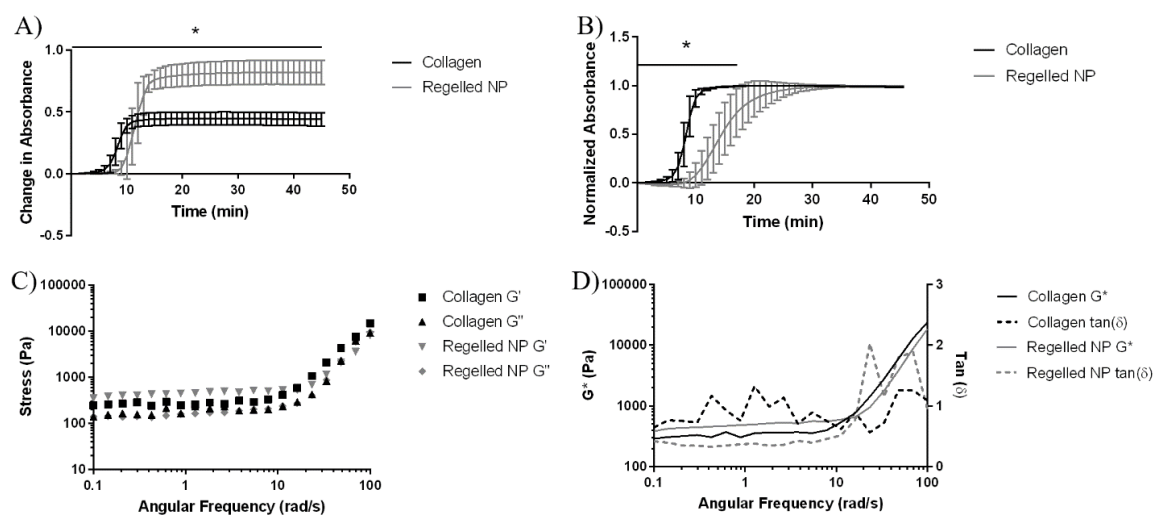

Figure 6. Gelation and mechanical properties of the regelled NP compared to collagen controls. A) The change in absorbance measured over time of collagen and regelled NP demonstrate a large and significant difference, suggesting that the regelled NP becomes more opaque than collagen. B) The normalized absorbance of the gels suggests that collagen only reaches its maximum value much sooner than the regelled NP. C) Rheology comparing the storage (G') and loss (G") moduli between collagen and regelled NP, suggests that regelled NP is weaker than collagen. There were no significant differences between the G" of either group but the G' of collagen was significantly different than that of regelled NP at 69.5 and 100 rad/s. D) Rheology comparing the dynamic shear modulus (G*) and tan(δ) of collagen and regelled NP suggest that regelled NP is weaker than collagen. G* of collagen was significantly different from that of regelled NP at 69.5 and 100 rad/s, while tan(δ) was significantly different at 23.4 rad/s. Error bars were omitted from C and D to improve clarity.

After discovering that the mechanical properties of the regelled NP were similar to

collagen, but low compared to native NP tissue, the microstructure of the regelled NP was

investigated to determine if there were any significant differences that could cause the difference in mechanical properties. SEM imaging revealed that collagen gels tended to have smaller, less organized fibers, compared to native tissue, decellularized NP tissue, and regelled NP, whereas control NP tissue had thicker, more dense collagen fibers, as well as cell debris covering much of the fiber surface (**Fig. 7A-H**). Decellularized NP had a looser fiber network, and the fibers were not as entangled compared to the other gels. The final regelled NP had thick fibers, similar to control NP, although fibers were less dense, more similar to decellularized NP. The diameters of the fibers were quantified for each group and were found to have no significant differences between any group, although regelled NP tended to have slightly thicker fibers compared to the other groups (**Fig. 7I**).
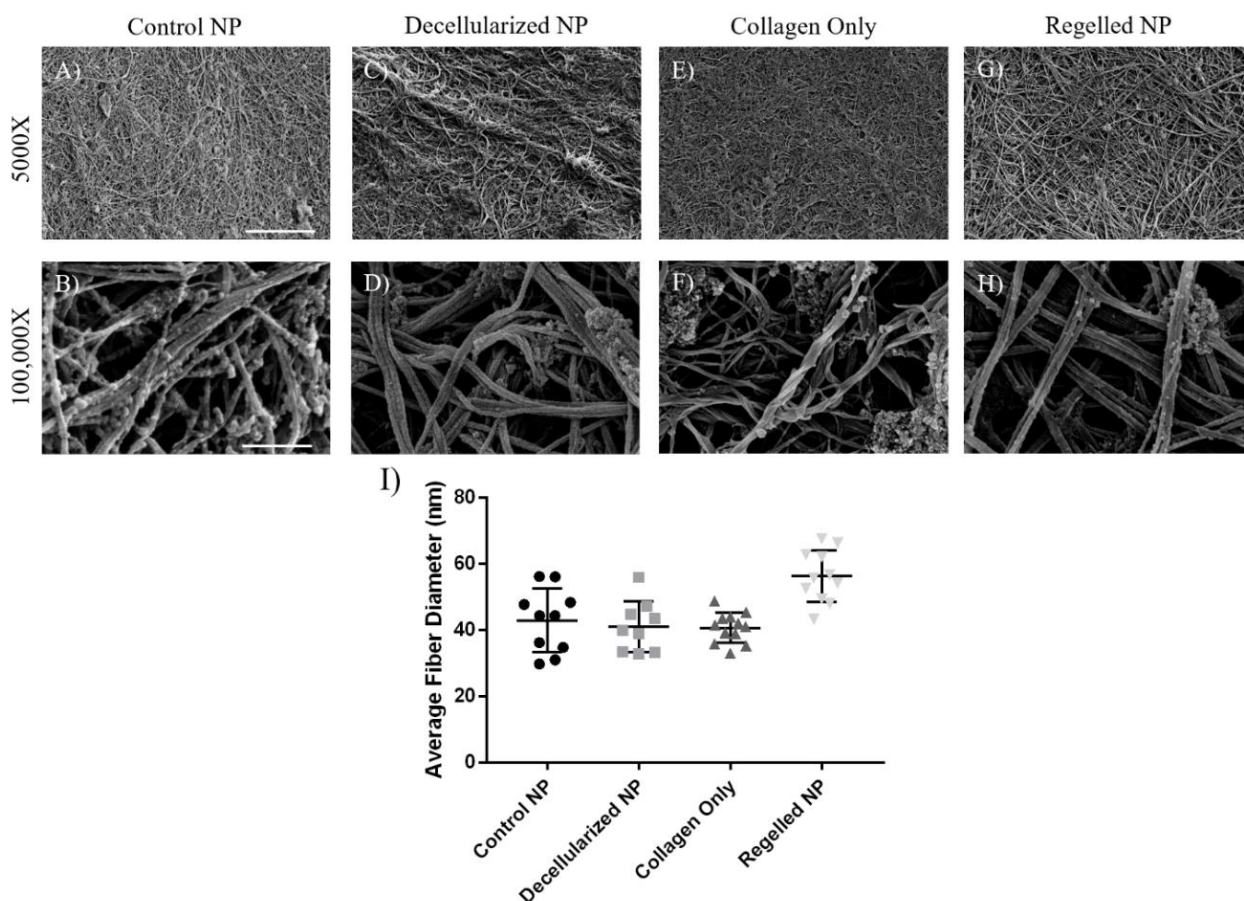
Figure 7. Scanning electron microscope images show similar fiber thickness between control NP (A, B), decellularized NP (C, D), collagen only (E, F), and regelled NP (G, H). Quantification of fiber diameter between groups. There were no significant differences between any group (I). Scale bar = 10 µm for 5000X and 0.5 µm for 100,000X.

2.3.1.4 Culture and Analysis of NP Cells with Regelled NP

Following the investigation of the physical properties of the regelled NP, the effects of the regelled NP was investigated on NP cells in order to verify that it could sustain native cell growth over time. Human NP cells were cultured in the regelled NP gels and DNA was measured to indicate whether cells proliferated over time while cultured within the gels. Regelled NP exhibited significant increases in DNA on days 3 and 7 compared to day 0, while the collagen group was significantly lower than the regelled NP group on day 3

(**Fig. 8A**). Increasing DNA indicated the gels do not inhibit cell proliferation. Normalized alamarBlue results showed that metabolic activity of human NP cells on day 7 cultured in regelled NP was significantly higher than every other day of that same gel (**Fig. 8B**). Normalized metabolic activity for day 7 regelled NP was also significantly greater than the day 7 collagen (**Fig. 8B**). The results of sGAG quantification reveal that regelled NP samples have a large amount of sGAG at day 0, which reduced over the first 3 days and subsequently starts to slowly increase over time, although not significantly (**Fig. 8C**). The control collagen gels have low sGAG that gradually increased over time, although not significantly. The hydroxyproline assay demonstrated a significant but minor decrease between days 0 and 1 in the regelled NP group, but there were no other differences within either group over the time course (**Fig. 8D**). The collagen group was significantly lower than the regelled NP group at each time point, but also did not exhibit any differences over the time course. These data demonstrate a constant collagen content over the 7-day time course for both samples. The sGAG:hydroxyproline ratio on day 0 was 4.25:1 and reduced to 0.162:1 by day 7.
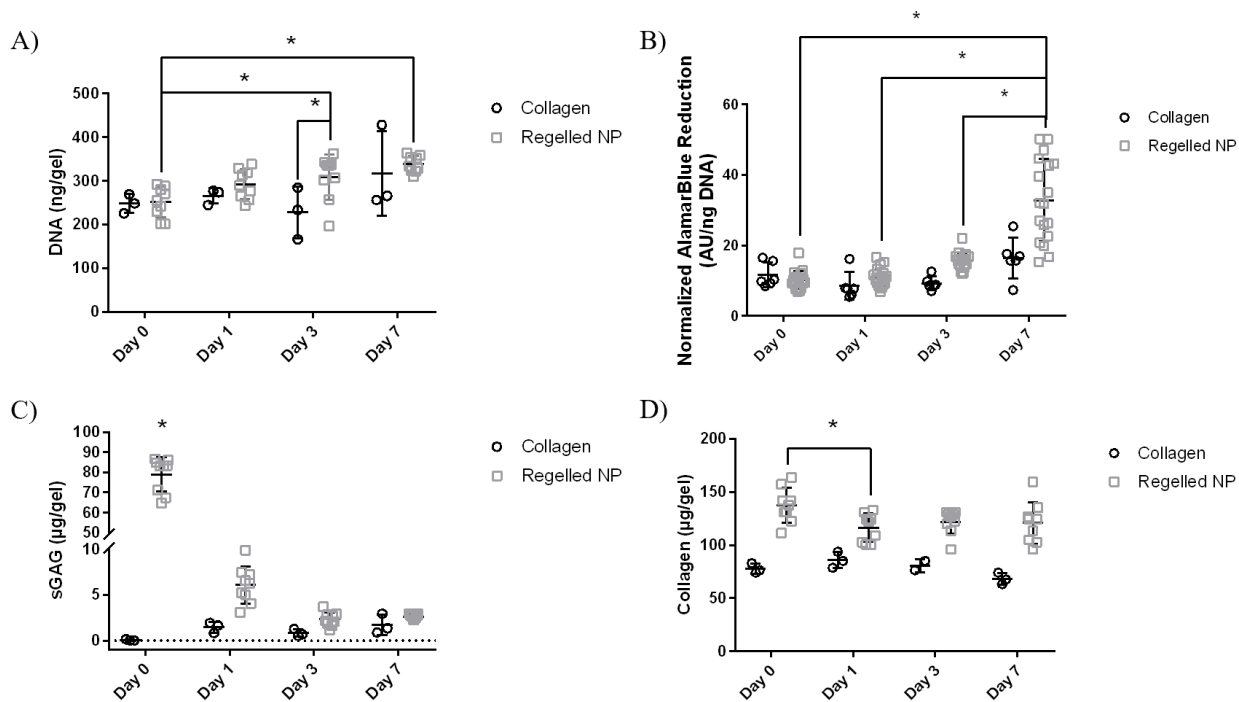
Figure 8. NP cells remain viable in regelled NP gels over 7 days and become more active compared to collagen. PicoGreen DNA results (A) demonstrated an increase from day 0 to day 7 in the regelled NP groups, while collagen on day 3 was decreased. AlamarBlue (B) showed a significant increase in metabolic activity of each group of gels normalized to DNA on day 7 in the regelled NP gels to all other time points. The regelled NP groups were also significantly greater than the collagen group on day 7. The sGAG quantification (C) revealed a significant decrease in the regelled NP groups from day 0 to the following days, however all groups appeared to increase in sGAG from day 3 to day 7, although not significant. Quantification of collagen content (D) was stable over time in both groups, with only day 0 and day 1 in the regelled NP group being significantly different. The collagen control group was significantly lower than the regelled NP at each time point. *Indicates significant difference $p < 0.05$.

2.3.1.5 Evaluation of Neuroinhibitory Properties of Regelled NP

To prevent pain, the regelled NP must exhibit neuroinhibitory properties, to be able to prevent nerve growth in the clinic. DRG neuroinhibition results demonstrated a significant reduction in number and distance of neurites growing into regelled NP compared to collagen controls. **Figure 9** shows representative images of DRGs cultured in the gel-within-gel model on day 15, with fluorescent staining of the neurites with NF-H. **Figure 10A and 10B** show representative images of the neurite length analysis. Maximum

neurite length in the inner gels was lower in regelled NP compared to collagen controls (1201.1$\pm$258.3 µm vs.1763.9$\pm$407.5 µm) although this difference was not significant (**Fig. 10C**). **Figure 10D and 10E** show representative images of the radial distance. Analysis revealed there was a significant reduction in the maximum radial distance, or the linear distance from the neurite crossing the boundary to the tip, of neurites in regelled NP samples compared to collagen controls (975.9$\pm$41.64 µm vs. 1601.3$\pm$381.1 µm) (**Fig. 10F**). **Figure 10G and 10H** show representative images of the Sholl analysis, which found that there were significantly fewer neurons in the regelled NP compared to collagen at all distances up to 700 µm away from the gel boundary, except at 600 µm (**Fig. 10I**). The second Sholl analysis demonstrated no significant differences in the number of neurites between collagen or regelled NP at any distance on the opposite side of the inner gel. The average distance of the DRGs from the boundary of each group were also calculated as 278.4$\pm$118.3 µm for collagen and 244$\pm$140.9 for regelled NP µm. These distances were not significantly different from each other. These data indicate that any residuals left in the regelled NP are not cytotoxic to neurons and their support cells in culture. Taken together, these data demonstrate the regelled NP has robust neuroinhibitory properties compared to collagen controls.
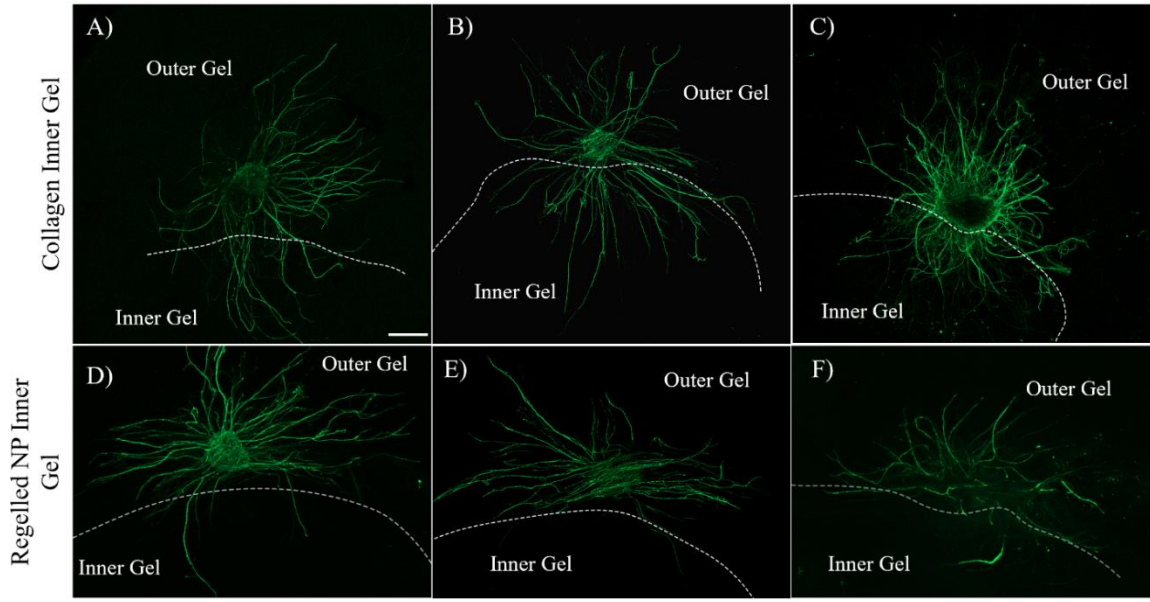
Figure 9. DRGs show reduced growth and altered morphology into the inner gel in regelled NP compared to collagen. Representative maximum projection confocal images of day 15 DRGs in regelled NP gels (D-F) and collagen gels (A-C). Scale bar = 500 µm.
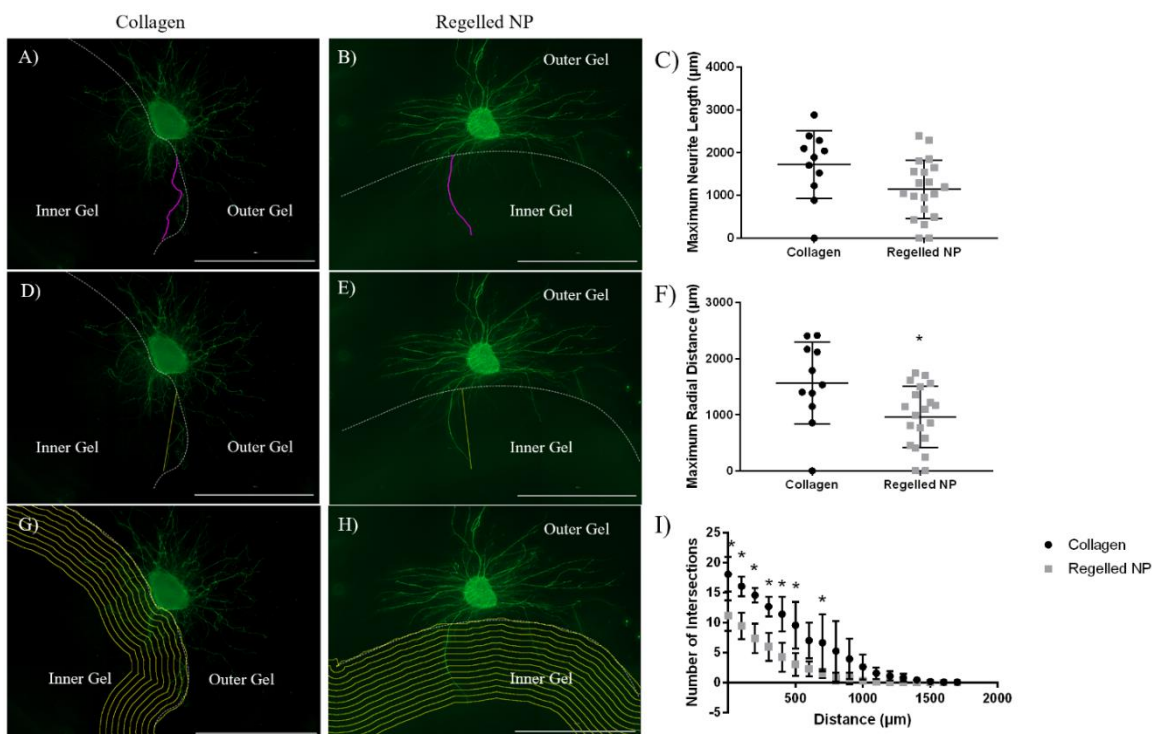
Figure 10. Neurite growth into regelled NP inner gels is significantly inhibited compared to collagen inner gels. Representative images (A,B) and analysis (C) for maximum neurite length into the inner gels. Representative images (D, E) and analysis (F) for maximum radial distance into the inner gels. Representative images of Sholl analysis (G,H) and quantification of the number of neurons at specific distances into the inner gel (I). Graphs C and F show the average and standard deviation of the gels individually to show the scattering of the individual points. Scale bar = 2000 μm. *Indicates significant difference p < 0.05.

2.4 DISCUSSION

Previous publications have developed NP decellularization methods with varying success in the removal of DNA and maintenance of extracellular matrix proteins [38-43, 85]. Some of these decellularization techniques have demonstrated high maintenance of glycosaminoglycans, key components of the NP that help to maintain osmotic pressure, as well as provide the NP with neuroinhibitory properties, yet no literature has demonstrated maintenance of the neuroinhibitory properties of the decellularized NP tissue scaffold. In this study, we successfully optimized a semi-high throughput decellularization process for

whole porcine NP, created a thermally gelling hydrogel from the decellularized NP, and demonstrated the regelled NP maintains cell viability and prevents nerve growth.

Several studies have found that most painful, degenerate discs contain nerves, due to a loss in neuroinhibition [25-27]. Reintroducing a neuroinhibitory gel has the potential to stop further ingrowth of nerves and halt the progression of disc-associated LBP. To investigate the neuroinhibitory properties of our regelled NP, we used our in vitro model [79] of innervation that involves culturing whole DRGs in an outer gel and allows the nerves to grow into an inner gel. In this study, the inner gel was composed of either the regelled NP or a matched collagen control gel. These data demonstrated that regelled NP had robust neuroinhibitory properties as exhibited by greater than two times fewer neurites at almost all distances up to 800 µm within the inner gel by the Sholl analysis. There are several factors that contribute to neuroinhibition in the body. The first contributing factor to neuroinhibition is the stiffness of the material that the nerve is growing into [86]. Our rheology data indicate that regelled NP and collagen have similar mechanical properties, therefore, mechanics is likely not a major contributor to the neuroinhibition seen in the regelled NP compared to collagen. The next contributing factor to neuroinhibition is the porosity of the material [87]. A porosity of ~80% was shown to promote the greatest nerve density and length with these values decreasing at 70 and 90% in a rat hemisection lesion [87]. SEM analysis revealed no significant difference in fiber diameter or fiber density between control NP, decellularized NP, collagen, and regelled NP. Although porosity cannot be calculated from SEM images, macroscopic evaluation of fibers and void space suggests similar fiber density and thus, likely similar porosity between all groups. Another factor contributing to neuroinhibition is the presence of neuroinhibitory molecules in the

material. Some common neuroinhibitory molecules include aggrecan, a proteoglycan present in the NP, chondroitin-6-sulfate, a major sGAG found on proteoglycans in the NP, and semaphorin3A, an axon guidance molecule in the nervous system [23, 24, 88]. While aggrecan and chondroitin-6-sulfate have been found in large quantities in the NP, semaphorin3A is demonstrated more in the outer annulus fibrosus with ~80% of cells expressing it, with a decreasing concentration into the NP, with only ~5% of cells expressing it [88]. We believe that our regelled NP likely contains more sGAGs and semaphorin 3A than collagen controls which may contribute to the neuroinhibitory properties. However, additional studies are needed to validate this claim.

When using decellularized tissue scaffolds, the removal of cellular DNA is crucial to the decellularization process to prevent an immune response when applied *in vivo*. It is speculated that during degeneration, there is infiltration of immune cells, which can recognize foreign cellular components and cause a host to reject the implanted material [89]. Thus, our removal of more than 99% of the original DNA from the tissue, as an indicator for cells, increases the chances of a host accepting the decellularized tissue scaffold. Due to the high removal of DNA and lack of alpha-gal found within the decellularized NP, it is unlikely that this tissue scaffold would cause an immune response due to species differences when implanted in a host. Porcine tissue has had clinical success previously with dermis (Fortiva, RTI Surgical, Inc.) and small intestinal submucosa (SIS, Cook Biotech), suggesting that porcine NP may also be implanted without problem after decellularization. Besides DNA removal, the other important aspect of decellularization is maintenance of native proteins. In the NP, the majority of the extracellular matrix is composed of sGAGs and type II collagen [90, 91]. The decellularization process used here

attempted to maintain as much of the native sGAGs and collagen as possible, to maintain the neuroinhibitory and structural capabilities of the tissue scaffold. Here, the sGAG maintenance was 74.0%, comparable to other NP decellularization processes which have a range of retentions between 55-97% [1, 38-44]. The normalized sGAG values presented here of 50.27 ± 5.40 µg/mg and 37.19 ± 5.27 µg/mg for control and decellularized NP, respectively, are generally lower than what has been determined in other work, which range from ~20 µg/mg to ~500 µg/mg in porcine NP [1, 38-44]. The large difference in sGAG across literature may be due to differences in species, animal age, and disc level. A common comparison used in NP decellularization is the ratio of sGAG:hydroxyproline as this ratio is an easy way to tell the amount of functional proteins compared to structural proteins found within the tissue scaffold. Here, this ratio was 10.16:1 in control tissue, 4.85:1 in decellularized NP, and 4.25:1 in the regelled NP. In comparison, the ratio of sGAG:hydroxyproline for healthy NP tissue is 27:1 [92], while other decellularized NP tissue scaffolds have been found at 21:1 [38], 2-4:1 [39], and ~8-20:1 [42]. These results suggest that the regelled NP is similar in the ratio of sGAG to collagen to decellularized NP tissue. Because the regelled NP is meant as a neuroinhibitory supplement, the sGAG:hydroxyproline ratio does not need to reach the levels of natural tissue. Further, our SEM images illustrated collagen fibers of similar orientation and thickness at each stage of the decellularization process, suggesting that our process retains the microstructure of a native NP.

Following decellularization, we were able to form digested NPs using an enzyme digestion process followed by collagen supplementation, which can then be injected through a small-bore needle and gel at 37 °C within 20 minutes to create the regelled NP.

The metabolic activity of the cells in the regelled NP increased over time compared to the collagen group, with a significant difference by day 7, suggesting that the cells in the regelled NP are more active compared to the collagen group. This may be due to the cells recognizing the decellularized tissue scaffold and acting on cues that the scaffold gives the cells, whereas the collagen gel would not have these same cues due to the lack of decellularized tissue. Similar phenomena have been demonstrated with pulmonary [93], preosteoblast [94], and kidney and mesenchymal stem cells [95] when cultured on decellularized porcine lung [93], tilapia skin [94], and porcine kidney tissues [95], with increases in metabolism by these cells when cultured on the decellularized tissue scaffolds. The increases in metabolic activity demonstrated in previous literature and in this thesis suggest that the cells recognize some aspect of the decellularized tissue and may act to remodel the tissue accordingly [95]. Increases in anabolic gene expression have also been demonstrated with stem cells cultured on decellularized NP tissue compared to controls lacking the decellularized tissue, which would suggest an increase in metabolism as well [42, 44]. In our study, the DNA assay showed a small but significant increase over time in the concentration of DNA in the regelled NP compared to collagen controls which suggests there was minimal cell death and the cells continued to proliferate over the course of the study. The significant increase in DNA in the regelled NP but not the collagen over 7 days suggests that some components in the decellularized NP are giving cues to the NP cells to proliferate, as the presence of decellularized tissue was the only difference between the two groups. Interestingly, there was a significant decrease in sGAG in the regelled NP observed from day 0 to 1. This may be due to diffusion of the sGAGs into the media due to the large surface area exposed to media in the 30 µL gels. Our re-gelled NPs cultured with sensory

neurons studies still exhibited robust neuroinhibitory properties, suggesting the resultant sGAG loss is either less in these larger gels, or the loss is not sufficient to reduce neuroinhibitory properties. Future work will examine the function of these scaffolds in vivo to verify the lack of an immune response as well as to probe the mechanism of neuroinhibition. In conjunction with the sGAGs, the levels of collagen were also investigated over time and showed few differences, with only days 0 and 1 in the regelled NP being significantly different. Between groups, the collagen and the regelled NP were significantly different at each time point, due to the collagen found naturally in the decellularized NP. Taken together, these results indicate that the regelled NP is not cytotoxic and may promote enhanced cell proliferation and remodeling compared to collagen gels, due to the increased metabolic activity of the cells in the regelled NP.

While the regelled NP has promise for preventing nerve growth in the disc, there are also some limitations. These include the regelled NPs low mechanical properties compared to human NP, which ranges in dynamic shear modulus from 7.4-19.8 kPa and tan δ of 0.424-0.577 [77, 78, 84], suggesting this material must be used in conjunction with native tissue to bear load. While these data suggest that the mechanical properties of the regelled NP are lower than native tissue, this is not a large limitation, because this gel is meant to act as a supplement to the NP, and not a total replacement. Another limitation of this research was the loss of sGAG from day 0 to day 1 in the regelled NP during the three-dimensional culture, which was most likely due to washing out of unbound sGAG during media changes due to diffusion; however, this did not seem to impact the neuroinhibition results. Another limitation of this work was that the regelled NP did not exhibit complete neuroinhibition, only partial, as some of the DRG neurites were still able to pass the inner

gel boundary. This feature will be investigated in the future by determining if neurites are traveling along the top or bottom of the gels instead of traveling through the gel. Supplementation of sGAG to the regelled NP may be possible to boost the regelled NP's neuroinhibitory properties. Future work that can be investigated include the effects of this gel on cultured stem cells and the gel's ability to differentiate stem cells towards a nucleus pulposus-like phenotype for NP regeneration, as well as the effects of LBP alleviation in vivo.

CHAPTER 3: Matrix Bound Nanovesicles

3.1 Review of Literature

3.1.1 Introduction to Matrix Bound Nanovesicles

Matrix Bound Nanovesicles (MBVs) are extracellular vesicles secreted by cells that are embedded within the extracellular matrix, instead of being secreted into the extracellular space, like exosomes or microvesicles. MBVs were recently discovered embedded within the extracellular matrix of urinary bladder matrix, small intestinal submucosa, dermis, brain, heart, muscle, ovary, pancreas, and tendon [68, 96-98]. Similar to microvesicles, MBVs range in size from 20-400 nm in diameter [96, 97, 99, 100], are secreted through blebbing of the plasma membrane [101-103], and contain various intravesicular proteins and micro RNA (miRNA), as well as lipids in the membrane [68, 96-99]. **Figure 11** demonstrates that MBVs are present in many different tissue types.
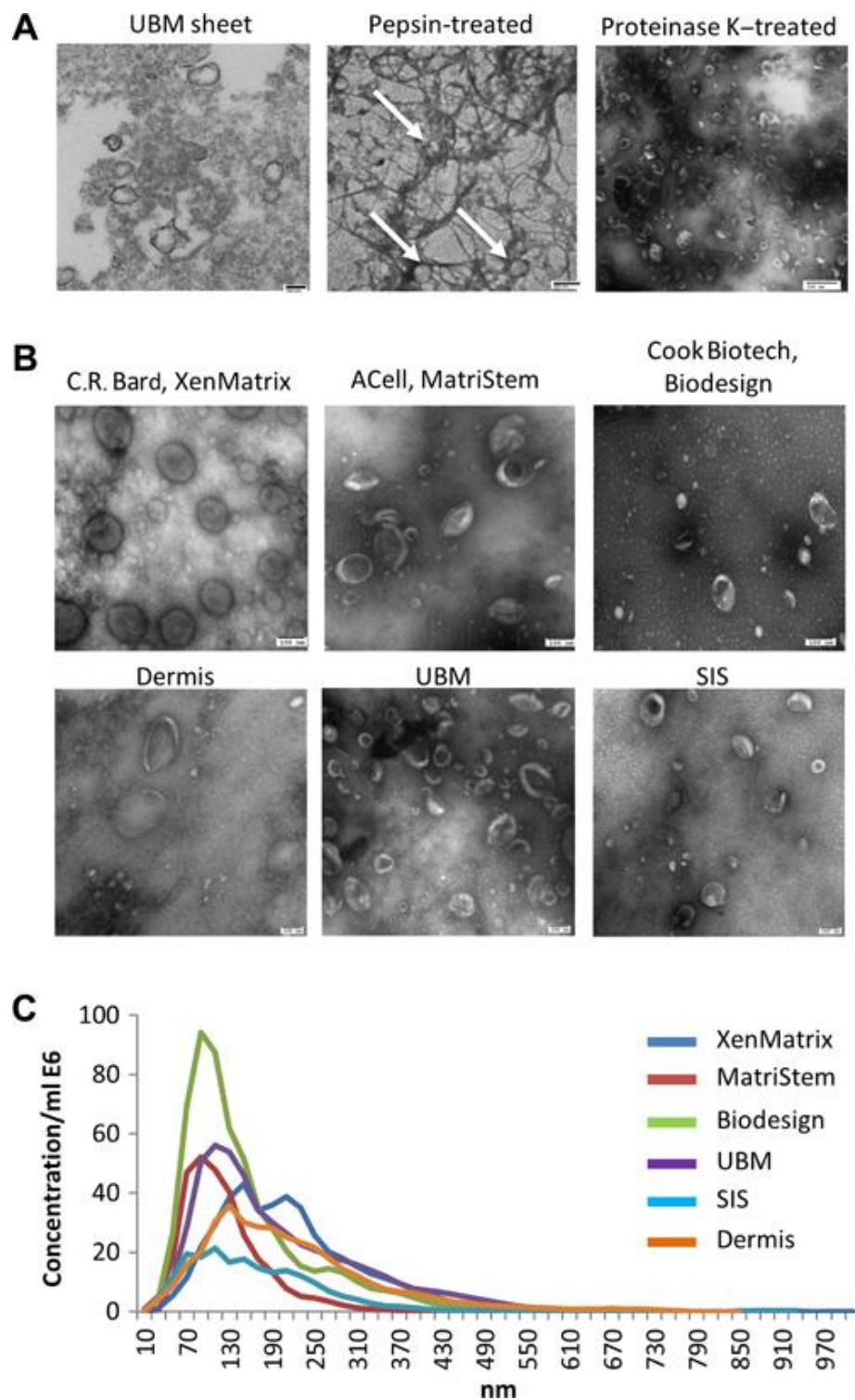
Figure 11. MBVs are present in many tissues. A) TEM images of MBVs in a urinary bladder matrix sheet either untreated, treated with pepsin, or treated with proteinase-K. B) TEM images of MBVs isolated from proteinase-K treated Xenmatrix, MatriStem, Biodesign, and decellularized porcine dermis, urinary bladder matrix, and small intestinal submucosa. C) Nanoparticle tracking analysis size data of MBVs isolated from various decellularized tissues [97].

Figure 12 demonstrates the difference in secretion and embedding between MBVs and some more common extracellular vesicles, exosomes and microvesicles. Previous research has shown that MBVs have immunomodulatory properties, specifically with macrophages [68, 69, 97]. It is possible that MBVs are contained within the decellularized NP tissue developed here and exhibit a tissue specific response. Thus, MBVs were investigated as part of this thesis as a possible mechanism of action for how the decellularized NP scaffolds interacted with macrophages and NP cells. Research from the first project demonstrated that NP cells remained viable within regelled NP and increased their metabolic activity, suggesting increased remodeling of the tissue, thus, the effect of MBVs derived from the decellularized NP tissue were investigated to determine if the MBVs within the regelled NP were a possible reason for this change. To research MBVs and understand the data that will be collected on them, it is important to consider how they are isolated, how they are characterized, what contents they may have, and how they interact with cells.
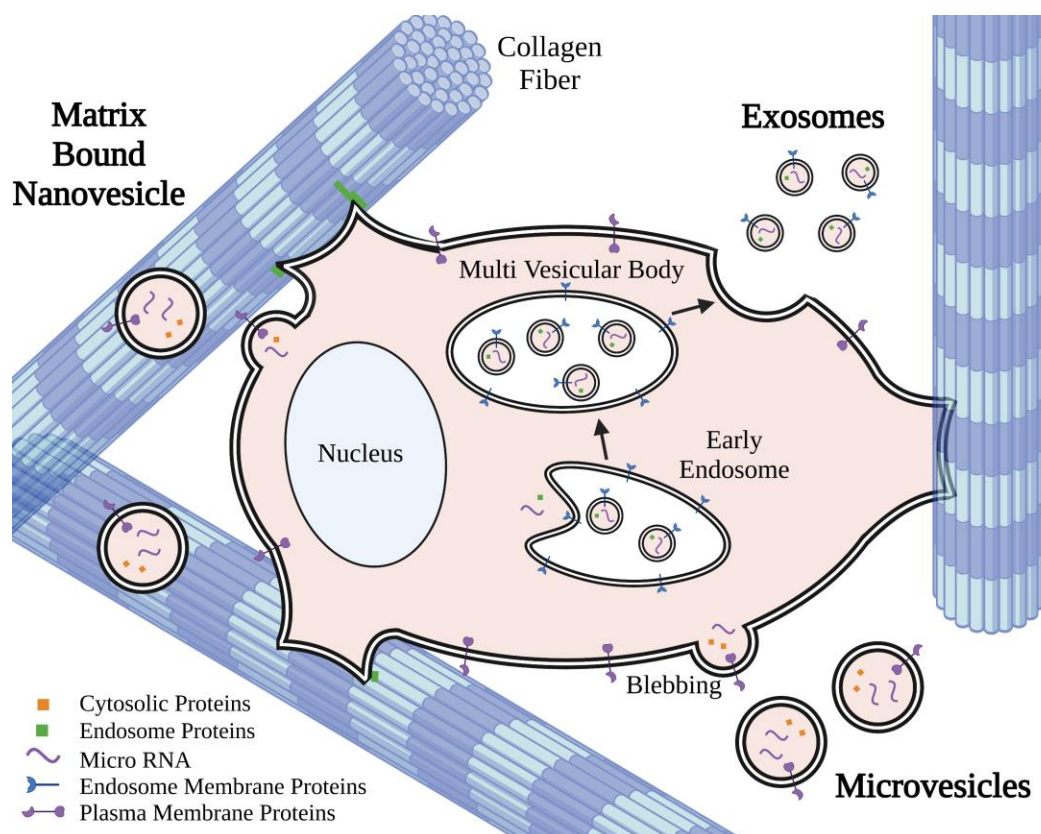
Figure 12. Different mechanisms of secretion of microvesicles, exosomes, and MBVs.

3.1.2 Isolation and Purification of MBVs from Tissue

Because MBVs are trapped within the extracellular matrix of tissues, as seen through transmission electron microscopy (TEM) and scanning electron microscopy (SEM) of whole decellularized tissues [96, 104], they are more difficult to isolate than other vesicles such as exosomes or microvesicles. The isolation process for MBVs involves the disruption and/or digestion of the surrounding tissue matrix [97]. However, disruption of the tissue can lead to large amounts of contaminating protein in solution with the MBVs that must be removed. Multiple isolation methods have been developed for similar vesicles like exosomes and can be adapted for MBVs. The methods that have had some success for MBV isolation so far include: 1) differential centrifugation, 2) tangential flow filtration, 3) size exclusion chromatography, and 4) density gradient centrifugation [99, 105]. All

methods to isolate EVs attempt to increase yield, or the number of EVs isolated, while trying to maintain high purity, or the ratio of the number of isolated EVs to the amount of contaminating protein. Different methods of digesting tissue can lead to varying yields due to the differences in how the tissue is digested, even when using the same isolation method, however, the yields still follow the same general trends as described below [99].

Differential centrifugation is generally considered the gold standard to isolate exosomes due to its simplicity and relative ease of use [106-110]. Differential centrifugation involves centrifuging a solution at increasing speeds to remove large contaminants, ending with a final centrifugation at greater than 100,000 x g, to pellet down the nanoscale vesicles [106, 107, 109-111]. While differential centrifugation is relatively easy to perform and is able to remove large contaminants, it requires a specialized ultracentrifuge and is unable to separate small vesicles from other small contaminants such as protein aggregates [105, 112]. This method of isolation generally has a high yield of particles but also a relatively high concentration of contaminating proteins [99]. Differential centrifugation is the most commonly used method to isolate MBVs at this time, although methods (or combinations of methods) that result in an increased purity may become more common [68, 69, 96, 97, 100, 113]. The current method that has been used to isolate MBVs from dermis, urinary bladder matrix, and small intestinal submucosa did so through digestion using collagenase, followed by centrifugation at 500 x g for 10 minutes, 2500 x g for 20 minutes, and 10,000 x g for 30 minutes, each repeated three times [97]. The supernatant was then centrifuged at 100,000 x g for 70 minutes and passed through a 0.22 µm filter [97]. Investigation into the presence of RNA and the effects on cells demonstrated that the MBVs were biologically active and could modulate the cell

phenotype [97]. While this process has been adapted slightly over time, it still remains very similar to this process.

Density gradient centrifugation is similar to differential centrifugation except that the final ultracentrifugation involves the use of a density gradient, often sucrose based, to further separate out particles. Because vesicles have a different density than contaminating protein, they should be found in different locations in the density gradient [105, 112]. This process involves the use of an ultracentrifuge, as well as a density gradient solution, to better purify the isolated EVs compared to just differential centrifugation, usually at the cost of yield [105, 112]. Density gradient centrifugation was first developed for exosomes, where it had slightly worse yield than differential centrifugation and tangential flow filtration but higher purity than these two methods [107, 114-116]. This method was also used to isolate urinary bladder matrix MBVs and tended to have worse yield than differential centrifugation, ultrafiltration, and size exclusion chromatography [99]. Along the same lines, this method tended to have higher purity compared to the other three isolation methods [99].

Tangential flow filtration is another method used to isolate exosomes that could be applied to MBVs. During tangential flow filtration, a solution is passed across a filter and anything smaller than the pore size of the filter is allowed to pass through. This method of isolation has been performed with exosomes with good yield, however, the purity of the sample remains low [117-119]. Tangential flow filtration is easy to perform, is easily scalable from small volumes such as single milliliters up to large volumes such as several liters and is relatively fast. The drawbacks to using tangential flow filtration are that it traditionally requires a specialized system to perform, although smaller tube and

centrifuge-based systems have been developed, such as the Corning Spin-X tubes (431482). Tangential flow filtration has the same problem as differential centrifugation in that it separates particles non-specifically and thus has problems with protein contamination [120, 121]. This method of isolation has been used previously with MBVs from urinary bladder matrix, which showed a high MBV yield but had the largest concentration of contaminating protein out of all methods tested, which is similar to results from exosome isolations [99, 118].

Size exclusion chromatography is a method often used by biologists and chemists to separate molecules or particles based on size and has been used to isolate exosomes as well. To perform size exclusion chromatography, a solution is passed through a column of beads and depending on the size of the particle being isolated, the particles will pass through the column at different speeds and thus fractions of the elute can be collected. Size exclusion chromatography is becoming more widely used to isolate small vesicles due to its availability, relative ease of use, and the great purity of isolated vesicles compared to other methods [120, 121]. Previous literature isolating exosomes with size exclusion chromatography has demonstrated excellent results in terms of purity, but low yields of particles [106, 111, 122, 123]. Some downsides of size exclusion chromatography are that it has low flow through and that it is difficult to control the electrostatic and hydrophobic interactions that occur, which can cause the isolation to become less pure [122, 124]. Size exclusion chromatography has been previously used to isolate urinary bladder matrix MBVs, followed by ultrafiltration to concentrate the MBVs [99]. The combination of size exclusion chromatography and filtration methods had a lower yield compared to the other

methods, except density gradient centrifugation, although it had the second lowest concentration of contaminating proteins, causing it to be pure [99].

There have been other studies comparing methods of isolation in other vesicles to try to determine the best method for MBV isolation, although there is no current consensus [125-128]. The best method to isolate MBVs may be tissue dependent, due to the different methods needed to digest tissues, and may involve the use of two methods together. Previous work has combined differential centrifugation, tangential flow filtration, and size exclusion chromatography to isolate exosomes from blood plasma, which demonstrated a very low amount of contaminating protein, coupled with a moderate particle yield compared to each isolation method alone [129]. Preliminary work in our lab on decellularized nucleus pulposus tissue has demonstrated that differential centrifugation followed by tangential flow filtration results in a concentrated solution of MBVs that appears to be relatively pure as well. More research in this area needs to be performed to determine the best methods or combination of methods to isolate MBVs with high yield and purity.

3.1.3 Characterization of MBV Size

Characterization of MBV size is important to verify the presence and quantity of MBVs, and to separate them from other EVs. Due to the similar sizes and compositions of exosomes and MBVs, the characterization methods often used for exosomes can also be used for MBVs.

Often, the first way to characterize EVs is to measure their size. For EVs these methods often include: TEM or SEM to visualize the size and morphology of the EVs, as well as staining to verify presence of lipids in the membrane [130, 131] and nanoparticle

tracking analysis, to determine the size and concentration [130, 132]. Some other, less often used methods to characterize size of EVs include dynamic light scattering, atomic force microscopy, tunable resistive pulse sensing, and flow cytometry, although special techniques need to be used such as aggregating the EVs, due to their small size [133-139]. At this time, only TEM, SEM, and nanoparticle tracking analysis have been conducted on MBVs to characterize their size, which was determined to be between 20-400 nm in diameter in urinary bladder matrix, small intestinal submucosa, and dermis, both before and after being isolated from the tissues [68, 69, 96, 97, 99, 100, 140].

3.1.4 MBV Cargo and Surface Markers

Characterization of the cargo of MBVs is important to determine their potential roles in matrix homeostasis and cell signaling. MBVs have been shown to contain various intravesicular miRNA and proteins, as well as membrane lipids, all of which can be used for cell signaling [68, 69, 96, 97, 99, 100, 140]. miRNAs have a wide range of applications in MBVs, including cell signaling and modulation of cell phenotype, while lipids protect the intravesicular contents from degradation and can act as another method of signal transduction. Analysis of the miRNA and lipid profiles of MBVs from different tissues demonstrated that the "fingerprint" of these molecules is different between MBVs from different tissue sources, as well as from parent cells and other extracellular vesicles secreted from the same cells [96, 97]. While miRNA and lipids are important MBV cargo to be investigated, they were not included within the scope of this thesis due to time constraints and a lack of knowledge on the miRNA cargo of MBVs, thus, only previous work investigating the protein content of MBVs will be discussed.

MBVs contain various proteins as their cargo and on their surface, much like other EVs. Proteins contained within the MBVs can play many roles, including cell signaling, remodeling of the extracellular matrix, or immune modulation. Research performed to date has used various cytokine arrays and Western blots to determine specific protein contents in MBVs. For example, MBVs from porcine small intestinal submucosa and mouse small intestinal submucosa contained high levels of IL-33, Reg3G, CD26, Endostatin, IL28, VEGF, ICAM-1, and CD142 [68], as shown in **Figure 13**. The MBVs were isolated from their respective tissues using differential centrifugation and the content of 111 proteins were measured using a cytokine array (ARY028, R&D Systems) [68]. It was noted that IL-33 was contained at high levels in both types of MBVs, thus, IL-33 was investigated more closely as a regulator of macrophage phenotype and was determined to be necessary for MBVs to polarize macrophages towards an M2-like phenotype [68]. However, depending on the environment, IL-33 can also induce an M1-like phenotype in macrophages when there is a lack of type 2 cytokines such as IL-4 or IL-13 [141]. Besides IL-33, important proteins such as VEGF, which regulates vascularization; ICAM-1, an adhesion molecule that is involved in activation of the immune system; and CD26, which regulates the immune response, signal transduction, and apoptosis; were all present at high levels in the MBVs from small intestinal submucosa [68, 142-147].
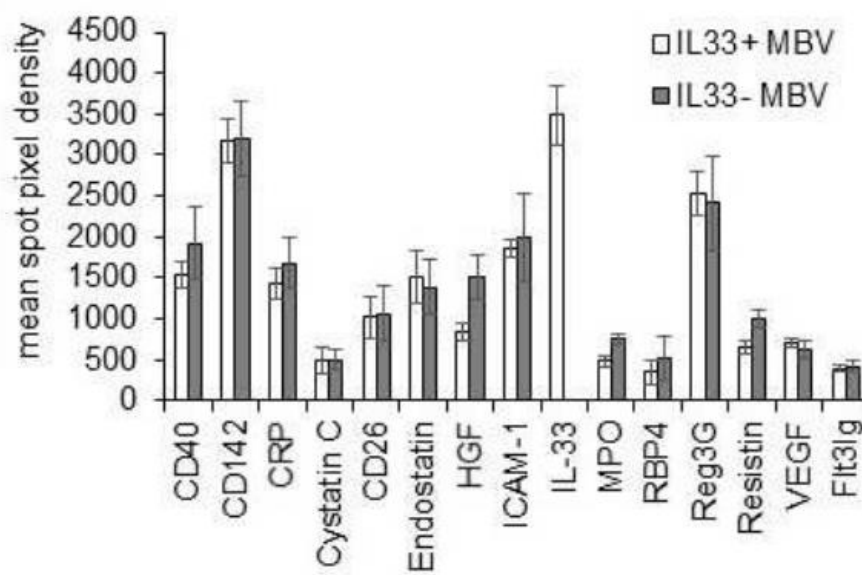
Figure 13. The most prevalent proteins contained within small intestinal submucosa MBVs [68].

Additional research may reveal certain surface markers that are conserved between MBVs and may be used as specific MBV markers, similar to CD9, CD63, TSG101, Alix, and CD81 in exosomes, although no MBV specific markers have been identified at this time [101, 148-150]. It is likely that the concentrations of proteins vary in MBVs from different tissues, due to the variable roles that they may need to play, and that the miRNA and lipid profiles also differ between MBV types. Further research into the protein contents and cell surface markers of MBVs may elucidate their roles in the extracellular matrix and determine various markers that differentiate them from other EVs.

3.1.5 Influence of MBVs on Macrophages

Unlike other EVs, MBVs are embedded within the tissue and are believed to be released during tissue remodeling, as the only method to isolate MBVs currently is to disrupt the surrounding tissue. Because MBVs are only revealed when tissue is broken down and they contain miRNA, proteins, and lipids that affect cells, it is important to

investigate what occurs when different relevant cells are exposed to MBVs. For this reason, various work has explored the effect of specific tissue derived MBVs on macrophage function and their potential therapeutic effects.

Macrophages play many roles in the body: they are the body's first of line of defense against pathogens in the innate immune system and act as antigen presenting cells to activate the adaptive immune system. Macrophages also act as mediators of inflammation and repair during tissue damage and release cytokines and enzymes depending on their polarization [151, 152]. It is believed that because macrophages are present at sites of tissue breakdown, they would be exposed to MBVs during release and may phagocytose MBVs, and thus alter their phenotype [151, 152]. This is due to the fact that MBVs can only be isolated after digestion of the tissue, which is similar to the degeneration of the tissue in vivo. Several studies have also demonstrated that MBVs can modulate macrophage phenotype, which will be described here [153-156].

Prior work demonstrated that decellularized urinary bladder matrix, small intestinal submucosa, and dermis tissue scaffolds polarized macrophage phenotype away from an M1-like phenotype, towards an M2-like phenotype [153-156]. After MBVs were identified in small intestinal submucosa and urinary bladder matrix tissue scaffolds, it was hypothesized that they may be the mechanism of polarizing macrophage phenotype [69, 97]. Therefore, recent studies have examined the effects of MBVs compared to decellularized tissue scaffold on macrophage phenotype. The researchers compared the effects of isolated urinary bladder matrix and small intestinal submucosa MBVs to the effects of the whole decellularized tissue scaffolds on naïve, M2, and M1 macrophages [68, 69, 97]. The results of initial experiments found that MBVs tended to polarize

macrophages towards M2-like phenotypes, similarly to the decellularized tissue scaffolds that the MBVs were isolated from, as demonstrated in **Figure 14** [69, 97]. Continuation of this research saw that IL-33 was present in MBVs from both porcine and mouse small intestinal submucosa [68]. IL-33 is a known mediator of M2-like phenotype in macrophages, and MBVs from animals lacking this cytokine had a drastic reduction in M2-like response in macrophages [68]. Taken together, the results of these experiments demonstrate that MBVs can modulate macrophage phenotype, similarly to the whole tissue they are derived from, and this modulation is dependent upon the molecules that are found within the MBVs.
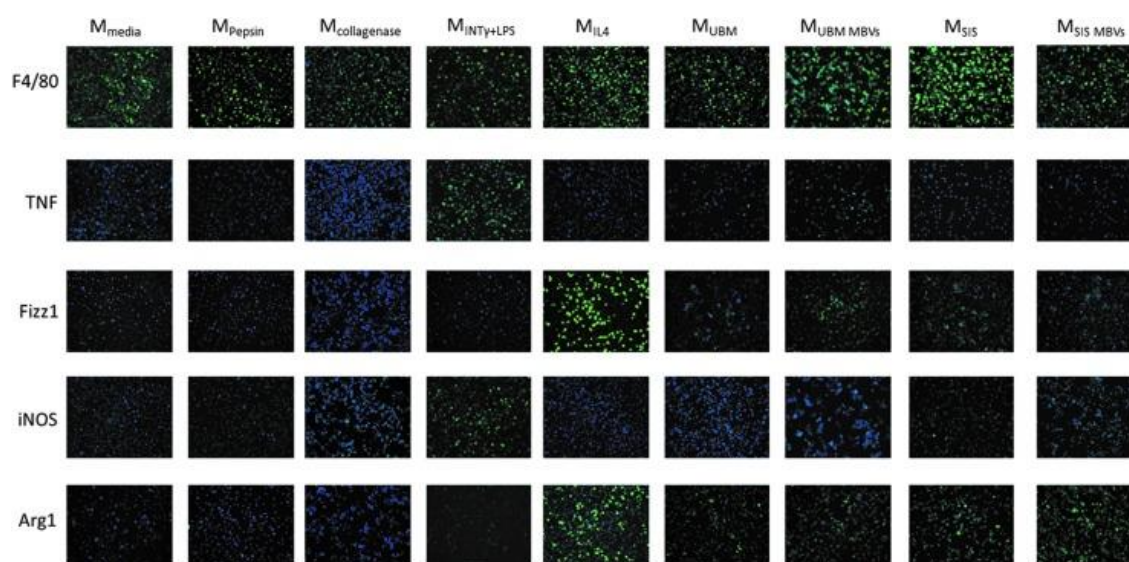

Figure 14. MBVs recapitulate extracellular matrix effects on macrophage phenotype. Macrophages were grown and treated either with the controls demonstrated, 250 µg/mL ECM, or 25 µg/mL MBVs. The macrophages were then stained for M1-like markers (TNF and iNOS), M2-like markers (Fizz1 and Arg1), or a pan marker (F4/80) and all treatments were counterstained with DAPI. There was high signal in the Fizz1 and Arg1 stained macrophages when treated with urinary bladder matrix, small intestinal submucosa, and the MBVs isolated from those tissues [69].

MBVs have the potential to alter the macrophage response and thus potentially drive tissue repair and regeneration, due to the ability of the macrophages to become polarized towards a pro-remodeling, M2 phenotype, however, the potential of MBVs to

induce this change must be investigated further. Anti-inflammatory MBVs may be an excellent therapeutic approach to help shift the immune response and aid in tissue repair. MBVs embedded in diseased tissue may also aid in immune system avoidance through macrophages, allowing the disease to progress. In either case, continued research on the effect of MBVs from novel tissues is needed to further increase the knowledge of this young field.

3.1.6 Summary for MBVs

MBVs are a recent discovery and so the knowledge on them is currently limited. It is believed, however, that MBVs are novel, nano-scale vesicles secreted by cells and embedded within the surrounding extracellular matrix. MBVs are similar in size and shape to other types of EVs, like exosomes and microvesicles, but MBVs differ from these other vesicles because they are embedded within the extracellular matrix and can be isolated following digestion of the tissue. MBVs are likely present in some quantity in all tissues and are specific to the cells that secreted them, indicated by a different lipid profile than exosomes and parent cells. However, more research on whether MBVs can be found in other unique tissues needs to be performed to confirm this belief. MBVs encompass cell specific miRNA, proteins, and lipids, either inside of the MBV, or on the membrane. Once the surrounding matrix starts to degrade, MBVs are thought to be released and can be taken up by cells, as noted that the only method to currently isolate MBVs is to digest the decellularized tissue, however, MBV release and uptake has not been studied in vivo at this time. Preliminary research has demonstrated that macrophages are polarized towards an M2-like phenotype when cultured with MBVs from small intestinal submucosa and urinary bladder matrix. The results discussed in this thesis demonstrate that MBVs may recapitulate the effects of their source tissue on macrophages, even when the source tissue

causes an inflammatory response, however, more research must be done in MBVs isolated

from novel tissues to confirm. Because MBVs are a recent discovery, not much is known

about how they function within tissues or the true reason they are secreted by cells. The

MBV arm of this thesis attempted to investigate whether MBVs could be found in NP

tissue, and to elucidate any differences between NP MBVs and previously described

MBVs. This project arm also attempted to demonstrate the effects of MBVs on cells and

determine what roles the MBVs may play in the NP.

3.2 METHODS
3.2.1 Isolation and Characterization of Matrix Bound Vesicles in Decellularized Porcine Nucleus Pulposus Tissue
3.2.1.1 Isolation of MBVs

MBVs were isolated according to a previously developed protocol with minor

modifications [97, 113, 140]. This method was chosen because it was known to work for

MBVs and is considered the gold standard for MBV isolation. This method also did not

require previous training to perform. Briefly, lyophilized, crushed decellularized tissue (see

"Whole Disc Decellularization" above) was digested in 5-20 mg increments in 1 mL of

100 ng/mL Liberase DL (05401160001, Sigma-Aldrich) for 12 hours at room temperature,

spinning on a tube revolver at a setting of 10 (88881001, Thermo Scientific). The digest

solution was then centrifuged 3 x 10,000 x g for 30 minutes while moving the supernatant

to new tubes to remove large contaminants. Following the centrifugation, the digest was

passed through a 0.22 µm filter (229747, Celltreat), to remove large contaminants. The

resulting solution was then centrifuged in 8x1 cm ultracentrifuge tubes at 100,000 x g at 4

°C for 70 minutes on a Beckman Coulter Optima L-100K Ultracentrifuge with a Ti90 rotor.

Once pelleted, the supernatant was poured off and the pellet was resuspended with 500-

1000 µL of 1X PBS. To break apart protein aggregates, the solution was passed through a

27G needle (305136, Beckton Dickinson). The solution was then filtered twice using a

Corning Spin-X centrifuge tube at 4000 x g for 15 minutes at 4 °C. After each

centrifugation, the top of portion of the tube was resuspended in 1 mL of sterile 1X PBS.

This step was added to further isolate the MBVs from contaminating small

proteins/molecules, as they would pass through the filter, while the MBVs would not.

3.2.1.2 Determining Concentration of MBVs Using Nanoparticle Tracking Analysis

To be able to determine MBV size and concentration, the isolated MBVs were

imaged using a Malvern NanoSight NS300. The MBVs were diluted 1:60 and 3x1 minute

videos were taken at an infusion rate of 100, camera level 15, camera shutter 1206, camera

gain 366, camera histogram 3294, and a detection threshold of 4. A total of n=3 MBV

isolation batches were analyzed with 3 videos of each batch.

3.2.1.3 Imaging MBVs Using Transmission Electron Microscopy

To be able to view the MBVs, they were imaged using a transmission electron

microscope. Three batches of MBVs were isolated and resuspended. 10 µL of the

suspensions were mixed 1:1 with 4 % PFA in a microcentrifuge tube. 3-5 µL of the fixed

MBVs were added dropwise to TEM grids (01824, Ted Pella) and the drops were allowed

to dry before adding another drop. Following fixation, uranyl acetate was added the grids

as a negative stain to visualize lipids. The grids were stored at room temperature in a

desiccator until needed. The grids were imaged at 200 kV using a FEI Technai Osiris

(scanning) TEM with a high-angle angular dark-field (HAADF) detector and at 80 kV on

a Hitachi H7500. Using the Technai Osiris, energy-dispersive X-ray spectroscopy (EDX)

data was also collected from one image of MBVs to determine the elemental composition.

3.2.1.4 Protein Content Quantification of MBVs

The protein content of the MBVs was determined using an R&D Proteome profiler Mouse XL Cytokine Array (ARY028, R&D Systems). This cytokine array was chosen because it measured a wide variety of different proteins and included molecules that were important for this research, such as various interleukins, as well as pro- and anti-inflammatory cytokines and chemokines. Triton X-100 was added to the MBVs to a concentration of 1% and frozen at -80 °C to lyse the vesicles. The MBVs were then thawed, and the assay was performed according to manufacturer's instructions. Briefly, the membranes were blocked using a provided solution. The membranes were then incubated with the lysed MBV solution overnight at 4 °C. The MBV solution was removed, and the membranes were washed. A solution of detection antibodies was added to the membranes, after which the membranes were washed. The membranes were then incubated in a solution of streptavidin-HRP, followed by a short incubation with the provided chemi-luminescent substrate. The membranes were imaged for 10 minutes using a Bio Rad Chemi Doc XRS+ with Image Lab Software. The adjusted pixel density was used to quantify the amount of each cytokine present on each membrane by drawing a circle with an area of 1.9 mm^2 around each dot. The average of the outside pixels along the circle was then subtracted from each pixel inside of the circle and the pixel density was then determined inside each circle. The values determined from the software were then normalized to the mass of protein added to each membrane, determined from the BCA assay. Each protein was dotted in duplicate on each membrane. A total of n=3 membranes were analyzed, with each membrane analyzing a different isolation batch of MBVs.

3.2.2 Determining Effects of Matrix Bound Vesicles on Cells

Macrophages were chosen for this experiment because they are the chief innate immune cell of the body. In cases of disc degeneration or herniation, they would be the first immune cell to arrive and initiate some form of response, either pro-regenerative or pro-inflammatory. NP cells were also chosen to be exposed to the MBVs because NP cells are native to the disc and are immediately be exposed to MBVs during degeneration, thus how they react is important to analyze.

3.2.2.1 MBV Preparation

MBVs were prepared as described above in "3.2.1.1 Isolation of MBVs". Briefly, three different isolations, each using decellularized tissue from at least 2 different spines, were digested and centrifuged accordingly. Following the analysis of the size, concentration, and contents, the three isolations were combined into one stock MBV solution. This stock MBV solution was then used to prepare various medias for culturing both macrophages and NP cells at concentrations of 5, 10, and 15 µg/mL MBVs determined using the BCA assay. Preliminary work had used the same concentrations of MBVs and demonstrated a dose dependent response of macrophages.

3.2.2.2 Isolation of Macrophages

Macrophage precursors were isolated from mouse femur bone marrow through a previously established protocol in our lab. Briefly, macrophage precursors were isolated from CD1 mice according to established protocols [157]. Briefly, the tibia and femur were resected from the mouse and placed in Dulbecco's phosphate-buffered saline (DPBS) (14190136, Thermo Fisher). Muscle and ligamentous tissue were then trimmed off the bones and the bones were transferred to fresh DBPS. The metaphysis was removed from each end of the bone and the marrow was flushed into a 50 mL conical tube using a 25-

gauge needle and cold DPBS. Non-cellular material was removed by straining the cell suspension through a 70 µm filter (08-771-2, Fisher Scientific). The cell suspension was then pelleted via centrifugation at 500 x g for 10 minutes. Contaminating red blood cells were lysed by incubating the cell pellet for 5 minutes in 3 mL of ACK lysis buffer (A1049201, Fisher Scientific). Finally, the cells were counted and frozen down at 6 million cells/mL in 70% FBS, 20% DMEM:F12 and 10% dimethyl sulfoxide.

3.2.2.3 Macrophage cell culture

Mouse bone marrow was plated at 6 million cells/mL in non-treated 48 well plates (82051-004, VWR) and cultured with complete macrophage media for six days to drive cells to macrophage phenotype [157]. Macrophages were cultured in 300 µL of Complete Macrophage Cell Media (88% DMEM:F12 (SH0023.01, Cytiva), 10% fetal bovine serum (26-140-079, Fisher Scientific), 1% penicillin/streptomycin (15-140-122, Fisher Scientific), 1% GlutaMax (35050-061, Life Technologies), and 50 ng/mL macrophage-colony stimulating factor (M9170, Sigma-Aldrich)), which was half-changed every two to three days. The macrophages were grown to confluency in normoxia at 37 °C before being used. Primary macrophages were used in the following experiments to negate the effects of dedifferentiation. Cells from three different mice were used in these experiments to account for cell variability. Once the macrophages reached 80% confluence, interferon-δ (IF005, Fisher Scientific) was added to the media in half of the wells to a concentration of 20 ng/mL. The cells were allowed to incubate for 4 hours at 37 °C at normoxia before all media was removed and replaced with either 300 µL complete macrophage cell media in the untreated wells or 300 µL of complete macrophage cell media containing 100 ng/mL lipopolysaccharide (LPS) (L4516, Sigma-Aldrich) in the interferon-δ treated wells. The cells incubated for 24 hours with or without LPS at 37 °C in normoxia. The cells that

received no polarization treatment were maintained as naïve macrophages, while the cells that were treated with interferon-δ and LPS were M1-like. M2-like macrophages were obtained by treating the macrophages with 20 ng/mL of IL-4 and Il-13, instead of treatment with MBVs.

3.2.2.4 Treating Macrophages with MBVs

Following polarization, the media was removed and frozen for later use in assays, then replaced with media containing 0, 5, 10, 15 µg/mL of MBVs or 20 ng/mL of IL-4 and IL-13, with or without 100 ng/mL of LPS, depending on whether the cells were naïve or M1. The cells incubated for 48 hours at 37 °C in normoxia before the media was removed and frozen for use in assays, and the cells were fixed in 4% PFA for 15 minutes. This study included in-plate duplicates of each treatment, with three different plates of cells, each from a different mouse.
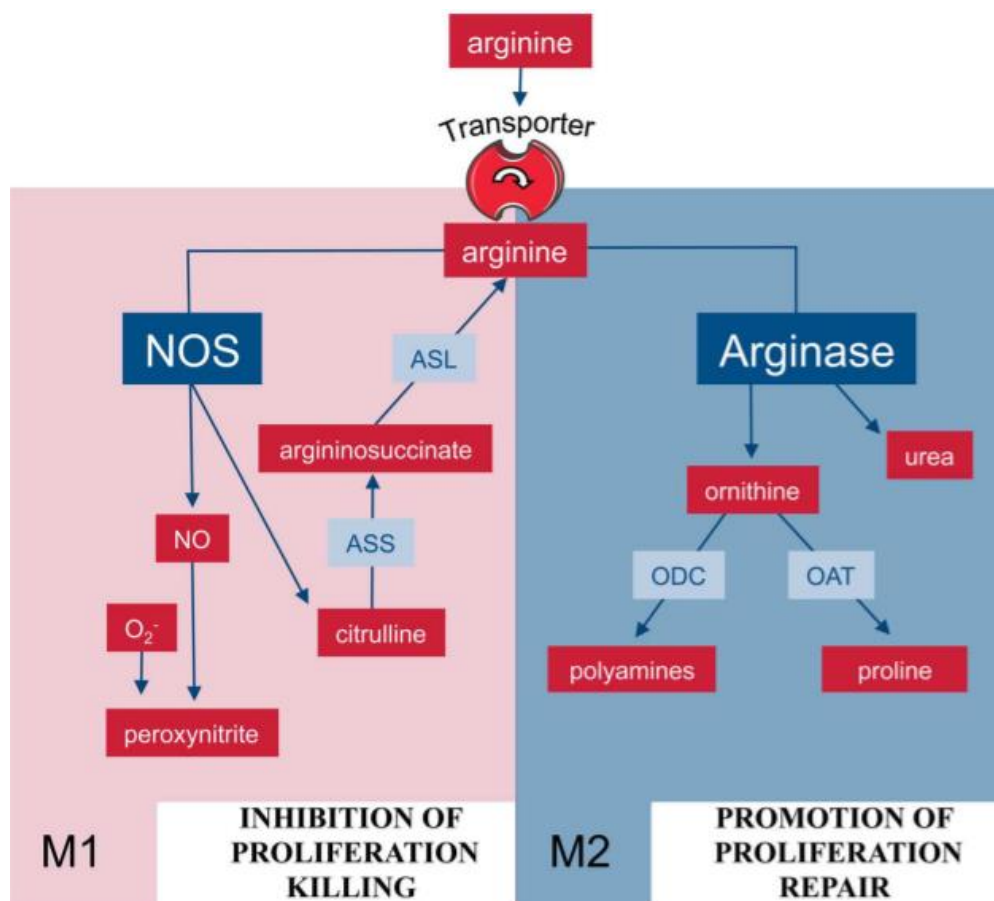
Figure 15. The different pathways macrophages take to metabolize arginine, based on their phenotype. Macrophages metabolize arginine depending upon their polarization. If polarized towards M1, they metabolize arginine to nitric oxide and citrulline, whereas when M2, they metabolize arginine to ornithine and urea. The divergence in metabolism can be taken advantage of by measuring the concentrations of various downstream products to easily determine the phenotype of a population of macrophages [158].

3.2.2.5 Urea and Nitrite Assays on Macrophage Media

Both the urea and nitrite assays were conducted to determine the phenotype of

macrophages non-destructively, due to the divergent metabolism of macrophages based on

activation. M1 macrophages produce more nitrite from arginine while M2 macrophages

produce urea. **Figure 15** [158] demonstrates how macrophages can break down arginine to

produce either nitrite or urea, depending on their phenotype. The M1-likeness can be

determined by the ratio of nitrite/urea, which should be independent of the number of

macrophages. Thus, a urea assay (DIUR-100, BioAssay Systems) was conducted on media taken from the macrophages treated with MBVs, induplicate, according to the manufacturer's instructions. Briefly, a standard curve was made and 50 µL of both the standard and samples were pipetted in duplicate into a 96 well plate. 200 µL of the working reagent was added to each well and the plate was allowed to incubate at room temperature, in the dark, for 50 minutes, before having the absorbance of each well be read on a plate reader at 430 nm.

For the nitrite assay (PAG2930, VWR), a standard curve was made and 50 µL of both the standard and samples were pipetted in duplicate into a 96 well plate. 50 µL of the Sulfanilamide solution was added to each well and the plate was allowed to incubate at room temperature, in the dark, for 10 minutes. 50 µL of the NED solution was then added to each well and the plate was allowed to incubate at room temperature, in the dark, for another 10 minutes before having the absorbance of each well be read on a plate reader at 535 nm.

3.2.2.6 NP cell culture

Human NP cells (4800, ScienCell) were cultured in a 48 well plate (82051-004, VWR) coated with 0.15 µg of Poly-L-Lysine per well (0413, ScienCell). NP cells were cultured in 300 µL of Complete Nucleus Pulposus Cell Media (4801, ScienCell), which was changed every two to three days. The NP cells were grown to confluency in normoxia at 37 °C before being used. Passage 2 NP cells were used in the following experiments to negate the effects of dedifferentiation. These cells were acquired from single, fetal donor and the identity of the cells was verified by the company through immunofluorescence with

antibodies for fibronectin and vimentin (ScienCell). Three different donors were used in these experiments to account for donor variability.

3.2.2.7 Treating NP cells with MBVs

Once the NP cells reached 80% confluence, all media was removed and frozen for later analysis, then replaced with either 300 µL complete NP cell media or 300 µL of complete NP cell media containing 10 ng/mL IL-1β (200-01B, PeproTech). The cells incubated for 24 hours with or without IL-1β at 37 °C in normoxia before the media was removed and frozen, then replaced with 300 µL of complete NP cell media, with or without IL-1β, and 30 µL of CCK-8 solution (ab228554, Abcam). The cells incubated for 2 hours at 37 °C in normoxia before the CCK-8 media was removed and read according to the manufacturer's instructions, and the media was replaced with complete NP cell media containing 0, 5, 10, or 15 µg/mL of MBVs, with or without 10 ng/mL of IL-1β, depending on the group. The cells incubated for 48 hours at 37 °C in normoxia before the media was removed and frozen, then replaced with 300 µL of complete NP cell media, with or without IL-1β, and 30 µL or CCK-8 solution. The cells incubated for 2 hours at 37 °C in normoxia before the CCK-8 media was removed and read and the cells were fixed in 4% PFA for 15 minutes. The CCK-8 data was used to determine the number of cells before and after treatment with MBVs. The number of cells was determined by creating a standard curve of cells and conducting the CCK-8 assay on them as described. Brightfield images were taken every day using an ISS VistaVision microscope to observe morphological changes in the NP cells. This study included in-plate duplicates of each treatment, with three different plates of cells, all with a different donor.

3.2.3 Statistical Analyses

Statistical analysis was conducted using the GraphPad Prism 7.03 software. Statistical significance was determined in the nitrite and urea assays using a two-way ANOVA with multiple comparisons within each group and of the same treatment between groups. Significance was determined in the CCK-8 analysis using a two-way ANOVA. Significance was set as $p \leq 0.05$ for all analyses. Error bars for all graphs represent the standard deviation.

3.3 RESULTS

3.3.1 Isolation and Characterization of Matrix Bound Vesicles in Decellularized Porcine Nucleus Pulposus Tissue

3.3.1.1 Isolation and Size Quantification of MBVs

Following isolation of MBVs from the decellularized porcine NP tissue, the physical characteristics of the MBVs were investigated to compare to previously described MBVs. The total average diameter of the MBVs was 114.4 ± 12.75 nm. The distribution of the sizes of MBVs determined from the nanoparticle tracking analysis are shown in **Figure 16**. The size data collected from the nanoparticle tracking analysis demonstrated that the MBVs isolated here were of similar size to previously described MBVs from other tissues [68, 69, 96, 97, 99, 100, 140]. Following the nanoparticle tracking analysis, a BCA protein assay was conducted to determine the total protein content of the MBVs. The average amount of protein isolated from each crush was 0.314 ± 0.052 µg/mg tissue.
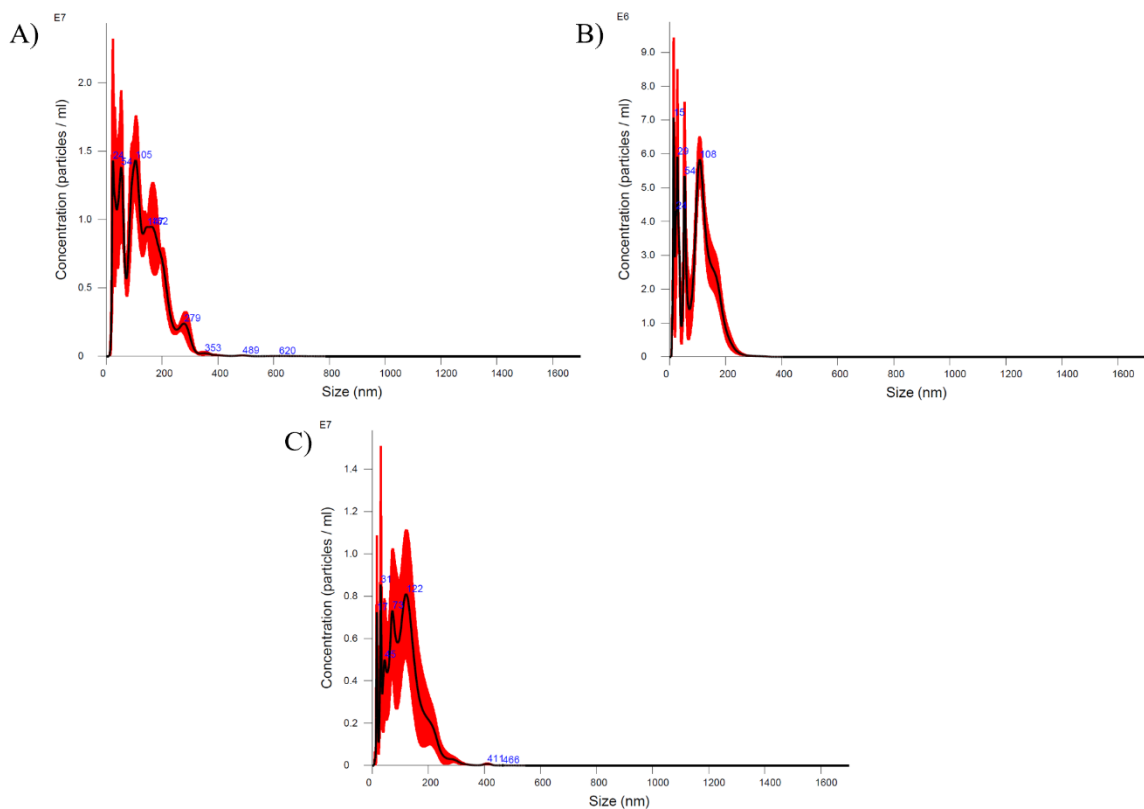
Figure 16. Size distributions of MBVs using nanoparticle tracking analysis. The size distributions of the MBVs were determined as previously described using nanoparticle tracking analysis. Each graph shows the average size distribution across three videos, for different MBV isolations.

3.3.1.2 Imaging MBVs Using Transmission Electron Microscopy

Following the verification that there were protein and particles present from the digestion and isolation of MBVs from decellularized NP tissue, three batches of MBVs were imaged using a TEM. **Figure 17 A and B** shows representative images of the MBVs which show a mostly rounded shape, with small crystalline formations located inside. **Figure 17 C** demonstrates MBVs stained with uranyl acetate, demonstrating the presence of lipids, which suggests a lipid membrane. This was an important finding, because the presence of lipids in these vesicles suggests that they are secreted from cells and adds evidence that these particles are truly MBVs. **Figure 17D** shows an EDX spectrum of the elemental composition of the MBVs. This spectrum shows high contents of calcium,

phosphorus, potassium, magnesium, and chlorine. The high levels of copper and oxygen are likely due to the copper grid and atmosphere, respectively.
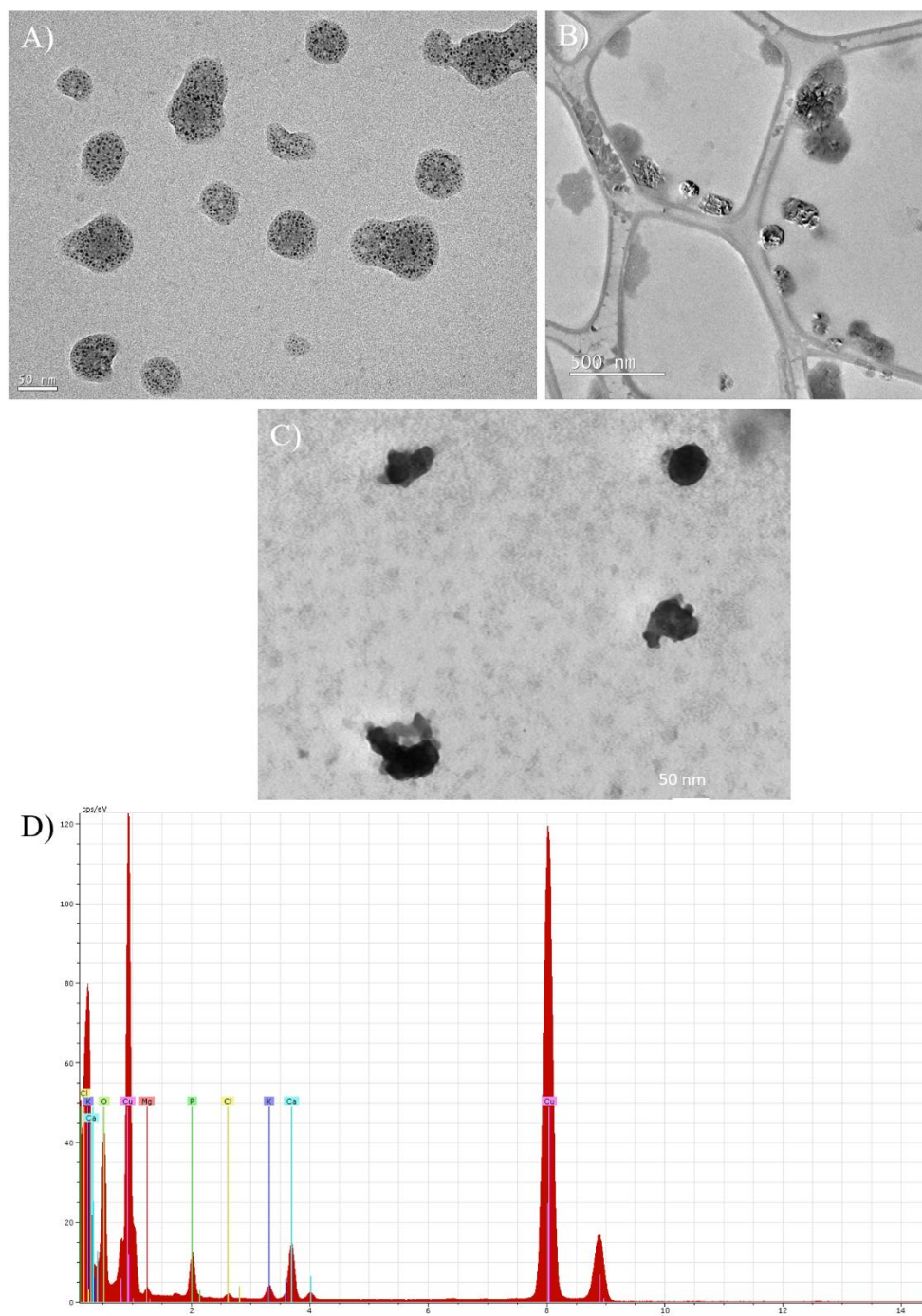

Figure 17. Representative Images of MBVs from two different isolations. A, B) Macroscopic images of MBVs from two different isolations demonstrated similarity in size and shape. C)

Macroscopic image of MBVs stained with uranyl acetate. D) EDX data of an MBV. The large copper spike is most likely due to the copper background from the grid.

3.3.1.3 Protein Content Quantification of MBVs

Once the physical characteristics of the NP MBVs had been investigated, the protein contents of the MBVs were next investigated. Selected protein content of the MBVs was analyzed using a 111-protein array to determine the contents of the MBVs and compare the most prevalent proteins with previous literature. **Figure 18A-C** shows images of the membranes. It was noted that the dots were slightly dim, which is due to the low mass of protein that was analyzed for each membrane (21.29, 47.3, and 13.24 μg respectively). **Figure 18D** demonstrates the average adjusted pixel density between all three membranes of the ten most prevalent proteins. These most prevalent proteins play roles in immune regulation (IL-33, CCL22, coagulation factor III, IL-1ra, IL-28A/B, LIF, and IL-1a), matrix homeostasis (MMP-2), and cell signaling (fetuin A and proprotein convertase 9).
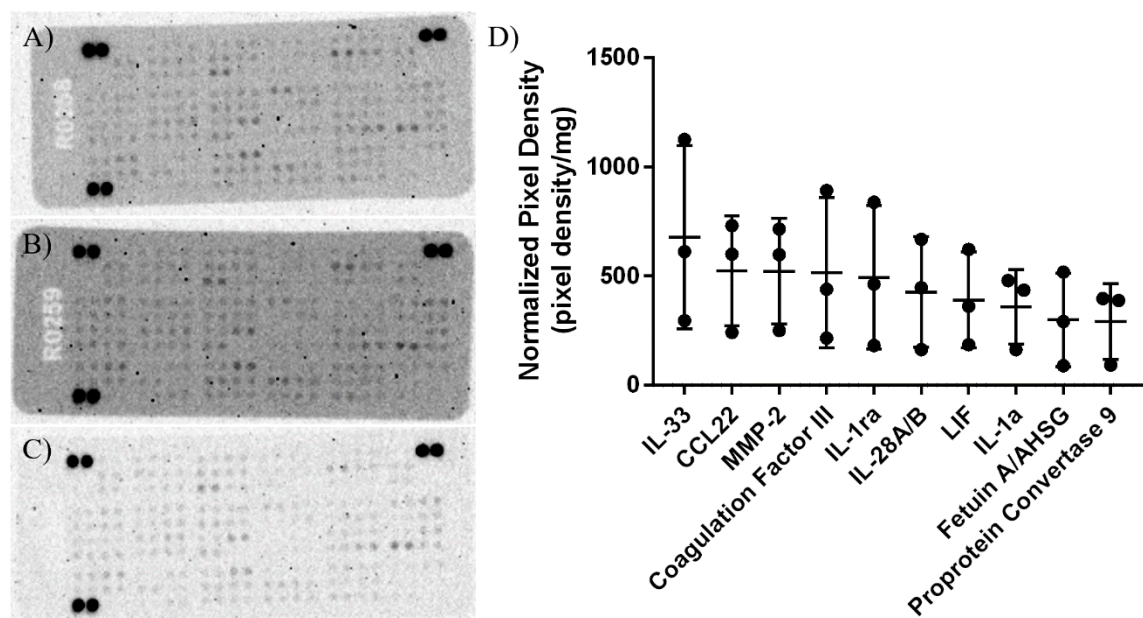
Figure 18. MBVs contain specific proteins. A-C) Representative images of each membrane with a different MBV isolation. D) A graph of the normalized adjusted pixel density of the 10 most prevalent proteins from the array.

3.3.2 Determining Effects of Matrix Bound Vesicles on Cells

3.3.2.1 Treating Macrophages with MBVs

Macrophages have been found to be present in degenerate NP tissue, most likely due to disruption of the AF to allow infiltration [89, 159]. Thus, we wanted to investigate the impact of the NP MBVs on macrophages to determine how the macrophages would react and if they would be able to act to repair the tissue. The specific phenotypes used here were naïve and M1-like macrophages as these would be the phenotypes that are most likely to be present in the degenerate NP. To investigate the effects of MBVs on both naïve and M1-like macrophages, macrophages were treated with concentrations of 0, 5, 10, and 15 µg/mL of MBVs for 48 hours in complete media. The media was removed and tested for urea and nitrite immediately before treatment and after treatment with MBVs. Nitrite was used as an indicator of an M1-like phenotype, while urea was used as an indicator of an M2-like phenotype. If low levels of both were present, this was an indicator of a naïve

phenotype. **Figure 19A-B** demonstrates the naïve macrophage readings. The naïve macrophages did not express readable amounts of nitrite before treatment with MBVs, however, after treatment, the nitrite significantly increased in a concentration dependent fashion with MBV concentration (**Fig. 19A**). In contrast, the naïve macrophages demonstrated low levels of urea expression before treatment with MBVs, however, after treatment with MBVs, there were no readable urea levels, except in the M2-like macrophages, which did not receive MBVs (**Fig. 19B**). **Figure 19C-D** demonstrates the M1-like polarized macrophage readings. The M1-like macrophages expressed high levels of nitrite both before and after treatment with MBVs, with the only significant differences occurring between 15 µg/mL of MBVs and 0 and 5 µg/mL and M2-like polarized macrophages after treatment (**Fig. 19C**). The M1-like macrophages demonstrated low levels of urea before treatment with MBVs, and no urea expression following MBV treatment, with significant decreases in the 0 and 10 µg/mL and the M2-like macrophages (**Fig. 19D**). Combined, these data demonstrate that NP MBVs polarize macrophages toward an M1-like phenotype if they are naïve and keep M1-like macrophages in and M1-like phenotype.
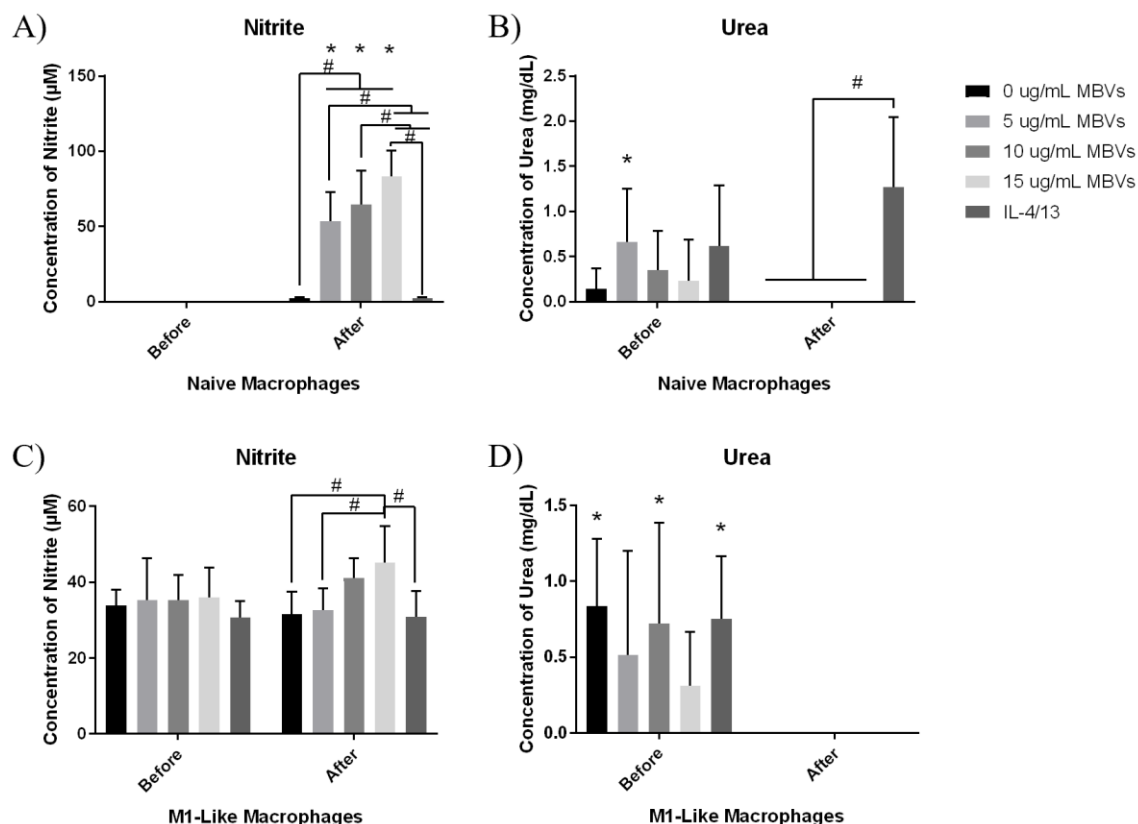
Figure 19. MBVs polarize macrophages towards an inflammatory phenotype. Graphs demonstrating the concentrations of nitrite (A and C) and urea (B and D) before and after treatment with MBVs. The groups were split naive (complete media) and M1-like (pretreated with interferon-δ, then LPS in complete media) macrophages. * Indicates significant difference $p < 0.05$ within the same treatment between the different times. # Indicates significant difference $p < 0.05$ of the within the same time but between different treatments.

3.3.2.2 Treating NP cells with MBVs

Similar to macrophages, NP cells were treated with varying concentrations of MBVs, both with and without treatment with IL-1β to create an inflammatory NP phenotype similar to the degenerate disc. **Figure 20A-D** shows representative images of the NP cells both before and after treatment with MBVs. It was noted that while the NP cells did not drastically change their morphology, they did begin to overlap during proliferation, as well as stop lining up in an orderly fashion, following treatment with MBVs, suggesting the MBVs had some effect on NP cell growth. The effect of MBVs on NP cell proliferation was also investigated. **Figure 20E and F** shows the number of

untreated and IL-1β treated cells calculated using the CCK-8 assay and a standard curve of NP cells before and after treatment with MBVs. The CCK-8 assay is used to measure the number of cells that are present. There were no significant differences present between any groups, indicating that the number of viable cells did not significantly change, however, all of the after-treatment readings have more cells than before. This suggests that the NP MBVs did not halt proliferation, which would be indicative of a senescent phenotype, common in degenerate discs.
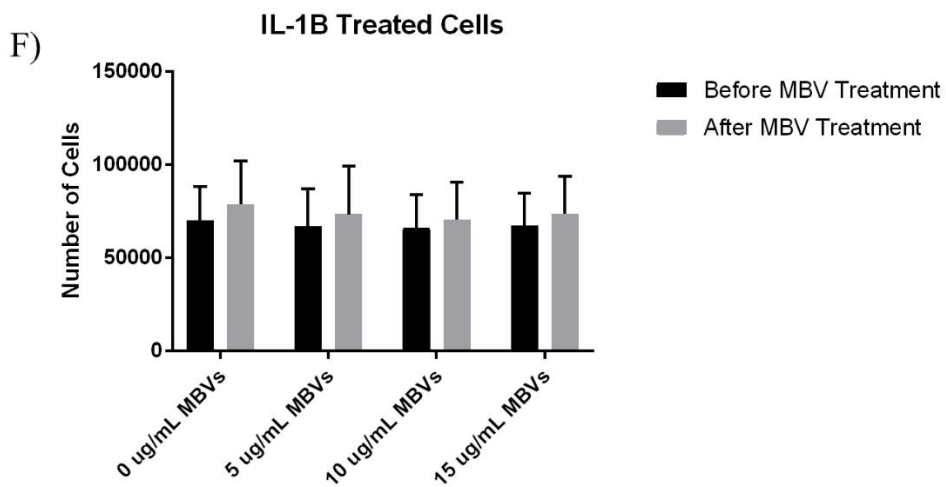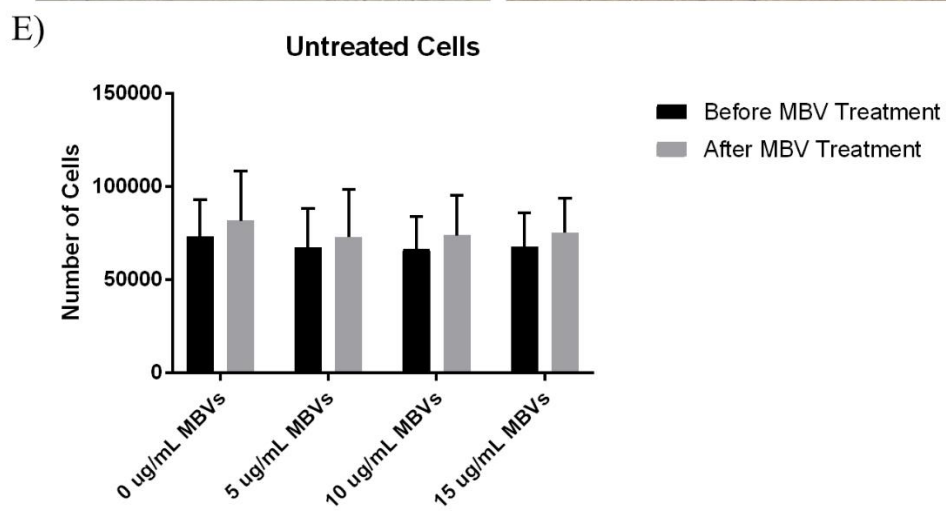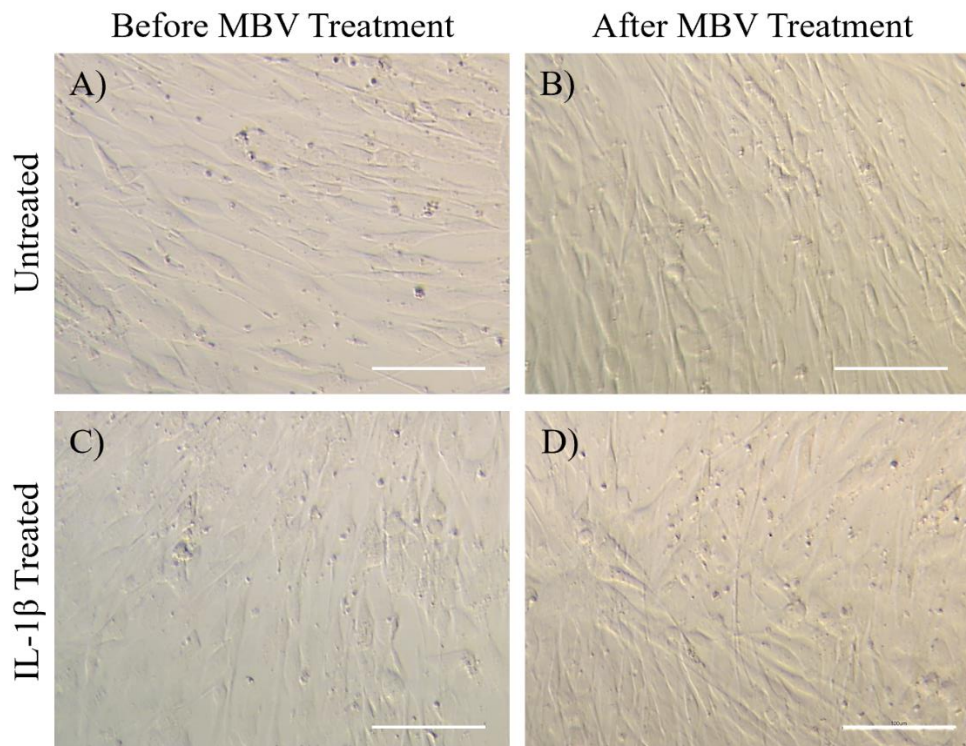
Before MBV Treatment   After MBV Treatment

A) B) C) D) Untreated IL-1β Treated

E) Untreated Cells
F) IL-1B Treated Cells

Figure 20. MBVs cause NP cells to grow on top of each other and stop lining up. A-D) Representative images of NP cells both before and after treatment with MBVs. E) The number of untreated cells before and after treatment with MBVs. F) The number of IL-1β treated cells before and after treatment with MBVs. There were no significant differences between any groups.

3.4 DISCUSSION

Decellularized tissue scaffolds have long been known to modulate cell function towards regeneration. Recent discoveries in urinary bladder matrix, small intestinal submucosa, and dermis have identified MBVs as one potential mechanistic pathway for modulation of cell function [68, 96-98]. To date, no one has explored the presence or function of MBVs in NP tissue, which, from the work presented here, appears to behave differently compared to previously described MBVs.

The cell culture experiments revealed that naïve macrophages treated with MBVs secreted much more nitrite and much less urea compared to before MBV treatment, which suggests NP MBVs are pro-inflammatory. Interestingly, if the macrophages were already polarized towards an M1-like phenotype, they secreted relatively similar levels of nitrite, regardless of treatment. In contrast, macrophages generally secreted urea no matter the polarization before treatment with MBVs but only produced urea when polarized towards an M2-like phenotype following treatment with MBVs. These results suggest that the NP MBVs isolated here polarize both naïve and M1-like macrophages toward an M1-like phenotype, which is different to previous literature, which suggested that MBVs from urinary bladder matrix and small intestinal submucosa polarized macrophages towards an M2-like phenotype [68, 69]. This result suggests that NP MBVs cause cells to act similarly to when they treated with the whole decellularized tissue. In fact, this result has already been investigated in urinary bladder matrix and small intestinal submucosa, as both of these whole tissues also polarized macrophages towards an M2-like phenotype [69, 97]. NP

tissue, on the other hand, causes an inflammatory, M1-like response, even when decellularized and placed within a host [39]. It appears that instead of only acting in an anti-inflammatory manner, as was originally believed, MBVs are dependent upon their parent tissue, and have effects similar to the tissue as a whole. Further research into the causes of these differences between MBVs derived from different tissues needs to be performed, however, one possibility is that MBVs are the mediators of tissue breakdown. Because tissues are different, they also have different methods of breakdown and remodeling. In the case of the NP, this tissue naturally breaks down over time and lacks a method to remodel, and so the MBVs mimic this response to cells. On the other hand, the tissues that MBVs have been isolated from previously and have been shown to modulate macrophages toward an M2-like phenotype; urinary bladder matrix, small intestinal submucosa, and dermis; are all tissues that have high turnover and are constantly remodeling. In these tissues, macrophages would be much more inclined to aid in the remodeling process compared to the NP. Thus, the MBVs from these tissues also mimic this remodeling response in cells.

Following the investigation into the effects of MBVs on cells, the cargo of the MBVs were also investigated. MBVs contain miRNA, proteins, and lipids that can have effects on cells and the surrounding tissue. Due to time constraints as well as a lack of information on miRNA present in MBVs, only protein cargo of MBVs were investigated in this thesis. The most prevalent proteins from NP MBVs were IL-33 and MMP-2. IL-33 is a member of the IL-1 family and plays many roles in macrophage activation, showing roles in polarizing macrophages to both M1- and M2-like phenotypes [160]. This is most likely due to its role in regulating the expression of IL-1ra on many different cell types,

including macrophages [160]. IL-33 is generally considered as an alarm signal for cell or tissue damage [160]. In most tissues, IL-33 activates Treg and Th2 cells to then secrete IL-4 and IL-13 [160, 161]. Increased secretion of IL-4 and IL-13 polarize macrophages towards an M2-like response [160, 161]. However, if these and other M2 cytokines are not present in large enough quantities or pro-inflammatory cytokines, like IL-12 are present, IL-33 can cause macrophages to instead be polarized ed towards an M1-like phenotype [161]. The data collected here suggested that NP MBVs polarize macrophages towards an M1-like phenotype. One reason this may occur is that anti-inflammatory cytokines are not present in enough quantities to offset the effect of pro-inflammatory cytokines on IL-33 receptor expression on macrophages, polarizing them towards an M1-like phenotype. IL-33 was investigated thoroughly as being a key regulator of macrophage phenotype in MBVs, to polarize them towards an M2-like phenotype, in small intestinal submucosal MBVs [68]. MBVs from small intestinal submucosa required IL-33 to polarize macrophages towards an M2-like phenotype, as MBVs isolated from the small intestinal submucosa of IL-33 negative animals resulted in activation of macrophages towards an M1-like phenotype, instead of the M2-like phenotype from IL-33 positive animals [68]. Our results indicate that IL-33 is present in NP MBVs, however, macrophages cultured with the NP MBVs appeared to become polarized towards an M1-like phenotype, which is different to previous literature. This suggests that while IL-33 is important in MBV mediated macrophage polarization, there are other factors that should be considered as well, that are different between the two types of MBVs.

MMP-2 is a matrix metalloproteinase that is involved in the breakdown of the extracellular matrix, specifically type IV collagen, and is thought to be involved in multiple

pathways involved in vascularization and the nervous system through regulation of growth of new vasculature and neurons [162, 163]. Previous literature on small intestinal submucosa found most MBV solutions contained some MMP-2 but not at the levels demonstrated here, which may be due to the different tissue sources of the MBVs [68]. The other most prevalent proteins included CCL22, Coagulation Factor II (CD142), IL-1ra, IL-28A/B, LIF, IL-1α, Fetuin A, and Proprotein Convertase 9. Of these proteins, Coagulation Factor III [164], IL-28A/B [165], LIF [166], and IL-1α [167] act as pro-inflammatory cytokines, however, IL-28A/B can play both pro- and anti-inflammatory roles [165]. CCL22, IL-1ra, and Fetuin A act as anti-inflammatory cytokines, with CCL22 invoking a type II immune response [168], IL-1ra acting as a competitive inhibitor of IL-1α and IL-1β [169], and Fetuin A acting to inhibit pathogen associated molecular pattern activation of innate immune cells [170]. Lastly, Proprotein Convertase 9 plays minimal roles in inflammation, instead acting as a processor or protein precursors [171]. Overall, the majority of prevalent proteins in NP MBVs have some pro-inflammatory or degradative roles, with only a few of the proteins acting to oppose the others. In comparison, MBVs from small intestinal submucosa contained more proteins involved in other pathways besides inflammation such as endostatin, a regulator of angiogenesis [172], HGF, a regulator of cell growth and motility [173], MPO, an antimicrobial agent [174], and Reg3G, an immunosuppressive [68, 175]. Another key protein found in small intestinal submucosa was CD40, which is a costimulatory cytokine required for immune cell response, and was not very prevalent in NP MBVs [65]. The lack of CD40 may be one reason that NP MBVs polarized macrophages toward an M1-like response, whereas MBVs from other tissues polarized macrophages towards an M2-like response.

Other important cytokines that were present in our NP MBVs but not the most prevalent, include IL-7, CXCL10, IL-10, and IL-13 and ranking 11, 20, 21, and 29 respectively. IL-7 is involved in B and T cell activation, as well as bone homeostasis [176, 177]. CXCL10, otherwise known as interferon gamma-induced protein 10, is a chemokine for macrophages, T cells, and other immune cells, and also inhibits angiogenesis [178, 179]. IL-10 is a key anti-inflammatory cytokine that inhibits the activity of most immune cells and polarizes macrophages towards an M2-like phenotype [180, 181]. Lastly, IL-13 is a key anti-inflammatory cytokine, and plays many roles in immune cells [182]. While the protein content of the MBVs is important and likely played key roles in the effects on cells, the miRNA and lipid contents that were not investigated, most likely also aided in the cell effects. Future work should investigate the miRNA and lipid cargo of the NP MBVs to better determine their roles in the effect the MBVs had on cells. miRNA likely plays a large role in modulation of cell phenotype, as previous literature demonstrated the presence of some miRNA in MBVs from urinary bladder matrix and small intestinal submucosa that highly expressed miRNA involved in modulation of macrophage phenotype [96, 99]. Lipids of MBVs are also important to investigate, as it is known that they can be used for cellular signaling, however, much less is known about the roles of lipids in MBVs. Along with the investigation into miRNA and lipid cargo, the effects of the various proteins that were prevalent within MBVs can also be investigated for their specific roles in the effects the MBVs had on cells.

NP cells were cultured and treated with MBVs similarly to the macrophages. Instead of polarizing the NP cells using LPS, IL-1β was used as it is a common pro-inflammatory cytokine found within the degenerated disc. Before treatment with MBVs,

the NP cells appeared to align in rows, even when treated with IL-1β. However, after treatment with any concentration of MBVs, the NP cells started to become less organized and started to overlap with each other. While there was no visible change in NP cell morphology, this overlapping is an indicator of altered cellular function. It was also noted that the NP cells continued proliferating during the MBV treatment, suggesting that the cells did not become senescent, which often occurs in mid to late-stage disc degeneration. More research to determine what is happening to the NP cells, as well as what causes the MBVs to have these effects must be performed. These experiments could include evaluating the gene expression changes of known NP markers ACAN, COL2, or SOX9, as well as possibly treating the NP cells with MBVs from other tissues that are known to promote a remodeling phenotype and determine if NP cells have the capacity to regenerate the degenerate NP if given the current signals.

TEM and NanoSight analysis determined that there were particles isolated from the decellularized tissue scaffold with the same size and appearance as previously determined MBVs, however, there appeared to be a crystalline formation within the MBVs that had not been seen previously. One hypothesis for these crystals is that they are similar to the calcifying nodes of matrix vesicles, as the MBVs isolated here are secreted by chondrocyte-like cells, which secrete matrix vesicles in other parts of the body, and calcium was present in the EDX of the MBVs [111]. Further research will need to be performed to fully elucidate what the crystalline formations are.

The first limitation of the MBV project arm was that it required vast amounts of decellularized tissue to generate usable amounts of MBVs. The average tissue requirement was 3.18 mg to isolate 1 µg of MBVs. To ensure that all experiments could be performed,

the amount of MBVs used for the protein array was lower than what was suggested by the manufacturer, which led to dim readings and increased noise. To combat this limitation, MBV isolations specifically for protein determination should be performed, to ensure adequate mass of proteins. This study also did not investigate the total protein content of NP MBVs, only the proteins that could be read using the cytokine array. This means that no knowledge was obtained on other, possibly important proteins. In the future, further studies investigating a wider range of proteins, using either another protein array or mass spectrometry, should be used to get a better understanding of the protein contents of MBVs. Along with the fact that only a select few proteins were analyzed using the cytokine array, neither miRNA nor lipids were investigated in any capacity in this work. miRNA most likely play a large role in cell phenotype modulation and could account for some of the differences between NP MBVs and other MBVs that were noticed. Future work should investigate the total miRNA contents of NP MBVs and compare this to the contents of other MBVs. Another limitation of this study was that only one isolation method was used here. It is possible that the amount of decellularized tissue needed to isolate usable amounts of MBVs could be decreased using another isolation method that was discussed in the literature review section. For the readings of nitrite and urea from macrophage media, many of the values were unreadable, making analysis difficult. A few reasons for this include that the values were actually very low or that the assays were not sensitive enough to measure such small readings. In the future, some solutions to this problem would be to either use more sensitive assays or to culture the macrophages for longer, to allow the analytes to accumulate further. Another limitation is that the NP cells did not react very much to the MBVs, so it was difficult to visually determine how the MBVs impacted them,

unlike the macrophages, which were very easy to visually tell differences between the treatments. The work with NP cells and MBVs was preliminary and suggests that further work would be useful to further elucidate the effects of NP MBVs on the native NP cells.

Chapter 4: Conclusions

The decellularization and gelation process developed here for porcine nucleus pulposus is not cytotoxic and the resulting gel exhibits neuroinhibitory properties, which could be explored in the future for the treatment of low back pain. This decellularized NP tissue scaffold can be engineered into a thermally forming injectable gel, which would improve the ability to translate to the clinic. The presence of matrix bound nanovesicles was also investigated in the decellularized NP. MBV-like vesicles could be isolated from the NP tissue but, unexpectedly, treating macrophages and NP cells with the MBVs polarized them towards an unhealthy, inflammatory phenotype, contrary to expectation based on the results of previous literature. While the results of macrophages treated with MBVs presented in this thesis may be different to previous literature, the NP MBVs appear to have the same effect on macrophages as the whole NP tissue. Instead of acting in a pro-regenerative manner independent of the tissue they are derived from, it appears that MBVs act in a similar manner to how treatment with the whole parent tissue would result. More research must be performed to verify the results demonstrated here, especially in unique tissues that have different properties to the ones investigated previously. This research also further increased the knowledge in the field of MBVs and raised new questions on the effects of tissue specific MBVs on cells, as well as their source tissue.

Acknowledgements

References

[1] R.A. Wachs, E.N. Hoogenboezem, H.I. Huda, S. Xin, S.L. Porvasnik, C.E. Schmidt, Creation of an injectable in situ gelling native extracellular matrix for nucleus pulposus tissue engineering, The Spine Journal 17(3) (2017) 435-444.

[2] G.B. Andersson, Epidemiological features of chronic low-back pain, The lancet 354(9178) (1999) 581-585.

[3] A. Navani, L. Manchikanti, S.L. Albers, R.E. Latchaw, J. Sanapati, A.D. Kaye, S. Atluri, S. Jordan, A. Gupta, D. Cedeno, Responsible, safe, and effective use of biologics in the management of low back pain: American Society of Interventional Pain Physicians (ASIPP) guidelines, Pain physician 22(1) (2019) S1-S74.

[4] A.L. Binch, A.A. Cole, L.M. Breakwell, A.L. Michael, N. Chiverton, L.B. Creemers, A.K. Cross, C.L. Le Maitre, Nerves are more abundant than blood vessels in the degenerate human intervertebral disc, Arthritis research & therapy 17(1) (2015) 1-10.

[5] B. Wu, L. Yang, B. Peng, Ingrowth of nociceptive receptors into diseased cervical intervertebral disc is associated with discogenic neck pain, Pain Medicine 20(6) (2019) 1072-1077.

[6] E. Park, S. Moon, H. Suh, S. Hochman, M.-G. Lee, Y. Kim, I. Jang, H. Han, Disc degeneration induces a mechano-sensitization of disc afferent nerve fibers that associates with low back pain, Osteoarthritis and cartilage 27(11) (2019) 1608-1617.

[7] A. Freemont, A. Watkins, C. Le Maitre, P. Baird, M. Jeziorska, M. Knight, E. Ross, J. O'brien, J. Hoyland, Nerve growth factor expression and innervation of the painful intervertebral disc, The Journal of pathology 197(3) (2002) 286-292.

[8] P. Kalakoti, S. Missios, T. Maiti, S. Konar, S. Bir, P. Bollam, A. Nanda, Inpatient outcomes and postoperative complications after primary versus revision lumbar spinal fusion surgeries for degenerative lumbar disc disease: a national (nationwide) inpatient sample analysis, 2002–2011, World neurosurgery 85 (2016) 114-124.

[9] T. Ibrahim, I. Tleyjeh, O. Gabbar, Surgical versus non-surgical treatment of chronic low back pain: a meta-analysis of randomised trials, International orthopaedics 32(1) (2008) 107-113.

[10] D. Beckerman, M. Esparza, S.I. Lee, S.H. Berven, S.S. Bederman, S.S. Hu, S. Burch, V. Deviren, B. Tay, P.V. Mummaneni, Cost Analysis of Single-Level Lumbar Fusions, Global spine journal 10(1) (2020) 39-46.

[11] J.R. Engsberg, L.G. Lenke, A.K. Reitenbach, K.W. Hollander, K.H. Bridwell, K. Blanke, Prospective evaluation of trunk range of motion in adolescents with idiopathic scoliosis undergoing spinal fusion surgery, Spine 27(12) (2002) 1346-1354.

[12] A. Katsuura, S. Hukuda, Y. Saruhashi, K. Mori, Kyphotic malalignment after anterior cervical fusion is one of the factors promoting the degenerative process in adjacent intervertebral levels, European spine journal 10(4) (2001) 320-324.

[13] J. Goffin, E. Geusens, N. Vantomme, E. Quintens, Y. Waerzeggers, B. Depreitere, F. Van Calenbergh, J. van Loon, Long-term follow-up after interbody fusion of the cervical spine, Clinical Spine Surgery 17(2) (2004) 79-85.

[14] P.P. Raj, Intervertebral disc: anatomy-physiology-pathophysiology-treatment, Pain Practice 8(1) (2008) 18-44.

[15] M.A. Adams, P.J. Roughley, What is intervertebral disc degeneration, and what causes it?, Spine 31(18) (2006) 2151-2161.

[16] T. Grunhagen, G. Wilde, D.M. Soukane, S.A. Shirazi-Adl, J.P. Urban, Nutrient supply and intervertebral disc metabolism, JBJS 88(suppl_2) (2006) 30-35.

[17] A. Maroudas, R. Stockwell, A. Nachemson, J. Urban, Factors involved in the nutrition of the human lumbar intervertebral disc: cellularity and diffusion of glucose in vitro, Journal of anatomy 120(Pt 1) (1975) 113.

[18] A. Nachemson, T. Lewin, A. Maroudas, M. Freeman, In vitro diffusion of dye through the end-plates and the annulus fibrosus of human lumbar inter-vertebral discs, Acta Orthopaedica Scandinavica 41(6) (1970) 589-607.

[19] L.M. Benneker, P.F. Heini, M. Alini, S.E. Anderson, K. Ito, 2004 Young Investigator Award Winner: vertebral endplate marrow contact channel occlusions and intervertebral disc degeneration, Spine 30(2) (2005) 167-173.

[20] C. Feng, H. Liu, M. Yang, Y. Zhang, B. Huang, Y. Zhou, Disc cell senescence in intervertebral disc degeneration: causes and molecular pathways, Cell Cycle 15(13) (2016) 1674-1684.

[21] C.L. Le Maitre, A.J. Freemont, J.A. Hoyland, Accelerated cellular senescence in degenerate intervertebral discs: a possible role in the pathogenesis of intervertebral disc degeneration, Arthritis research & therapy 9(3) (2007) R45.

[22] J. Rutges, R. Duit, J. Kummer, J. Bekkers, F. Oner, R. Castelein, W. Dhert, L. Creemers, A validated new histological classification for intervertebral disc degeneration, Osteoarthritis and cartilage 21(12) (2013) 2039-2047.

[23] W.E. Johnson, B. Caterson, S.M. Eisenstein, D.L. Hynds, D.M. Snow, S. Roberts, Human intervertebral disc aggrecan inhibits nerve growth in vitro, Arthritis & Rheumatism 46(10) (2002) 2658-2664.

[24] D. Purmessur, M.C. Cornejo, S.K. Cho, P.J. Roughley, R.J. Linhardt, A.C. Hecht, J.C. Iatridis, Intact glycosaminoglycans from intervertebral disc-derived notochordal cell-conditioned media inhibit neurite growth while maintaining neuronal cell viability, The spine journal 15(5) (2015) 1060-1069.

[25] A. Freemont, T. Peacock, P. Goupille, J. Hoyland, J. O'brien, M. Jayson, Nerve ingrowth into diseased intervertebral disc in chronic back pain, The lancet 350(9072) (1997) 178-181.

[26] B. Peng, W. Wu, S. Hou, P. Li, C. Zhang, Y. Yang, The pathogenesis of discogenic low back pain, The Journal of bone and joint surgery. British volume 87(1) (2005) 62-67.

[27] J. García-Cosamalón, M.E. Del Valle, M.G. Calavia, O. García-Suárez, A. López-Muñiz, J. Otero, J.A. Vega, Intervertebral disc, sensory nerves and neurotrophins: who is who in discogenic pain?, Journal of anatomy 217(1) (2010) 1-15.

[28] Y. Abe, K. Akeda, H.S. An, Y. Aoki, R. Pichika, C. Muehleman, T. Kimura, K. Masuda, Proinflammatory cytokines stimulate the expression of nerve growth factor by human intervertebral disc cells, Spine 32(6) (2007) 635-642.

[29] D. Purmessur, A.J. Freemont, J.A. Hoyland, Expression and regulation of neurotrophins in the nondegenerate and degenerate human intervertebral disc, Arthritis research & therapy 10(4) (2008) 1-9.

[30] J.-M. Zhang, J. An, Cytokines, inflammation and pain, International anesthesiology clinics 45(2) (2007) 27.

[31] H. Kimmel, M. Rahn, T.W. Gilbert, The clinical effectiveness in wound healing with extracellular matrix derived from porcine urinary bladder matrix: a case series on severe

chronic wounds, The Journal of the American College of Certified Wound Specialists 2(3) (2010) 55-59.

[32] N. Naderi, N. Joji, N.V. Kang, Use of dCELL (Decellularized Human Dermis) in Repair of Urethrocutaneous Fistulas or Glans Dehiscence, Plastic and Reconstructive Surgery–Global Open (2020).

[33] E. Bondioli, V. Purpura, C. Orlandi, A. Carboni, P. Minghetti, G. Cenacchi, G. De Luca, D. Capirossi, E. Nigrisoli, D. Melandri, The use of an acellular matrix derived from human dermis for the treatment of full-thickness skin wounds, Cell and tissue banking 20(2) (2019) 183-192.

[34] M.E. Franklin, J.M. Trevino, G. Portillo, I. Vela, J.L. Glass, J.J. González, The use of porcine small intestinal submucosa as a prosthetic material for laparoscopic hernia repair in infected and potentially contaminated fields: long-term follow-up, Surgical endoscopy 22(9) (2008) 1941-1946.

[35] B.K. Oelschlager, C.A. Pellegrini, J. Hunter, N. Soper, M. Brunt, B. Sheppard, B. Jobe, N. Polissar, L. Mitsumori, J. Nelson, Biologic prosthesis reduces recurrence after laparoscopic paraesophageal hernia repair: a multicenter, prospective, randomized trial, Annals of surgery 244(4) (2006) 481.

[36] Y. Liu, Z. Cao, H. Yang, Y. Shen, J. Chen, Porcine Small Intestinal Submucosa Mesh to Treat Inguinal Hernia in Young Adults Using Laparoscopic Inguinal Hernia Repair: A Retrospective Controlled Study, Surgical Laparoscopy Endoscopy & Percutaneous Techniques 30(4) (2020) 367-370.

[37] P.M. Crapo, T.W. Gilbert, S.F. Badylak, An overview of tissue and whole organ decellularization processes, Biomaterials 32(12) (2011) 3233-3243.

[38] J.J. Mercuri, S.S. Gill, D.T. Simionescu, Novel tissue-derived biomimetic scaffold for regenerating the human nucleus pulposus, Journal of biomedical materials research Part A 96(2) (2011) 422-435.

[39] J.J. Mercuri, S. Patnaik, G. Dion, S.S. Gill, J. Liao, D.T. Simionescu, Regenerative potential of decellularized porcine nucleus pulposus hydrogel scaffolds: stem cell differentiation, matrix remodeling, and biocompatibility studies, Tissue engineering Part A 19(7-8) (2013) 952-966.

[40] A. Hensley, J. Rames, V. Casler, C. Rood, J. Walters, C. Fernandez, S. Gill, J.J. Mercuri, Decellularization and characterization of a whole intervertebral disk xenograft scaffold, Journal of Biomedical Materials Research Part A 106(9) (2018) 2412-2423.

[41] L.K. Chan, V.Y. Leung, V. Tam, W.W. Lu, K. Sze, K.M. Cheung, Decellularized bovine intervertebral disc as a natural scaffold for xenogenic cell studies, Acta biomaterialia 9(2) (2013) 5262-5272.

[42] X. Zhou, J. Wang, X. Huang, W. Fang, Y. Tao, T. Zhao, C. Liang, J. Hua, Q. Chen, F. Li, Injectable decellularized nucleus pulposus-based cell delivery system for differentiation of adipose-derived stem cells and nucleus pulposus regeneration, Acta biomaterialia 81 (2018) 115-128.

[43] J. Xu, S. Liu, S. Wang, P. Qiu, P. Chen, X. Lin, X. Fang, Decellularised nucleus pulposus as a potential biologic scaffold for disc tissue engineering, Materials Science and Engineering: C 99 (2019) 1213-1225.

[44] L. Yu, Z.-J. Sun, Q.-C. Tan, S. Wang, W.-H. Wang, X.-Q. Yang, X.-J. Ye, Thermosensitive injectable decellularized nucleus pulposus hydrogel as an ideal

biomaterial for nucleus pulposus regeneration, Journal of Biomaterials Applications (2020) 0885328220921328.

[45] H. Cho, S.-H. Park, S. Lee, M. Kang, K.A. Hasty, S.-J. Kim, Snapshot of degenerative aging of porcine intervertebral disc: a model to unravel the molecular mechanisms, Experimental & molecular medicine 43(6) (2011) 334.

[46] D.O. Freytes, J. Martin, S.S. Velankar, A.S. Lee, S.F. Badylak, Preparation and rheological characterization of a gel form of the porcine urinary bladder matrix, Biomaterials 29(11) (2008) 1630-1637.

[47] J.M. Singelyn, J.A. DeQuach, S.B. Seif-Naraghi, R.B. Littlefield, P.J. Schup-Magoffin, K.L. Christman, Naturally derived myocardial matrix as an injectable scaffold for cardiac tissue engineering, Biomaterials 30(29) (2009) 5409-5416.

[48] J. Ungerleider, T. Johnson, N. Rao, K. Christman, Fabrication and characterization of injectable hydrogels derived from decellularized skeletal and cardiac muscle, Methods 84 (2015) 53-59.

[49] R.A. Pouliot, B.M. Young, P.A. Link, H.E. Park, A.R. Kahn, K. Shankar, M.B. Schneck, D.J. Weiss, R.L. Heise, Porcine lung-derived extracellular matrix hydrogel properties are dependent on pepsin digestion time, Tissue Engineering Part C: Methods 26(6) (2020) 332-346.

[50] B.B. Rothrauff, L. Coluccino, R. Gottardi, L. Ceseracciu, S. Scaglione, L. Goldoni, R.S. Tuan, Efficacy of thermoresponsive, photocrosslinkable hydrogels derived from decellularized tendon and cartilage extracellular matrix for cartilage tissue engineering, Journal of tissue engineering and regenerative medicine 12(1) (2018) e159-e170.

[51] J.M. Singelyn, P. Sundaramurthy, T.D. Johnson, P.J. Schup-Magoffin, D.P. Hu, D.M. Faulk, J. Wang, K.M. Mayle, K. Bartels, M. Salvatore, Catheter-deliverable hydrogel derived from decellularized ventricular extracellular matrix increases endogenous cardiomyocytes and preserves cardiac function post-myocardial infarction, Journal of the American College of Cardiology 59(8) (2012) 751-763.

[52] Y.-W. Chen, C.-C. Chen, H.Y. Ng, C.-W. Lou, Y.-S. Chen, M.-Y. Shie, Additive manufacturing of nerve decellularized extracellular matrix-contained polyurethane conduits for peripheral nerve regeneration, Polymers 11(10) (2019) 1612.

[53] S. Bordbar, N. Lotfi Bakhshaiesh, M. Khanmohammadi, F.A. Sayahpour, M. Alini, M. Baghaban Eslaminejad, Production and evaluation of decellularized extracellular matrix hydrogel for cartilage regeneration derived from knee cartilage, Journal of Biomedical Materials Research Part A 108(4) (2020) 938-946.

[54] S. Yasmeen, M.K. Lo, S. Bajracharya, M. Roldo, Injectable scaffolds for bone regeneration, Langmuir 30(43) (2014) 12977-12985.

[55] Q. Wang, S. Chen, D. Chen, Preparation and characterization of chitosan based injectable hydrogels enhanced by chitin nano-whiskers, Journal of the mechanical behavior of biomedical materials 65 (2017) 466-477.

[56] R.H.J. de Hilster, P.K. Sharma, M.R. Jonker, E.S. White, E.A. Gercama, M. Roobeek, W. Timens, M.C. Harmsen, M.N. Hylkema, J.K. Burgess, Human lung extracellular matrix hydrogels resemble the stiffness and viscoelasticity of native lung tissue, American Journal of Physiology-Lung Cellular and Molecular Physiology 318(4) (2020) L698-L704.

[57] C. Williams, K. Sullivan, L.D. Black III, Partially digested adult cardiac extracellular matrix promotes cardiomyocyte proliferation in vitro, Advanced healthcare materials 4(10) (2015) 1545-1554.

[58] C. Panebianco, J. Meyers, J. Gansau, W. Hom, J. Iatridis, Balancing biological and biomechanical performance in intervertebral disc repair: a systematic review of injectable cell delivery biomaterials, European cells & materials 40 (2020) 239.

[59] P.J. Murray, Macrophage polarization, Annual review of physiology 79 (2017) 541-566.

[60] F. Yang, X. Liao, Y. Tian, G. Li, Exosome separation using microfluidic systems: size-based, immunoaffinity-based and dynamic methodologies, Biotechnology Journal 12(4) (2017) 1600699.

[61] S.F. Badylak, J.E. Valentin, A.K. Ravindra, G.P. McCabe, A.M. Stewart-Akers, Macrophage phenotype as a determinant of biologic scaffold remodeling, Tissue Engineering Part A 14(11) (2008) 1835-1842.

[62] J.L. Dziki, B.M. Sicari, M.T. Wolf, M.C. Cramer, S.F. Badylak, Immunomodulation and mobilization of progenitor cells by extracellular matrix bioscaffolds for volumetric muscle loss treatment, Tissue Engineering Part A 22(19-20) (2016) 1129-1139.

[63] J.M. Fishman, M.W. Lowdell, L. Urbani, T. Ansari, A.J. Burns, M. Turmaine, J. North, P. Sibbons, A.M. Seifalian, K.J. Wood, Immunomodulatory effect of a decellularized skeletal muscle scaffold in a discordant xenotransplantation model, Proceedings of the National Academy of Sciences 110(35) (2013) 14360-14365.

[64] K. Sadtler, S.D. Sommerfeld, M.T. Wolf, X. Wang, S. Majumdar, L. Chung, D.S. Kelkar, A. Pandey, J.H. Elisseeff, Proteomic composition and immunomodulatory properties of urinary bladder matrix scaffolds in homeostasis and injury, Seminars in immunology, Elsevier, 2017, pp. 14-23.

[65] J.L. Dziki, L. Huleihel, M.E. Scarritt, S.F. Badylak, Extracellular matrix bioscaffolds as immunomodulatory biomaterials, Tissue Engineering Part A 23(19-20) (2017) 1152-1159.

[66] T.J. Keane, R. Londono, N.J. Turner, S.F. Badylak, Consequences of ineffective decellularization of biologic scaffolds on the host response, Biomaterials 33(6) (2012) 1771-1781.

[67] P. Simon, M. Kasimir, G. Seebacher, G. Weigel, R. Ullrich, U. Salzer-Muhar, E. Rieder, E. Wolner, Early failure of the tissue engineered porcine heart valve SYNERGRAFT® in pediatric patients, European journal of cardio-thoracic surgery 23(6) (2003) 1002-1006.

[68] G.S. Hussey, J.L. Dziki, Y.C. Lee, J.G. Bartolacci, M. Behun, H.R. Turnquist, S.F. Badylak, Matrix bound nanovesicle-associated IL-33 activates a pro-remodeling macrophage phenotype via a non-canonical, ST2-independent pathway, Journal of immunology and regenerative medicine 3 (2019) 26-35.

[69] L. Huleihel, J.G. Bartolacci, J.L. Dziki, T. Vorobyov, B. Arnold, M.E. Scarritt, C. Pineda Molina, S.T. LoPresti, B.N. Brown, J.D. Naranjo, Matrix-bound nanovesicles recapitulate extracellular matrix effects on macrophage phenotype, Tissue Engineering Part A 23(21-22) (2017) 1283-1294.

[70] N.Y. Ignat'eva, N. Danilov, S. Averkiev, M. Obrezkova, V. Lunin, Determination of hydroxyproline in tissues and the evaluation of the collagen content of the tissues, Journal of Analytical Chemistry 62(1) (2007) 51-57.

[71] I.O.f. Standardization, ISO 10993-5 Biological evaluation of medical devices, Tests for in vitro cytotoxicity, 2009, p. 34.

[72] I.O.f. Standardization, ISO 10993-12 Biological evaluation of medical devices, Sample preparation and reference materials, 2012.

[73] U. Galili, S. Shohet, E. Kobrin, C. Stults, B. Macher, Man, apes, and Old World monkeys differ from other mammals in the expression of alpha-galactosyl epitopes on nucleated cells, Journal of Biological Chemistry 263(33) (1988) 17755-17762.

[74] T.D. Johnson, S.Y. Lin, K.L. Christman, Tailoring material properties of a nanofibrous extracellular matrix derived hydrogel, Nanotechnology 22(49) (2011) 494015.

[75] Y. Li, E.P. Douglas, Effects of various salts on structural polymorphism of reconstituted type I collagen fibrils, Colloids and Surfaces B: Biointerfaces 112 (2013) 42-50.

[76] S. Morozova, M. Muthukumar, Electrostatic effects in collagen fibril formation, The Journal of chemical physics 149(16) (2018) 163333.

[77] J.C. Iatridis, L.A. Setton, M. Weidenbaum, V.C. Mow, Alterations in the mechanical behavior of the human lumbar nucleus pulposus with degeneration and aging, Journal of Orthopaedic Research 15(2) (1997) 318-322.

[78] J.C. Iatridis, L.A. Setton, M. Weidenbaum, V.C. Mow, The viscoelastic behavior of the non-degenerate human lumbar nucleus pulposus in shear, Journal of biomechanics 30(10) (1997) 1005-1013.

[79] S.M. Romereim, C.A. Johnston, A.L. Redwine, R.A. Wachs, Development of an in vitro intervertebral disc innervation model to screen neuroinhibitory biomaterials, Journal of Orthopaedic Research® 38(5) (2020) 1016-1026.

[80] J.M. Brown, J. Xia, B. Zhuang, K.-S. Cho, C.J. Rogers, C.I. Gama, M. Rawat, S.E. Tully, N. Uetani, D.E. Mason, A sulfated carbohydrate epitope inhibits axon regeneration after injury, Proceedings of the National Academy of Sciences 109(13) (2012) 4768-4773.

[81] M. Fornaro, A. Giovannelli, A. Foggetti, L. Muratori, S. Geuna, G. Novajra, I. Perroteau, Role of neurotrophic factors in enhancing linear axonal growth of ganglionic sensory neurons in vitro, Neural regeneration research 15(9) (2020) 1732.

[82] D.A. Sholl, Dendritic organization in the neurons of the visual and motor cortices of the cat, Journal of anatomy 87(Pt 4) (1953) 387.

[83] I.O.f. Standardization, Biological evaluation of medical devices, Part 5: Tests for in vitro cytotoxicity, 2009.

[84] N.L. Nerurkar, D.M. Elliott, R.L. Mauck, Mechanical design criteria for intervertebral disc tissue engineering, Journal of biomechanics 43(6) (2010) 1017-1030.

[85] L. Yu, Z.-J. Sun, Q.-C. Tan, S. Wang, W.-H. Wang, X.-Q. Yang, X.-J. Ye, Thermosensitive injectable decellularized nucleus pulposus hydrogel as an ideal biomaterial for nucleus pulposus regeneration, Journal of biomaterials applications 35(2) (2020) 182-192.

[86] K. Franze, The mechanical control of nervous system development, Development 140(15) (2013) 3069-3077.

[87] A.M. Thomas, M.B. Kubilius, S.J. Holland, S.K. Seidlits, R.M. Boehler, A.J. Anderson, B.J. Cummings, L.D. Shea, Channel density and porosity of degradable

bridging scaffolds on axon growth after spinal injury, Biomaterials 34(9) (2013) 2213-2220.

[88] S.K. Tolofari, S.M. Richardson, A.J. Freemont, J.A. Hoyland, Expression of semaphorin 3A and its receptors in the human intervertebral disc: potential role in regulating neural ingrowth in the degenerate intervertebral disc, Arthritis research & therapy 12(1) (2010) 1-11.

[89] K.R. Nakazawa, B.A. Walter, D.M. Laudier, D. Krishnamoorthy, G.E. Mosley, K.L. Spiller, J.C. Iatridis, Accumulation and localization of macrophage phenotypes with human intervertebral disc degeneration, The Spine Journal 18(2) (2018) 343-356.

[90] J. Antoniou, T. Steffen, F. Nelson, N. Winterbottom, A.P. Hollander, R.A. Poole, M. Aebi, M. Alini, The human lumbar intervertebral disc: evidence for changes in the biosynthesis and denaturation of the extracellular matrix with growth, maturation, ageing, and degeneration, The Journal of clinical investigation 98(4) (1996) 996-1003.

[91] D.S. Perie, J.J. Maclean, J.P. Owen, J.C. Iatridis, Correlating material properties with tissue composition in enzymatically digested bovine annulus fibrosus and nucleus pulposus tissue, Annals of biomedical engineering 34(5) (2006) 769-777.

[92] F. Mwale, P. Roughley, J. Antoniou, Distinction between the extracellular matrix of the nucleus pulposus and hyaline cartilage: a requisite for tissue engineering of intervertebral disc, Eur Cell Mater 8(58) (2004) 63-64.

[93] J.D. O'Neill, R. Anfang, A. Anandappa, J. Costa, J. Javidfar, H.M. Wobma, G. Singh, D.O. Freytes, M.D. Bacchetta, J.R. Sonett, Decellularization of human and porcine lung tissues for pulmonary tissue engineering, The Annals of thoracic surgery 96(3) (2013) 1046-1056.

[94] C.S. Lau, A. Hassanbhai, F. Wen, D. Wang, N. Chanchareonsook, B.T. Goh, N. Yu, S.H. Teoh, Evaluation of decellularized tilapia skin as a tissue engineering scaffold, Journal of tissue engineering and regenerative medicine 13(10) (2019) 1779-1791.

[95] J.D. O'Neill, D.O. Freytes, A.J. Anandappa, J.A. Oliver, G.V. Vunjak-Novakovic, The regulation of growth and metabolism of kidney stem cells with regional specificity using extracellular matrix derived from kidney, Biomaterials 34(38) (2013) 9830-9841.

[96] G.S. Hussey, C.P. Molina, M.C. Cramer, Y.Y. Tyurina, V.A. Tyurin, Y.C. Lee, S.O. El-Mossier, M.H. Murdock, P.S. Timashev, V.E. Kagan, Lipidomics and RNA sequencing reveal a novel subpopulation of nanovesicle within extracellular matrix biomaterials, Science advances 6(12) (2020) eaay4361.

[97] L. Huleihel, G.S. Hussey, J.D. Naranjo, L. Zhang, J.L. Dziki, N.J. Turner, D.B. Stolz, S.F. Badylak, Matrix-bound nanovesicles within ECM bioscaffolds, Science advances 2(6) (2016) e1600502.

[98] Y.C. Lee, Matrix-bound Nanovesicles as an Extracellular Source of Lysyl Oxidase, University of Pittsburgh, 2020.

[99] L.M. Quijano, J.D. Naranjo, S.O. El-Mossier, N.J. Turner, C. Pineda Molina, J. Bartolacci, L. Zhang, L. White, H. Li, S.F. Badylak, Matrix-Bound Nanovesicles: The Effects of Isolation Method upon Yield, Purity, and Function, Tissue Engineering Part C: Methods 26(10) (2020) 528-540.

[100] A. Faust, A. Kandakatla, Y. van der Merwe, T. Ren, L. Huleihel, G. Hussey, J.D. Naranjo, S. Johnson, S. Badylak, M. Steketee, Urinary bladder extracellular matrix hydrogels and matrix-bound vesicles differentially regulate central nervous system

neuron viability and axon growth and branching, Journal of biomaterials applications 31(9) (2017) 1277-1295.

[101] S.-i. Ohno, A. Ishikawa, M. Kuroda, Roles of exosomes and microvesicles in disease pathogenesis, Advanced drug delivery reviews 65(3) (2013) 398-401.

[102] K. Schara, V. Janša, V. Šuštar, D. Dolinar, J.I. Pavlič, M. Lokar, V. Kralj-Iglič, P. Veranič, A. Iglič, Mechanisms for the formation of membranous nanostructures in cell-to-cell communication, Cellular & molecular biology letters 14(4) (2009) 636-656.

[103] G. Camussi, M.-C. Deregibus, S. Bruno, C. Grange, V. Fonsato, C. Tetta, Exosome/microvesicle-mediated epigenetic reprogramming of cells, American journal of cancer research 1(1) (2011) 98.

[104] K.H. Hussein, K.-M. Park, K.-S. Kang, H.-M. Woo, Biocompatibility evaluation of tissue-engineered decellularized scaffolds for biomedical application, Materials Science and Engineering: C 67 (2016) 766-778.

[105] Z. Jiang, G. Liu, J. Li, Recent progress on the isolation and detection methods of exosomes, Chemistry–An Asian Journal 15(23) (2020) 3973-3982.

[106] T. Baranyai, K. Herczeg, Z. Onódi, I. Voszka, K. Módos, N. Marton, G. Nagy, I. Mäger, M.J. Wood, S. El Andaloussi, Isolation of exosomes from blood plasma: qualitative and quantitative comparison of ultracentrifugation and size exclusion chromatography methods, PloS one 10(12) (2015) e0145686.

[107] B.J. Tauro, D.W. Greening, R.A. Mathias, H. Ji, S. Mathivanan, A.M. Scott, R.J. Simpson, Comparison of ultracentrifugation, density gradient separation, and immunoaffinity capture methods for isolating human colon cancer cell line LIM1863-derived exosomes, Methods 56(2) (2012) 293-304.

[108] M. An, J. Wu, J. Zhu, D.M. Lubman, Comparison of an optimized ultracentrifugation method versus size-exclusion chromatography for isolation of exosomes from human serum, Journal of proteome research 17(10) (2018) 3599-3605.

[109] M.J. Kleijmeer, W. Stoorvogel, J.M. Griffith, O. Yoshie, H.J. Geuze, Selective enrichment of tetraspan proteins on the internal vesicles of multivesicular endosomes and on exosomes secreted by human B-lymphocytes, Journal of Biological Chemistry 273(32) (1998) 20121-20127.

[110] M.A. Livshits, E. Khomyakova, E.G. Evtushenko, V.N. Lazarev, N.A. Kulemin, S.E. Semina, E.V. Generozov, V.M. Govorun, Isolation of exosomes by differential centrifugation: Theoretical analysis of a commonly used protocol, Scientific reports 5(1) (2015) 1-14.

[111] M. Bottini, S. Mebarek, K.L. Anderson, A. Strzelecka-Kiliszek, L. Bozycki, A.M.S. Simão, M. Bolean, P. Ciancaglini, J.B. Pikula, S. Pikula, Matrix vesicles from chondrocytes and osteoblasts: Their biogenesis, properties, functions and biomimetic models, Biochimica et Biophysica Acta (BBA)-General Subjects 1862(3) (2018) 532-546.

[112] F. Momen-Heravi, L. Balaj, S. Alian, P.-Y. Mantel, A.E. Halleck, A.J. Trachtenberg, C.E. Soria, S. Oquin, C.M. Bonebreak, E. Saracoglu, Current methods for the isolation of extracellular vesicles, Biological chemistry 394(10) (2013) 1253-1262.

[113] Y. Van der Merwe, A.E. Faust, M.B. Steketee, Matrix bound vesicles and miRNA cargoes are bioactive factors within extracellular matrix bioscaffolds, Neural regeneration research 12(10) (2017) 1597.

[114] K. Li, D.K. Wong, K.Y. Hong, R.L. Raffai, Cushioned–Density Gradient Ultracentrifugation (C–DGUC): a Refined and High Performance Method for the Isolation, Characterization & Use of Exosomes, Methods in molecular biology (Clifton, NJ) 1740 (2018) 69.

[115] T. Yamada, Y. Inoshima, T. Matsuda, N. Ishiguro, Comparison of methods for isolating exosomes from bovine milk, Journal of Veterinary Medical Science (2012) 12-0032.

[116] Z. Zhang, C. Wang, T. Li, Z. Liu, L. Li, Comparison of ultracentrifugation and density gradient separation methods for isolating Tca8113 human tongue cancer cell line-derived exosomes, Oncology letters 8(4) (2014) 1701-1706.

[117] R.A. Haraszti, R. Miller, M. Stoppato, Y.Y. Sere, A. Coles, M.-C. Didiot, R. Wollacott, E. Sapp, M.L. Dubuke, X. Li, Exosomes produced from 3D cultures of MSCs by tangential flow filtration show higher yield and improved activity, Molecular Therapy 26(12) (2018) 2838-2847.

[118] S. Busatto, G. Vilanilam, T. Ticer, W.-L. Lin, D.W. Dickson, S. Shapiro, P. Bergese, J. Wolfram, Tangential flow filtration for highly efficient concentration of extracellular vesicles from large volumes of fluid, Cells 7(12) (2018) 273.

[119] Z. Han, C. Peng, J. Yi, D. Zhang, X. Xiang, X. Peng, B. Su, B. Liu, Y. Shen, L. Qiao, Highly efficient exosome purification from human plasma by tangential flow filtration based microfluidic chip, Sensors and Actuators B: Chemical 333 (2021) 129563.

[120] M.Y. Konoshenko, E.A. Lekchnov, A.V. Vlassov, P.P. Laktionov, Isolation of extracellular vesicles: general methodologies and latest trends, BioMed research international 2018 (2018).

[121] N. Ludwig, T.L. Whiteside, T.E. Reichert, Challenges in exosome isolation and analysis in health and disease, International journal of molecular sciences 20(19) (2019) 4684.

[122] K. Sidhom, P.O. Obi, A. Saleem, A review of exosomal isolation methods: is size exclusion chromatography the best option?, International Journal of Molecular Sciences 21(18) (2020) 6466.

[123] I. Lozano-Ramos, I. Bancu, A. Oliveira-Tercero, M.P. Armengol, A. Menezes-Neto, H.A.D. Portillo, R. Lauzurica-Valdemoros, F.E. Borràs, Size-exclusion chromatography-based enrichment of extracellular vesicles from urine samples, Journal of extracellular vesicles 4(1) (2015) 27369.

[124] K. Štulík, V. Pacáková, M. Tichá, Some potentialities and drawbacks of contemporary size-exclusion chromatography, Journal of biochemical and biophysical methods 56(1-3) (2003) 1-13.

[125] H. Kalra, C.G. Adda, M. Liem, C.S. Ang, A. Mechler, R.J. Simpson, M.D. Hulett, S. Mathivanan, Comparative proteomics evaluation of plasma exosome isolation techniques and assessment of the stability of exosomes in normal human blood plasma, Proteomics 13(22) (2013) 3354-3364.

[126] Y.-T. Tang, Y.-Y. Huang, L. Zheng, S.-H. Qin, X.-P. Xu, T.-X. An, Y. Xu, Y.-S. Wu, X.-M. Hu, B.-H. Ping, Comparison of isolation methods of exosomes and exosomal RNA from cell culture medium and serum, International journal of molecular medicine 40(3) (2017) 834-844.

[127] T. Yamashita, Y. Takahashi, M. Nishikawa, Y. Takakura, Effect of exosome isolation methods on physicochemical properties of exosomes and clearance of exosomes from the blood circulation, European Journal of Pharmaceutics and Biopharmaceutics 98 (2016) 1-8.

[128] T.K. Kurian, S. Banik, D. Gopal, S. Chakrabarti, N. Mazumder, Elucidating methods for isolation and quantification of exosomes: A review, Molecular Biotechnology (2021) 1-18.

[129] L. Muller, C.-S. Hong, D.B. Stolz, S.C. Watkins, T.L. Whiteside, Isolation of biologically-active exosomes from human plasma, Journal of immunological methods 411 (2014) 55-65.

[130] E. Van der Pol, F. Coumans, A. Grootemaat, C. Gardiner, I. Sargent, P. Harrison, A. Sturk, T. Van Leeuwen, R. Nieuwland, Particle size distribution of exosomes and microvesicles determined by transmission electron microscopy, flow cytometry, nanoparticle tracking analysis, and resistive pulse sensing, Journal of Thrombosis and Haemostasis 12(7) (2014) 1182-1192.

[131] J.-H. Deng, Z.-J. Li, Z.-X. Wang, J. Feng, X.-J. Huang, Z.-M. Zeng, Electron microscopy-based comparison and investigation of the morphology of exosomes derived from hepatocellular carcinoma cells isolated at different centrifugal speeds, Microscopy and Microanalysis 26(2) (2020) 310-318.

[132] R. Dragovic, G. Collett, P. Hole, D. Ferguson, C. Redman, I. Sargent, D. Tannetta, Isolation of syncytiotrophoblast microvesicles and exosomes and their characterisation by multicolour flow cytometry and fluorescence Nanoparticle Tracking Analysis, Methods 87 (2015) 64-74.

[133] T.A. Hartjes, S. Mytnyk, G.W. Jenster, V. van Steijn, M.E. van Royen, Extracellular vesicle quantification and characterization: common methods and emerging approaches, Bioengineering 6(1) (2019) 7.

[134] M.W. Graner, O. Alzate, A.M. Dechkovskaia, J.D. Keene, J.H. Sampson, D.A. Mitchell, D.D. Bigner, Proteomic and immunologic analyses of brain tumor exosomes, The FASEB Journal 23(5) (2009) 1541-1557.

[135] M. Kesimer, M. Scull, B. Brighton, G. DeMaria, K. Burns, W. O'Neal, R.J. Pickles, J.K. Sheehan, Characterization of exosome-like vesicles released from human tracheobronchial ciliated epithelium: a possible role in innate defense, The FASEB Journal 23(6) (2009) 1858-1868.

[136] S. Atay, C. Gercel-Taylor, M. Kesimer, D.D. Taylor, Morphologic and proteomic characterization of exosomes released by cultured extravillous trophoblast cells, Experimental cell research 317(8) (2011) 1192-1202.

[137] I. Kadiu, P. Narayanasamy, P.K. Dash, W. Zhang, H.E. Gendelman, Biochemical and biologic characterization of exosomes and microvesicles as facilitators of HIV-1 infection in macrophages, The Journal of Immunology 189(2) (2012) 744-754.

[138] S. Sharma, M. LeClaire, J. Gimzewski, Ascent of atomic force microscopy as a nanoanalytical tool for exosomes and other extracellular vesicles, Nanotechnology 29(13) (2018) 132001.

[139] R. Vogel, F.A. Coumans, R.G. Maltesen, A.N. Böing, K.E. Bonnington, M.L. Broekman, M.F. Broom, E.I. Buzás, G. Christiansen, N. Hajji, A standardized method to determine the concentration of extracellular vesicles using tunable resistive pulse sensing, Journal of extracellular vesicles 5(1) (2016) 31242.

[140] Y. van der Merwe, A.E. Faust, E.T. Sakalli, C.C. Westrick, G. Hussey, K.C. Chan, I.P. Conner, V.L. Fu, S.F. Badylak, M.B. Steketee, Matrix-bound nanovesicles prevent ischemia-induced retinal ganglion cell axon degeneration and death and preserve visual function, Scientific reports 9(1) (2019) 1-15.

[141] F.Y. Liew, J.-P. Girard, H.R. Turnquist, Interleukin-33 in health and disease, Nature Reviews Immunology 16(11) (2016) 676-689.

[142] N. Ferrara, The role of VEGF in the regulation of physiological and pathological angiogenesis, Mechanisms of angiogenesis (2005) 209-231.

[143] Y. Reiss, G. Hoch, U. Deutsch, B. Engelhardt, T cell interaction with ICAM-1-deficient endothelium in vitro: essential role for ICAM-1 and ICAM-2 in transendothelial migration of T cells, European journal of immunology 28(10) (1998) 3086-3099.

[144] A.W. Boyd, S.O. Wawryk, G.F. Burns, J.V. Fecondo, Intercellular adhesion molecule 1 (ICAM-1) has a central role in cell-cell contact-mediated immune mechanisms, Proceedings of the National Academy of Sciences 85(9) (1988) 3095-3099.

[145] F. Bühling, U. Junker, D. Reinhold, K. Neubert, L. Jäger, S. Ansorge, Functional role of CD26 on human B lymphocytes, Immunology letters 45(1-2) (1995) 47-51.

[146] E.P. Boonacker, E.A. Wierenga, H.H. Smits, C.J.V. Noorden, CD26/DPPIV signal transduction function, but not proteolytic activity, is directly related to its expression level on human Th1 and Th2 cell lines as detected with living cell cytochemistry, Journal of Histochemistry & Cytochemistry 50(9) (2002) 1169-1177.

[147] K. Sato, U. Aytac, T. Yamochi, K. Ohnuma, K. McKee, C. Morimoto, N. Dang, CD26/dipeptidyl peptidase IV enhances expression of topoisomerase II alpha and sensitivity to apoptosis induced by topoisomerase II inhibitors, British journal of cancer 89(7) (2003) 1366-1374.

[148] L. Zhu, Y. Shi, L. Liu, H. Wang, P. Shen, H. Yang, Mesenchymal stem cells-derived exosomes ameliorate nucleus pulposus cells apoptosis via delivering miR-142-3p: therapeutic potential for intervertebral disc degenerative diseases, Cell Cycle 19(14) (2020) 1727-1739.

[149] R. Drula, L.F. Ott, I. Berindan-Neagoe, K. Pantel, G.A. Calin, MicroRNAs from liquid biopsy derived extracellular vesicles: recent advances in detection and characterization methods, Cancers 12(8) (2020) 2009.

[150] C. Théry, K.W. Witwer, E. Aikawa, M.J. Alcaraz, J.D. Anderson, R. Andriantsitohaina, A. Antoniou, T. Arab, F. Archer, G.K. Atkin-Smith, Minimal information for studies of extracellular vesicles 2018 (MISEV2018): a position statement of the International Society for Extracellular Vesicles and update of the MISEV2014 guidelines, Journal of extracellular vesicles 7(1) (2018) 1535750.

[151] T.J. Koh, L.A. DiPietro, Inflammation and wound healing: the role of the macrophage, Expert reviews in molecular medicine 13 (2011).

[152] N. Fujiwara, K. Kobayashi, Macrophages in inflammation, Current Drug Targets-Inflammation & Allergy 4(3) (2005) 281-286.

[153] B.N. Brown, J.E. Valentin, A.M. Stewart-Akers, G.P. McCabe, S.F. Badylak, Macrophage phenotype and remodeling outcomes in response to biologic scaffolds with and without a cellular component, Biomaterials 30(8) (2009) 1482-1491.

[154] T.J. Keane, J. Dziki, E. Sobieski, A. Smoulder, A. Castleton, N. Turner, L.J. White, S.F. Badylak, Restoring mucosal barrier function and modifying macrophage phenotype

with an extracellular matrix hydrogel: potential therapy for ulcerative colitis, Journal of Crohn's and Colitis 11(3) (2017) 360-368.

[155] B.M. Sicari, J.L. Dziki, B.F. Siu, C.J. Medberry, C.L. Dearth, S.F. Badylak, The promotion of a constructive macrophage phenotype by solubilized extracellular matrix, Biomaterials 35(30) (2014) 8605-8612.

[156] B.N. Brown, R. Londono, S. Tottey, L. Zhang, K.A. Kukla, M.T. Wolf, K.A. Daly, J.E. Reing, S.F. Badylak, Macrophage phenotype as a predictor of constructive remodeling following the implantation of biologically derived surgical mesh materials, Acta biomaterialia 8(3) (2012) 978-987.

[157] X. Zhang, R. Goncalves, D.M. Mosser, The isolation and characterization of murine macrophages, Current protocols in immunology 83(1) (2008) 14.1. 1-14.1. 14.

[158] M. Rath, I. Müller, P. Kropf, E.I. Closs, M. Munder, Metabolism via arginase or nitric oxide synthase: two competing arginine pathways in macrophages, Frontiers in immunology 5 (2014) 532.

[159] R. Rothoerl, C. Woertgen, M. Holzschuh, K. Brehme, J. Rüschoff, A. Brawanski, Macrophage tissue infiltration, clinical symptoms, and signs in patients with lumbar disc herniation. A clinicopathological study on 179 patients, Acta neurochirurgica 140(12) (1998) 1245-1248.

[160] C. Cayrol, J.P. Girard, Interleukin-33 (IL-33): a nuclear cytokine from the IL-1 family, Immunological reviews 281(1) (2018) 154-168.

[161] A.B. Molofsky, A.K. Savage, R.M. Locksley, Interleukin-33 in tissue homeostasis, injury, and inflammation, Immunity 42(6) (2015) 1005-1019.

[162] N. NIH, MMP2 Matrix Metallopeptidase 2, 2021. https://www.ncbi.nlm.nih.gov/gene?Db=gene&Cmd=ShowDetailView&TermToSearch=4313.

[163] S.M. Agrawal, L. Lau, V.W. Yong, MMPs in the central nervous system: where the good guys go bad, Seminars in cell & developmental biology, Elsevier, 2008, pp. 42-51.

[164] C.T. Esmon, Role of coagulation inhibitors in inflammation, Thrombosis and haemostasis 86(07) (2001) 51-56.

[165] K. Blazek, H.L. Eames, M. Weiss, A.J. Byrne, D. Perocheau, J.E. Pease, S. Doyle, F. McCann, R.O. Williams, I.A. Udalova, IFN-λ resolves inflammation via suppression of neutrophil infiltration and IL-1β productionIFN-λ restricts neutrophil infiltration, The Journal of experimental medicine 212(6) (2015) 845-853.

[166] D. Knight, Leukaemia inhibitory factor (LIF): a cytokine of emerging importance in chronic airway inflammation, Pulmonary pharmacology & therapeutics 14(3) (2001) 169-176.

[167] J.L. Bankers-Fulbright, K.R. Kalli, D.J. McKean, Interleukin-1 signal transduction, Life sciences 59(2) (1996) 61-83.

[168] R.L. Rabin, CC, C, and CX3C Chemokines, (2003).

[169] C. Jacques, M. Gosset, F. Berenbaum, C. Gabay, The role of IL-1 and IL-1Ra in joint inflammation and cartilage degradation, Vitamins & Hormones 74 (2006) 371-403.

[170] H. Wang, A. E Sama, Anti-inflammatory role of fetuin-A in injury and infection, Current molecular medicine 12(5) (2012) 625-633.

[171] N. Scamuffa, F. Calvo, M. Chrétien, N.G. Seidah, A.M. Khatib, Proprotein convertases: lessons from knockouts, The FASEB Journal 20(12) (2006) 1954-1963.

[172] A.G. Marneros, B.R. Olsen, Physiological role of collagen XVIII and endostatin, The FASEB Journal 19(7) (2005) 716-728.

[173] R. Morishita, M. Aoki, Y. Yo, T. Ogihara, Hepatocyte growth factor as cardiovascular hormone: role of HGF in the pathogenesis of cardiovascular disease, Endocrine journal 49(3) (2002) 273-284.

[174] S.J. Klebanoff, Myeloperoxidase: friend and foe, Journal of leukocyte biology 77(5) (2005) 598-625.

[175] X. Liu, Z. Zhou, Q. Cheng, H. Wang, H. Cao, Q. Xu, Y. Tuo, L. Jiang, Y. Zou, H. Ren, Acceleration of pancreatic tumorigenesis under immunosuppressive microenvironment induced by Reg3g overexpression, Cell death & disease 8(9) (2017) e3033-e3033.

[176] J. Lorenzo, The effects of immune cell products (cytokines and hematopoietic cell growth factors) on bone cells, Osteoimmunology, Elsevier2016, pp. 143-167.

[177] A. Ma, R. Koka, P. Burkett, Diverse functions of IL-2, IL-15, and IL-7 in lymphoid homeostasis, Annu. Rev. Immunol. 24 (2006) 657-679.

[178] A.L. Angiolillo, C. Sgadari, D.D. Taub, F. Liao, J.M. Farber, S. Maheshwari, H.K. Kleinman, G.H. Reaman, G. Tosato, Human interferon-inducible protein 10 is a potent inhibitor of angiogenesis in vivo, The Journal of experimental medicine 182(1) (1995) 155-162.

[179] J.H. Dufour, M. Dziejman, M.T. Liu, J.H. Leung, T.E. Lane, A.D. Luster, IFN-γ-inducible protein 10 (IP-10; CXCL10)-deficient mice reveal a role for IP-10 in effector T cell generation and trafficking, The Journal of Immunology 168(7) (2002) 3195-3204.

[180] B. Stanic, W. Van De Veen, O.F. Wirz, B. Rückert, H. Morita, S. Söllner, C.A. Akdis, M. Akdis, IL-10–overexpressing B cells regulate innate and adaptive immune responses, Journal of Allergy and Clinical Immunology 135(3) (2015) 771-780. e8.

[181] D.F. Fiorentino, A. Zlotnik, T.R. Mosmann, M. Howard, A. O'garra, IL-10 inhibits cytokine production by activated macrophages, The Journal of immunology 147(11) (1991) 3815-3822.

[182] T.A. Wynn, IL-13 effector functions, Annual review of immunology 21(1) (2003) 425-456.